INTERPRETATION OF THE BMP MORPHOGEN GRADIENT DURING DORSAL-VENTRAL AXIAL PATTERNING

Hannah Greenfeld

A DISSERTATION

in

Cell and Molecular Biology

Presented to the Faculties of the University of Pennsylvania

in

Partial Fulfillment of the Requirements for the

Degree of Doctor of Philosophy

2020

Supervisor of Dissertation

_____

Mary C. Mullins, PhD
Professor of Cell and Developmental Biology

Graduate Group Chairperson

_____

Daniel Kessler, PhD
Professor of Cell and Developmental Biology

Dissertation Committee
Sarah Millar, PhD, Professor of Cell, Developmental, and Regenerative Biology
Ken Zaret, PhD, Joseph Leidy Professor of Cell and Developmental Biology
John Murray, PhD, Associate Professor of Genetics
Shawn Little, PhD, Assistant Professor of Cell and Developmental Biology

INTERPRETATION OF THE BMP MORPHOGEN GRADIENT DURING DORSAL-VENTRAL AXIAL PATTERNING

ACKNOWLEDGMENT

First, I would like to thank my thesis adviser Mary Mullins for her tremendous support and patience during my entire time in graduate school. She is truly dedicated to developing students into scientists through her commitment to rigorous science and by fostering skills beyond the bench. I admire her as both a scientist and as a mentor in and out of the lab. Thank you for allowing me to explore, learn, and grow; I could not have asked for a better environment to do my graduate work.

I am incredibly lucky to have worked with so many wonderful people, past and present, in the Mullins lab. Thank you for all the thoughtful feedback and discussions throughout the years. Special thanks to Joe Zinski for pioneering the pSmad5 imaging assay and paving the way for my project, Francesca Tuazon for being a wonderful bay-mate and providing so much support and inspiration, and Amy Kugath for her incredible amount of help and expertise. Thank you Ben Tajer, Robyn Allen, AJ Lucy, William Jones, Jira White, Jose Pelliccia, and Manami Kobayashi for making the lab such a fun place to work and for the countless hours of thoughtful feedback in lab meetings and practice talks.

Thank you to my committee members for their input over the years: Sarah Millar, Ken Zaret, Shawn Little, and John Murray have all provided valuable feedback and direction at every stage of the project.

I have also been inspired by my friends throughout my life, and they have been there to celebrate and commiserate with me during my time in graduate

school and beyond. Special thanks to Zoe Leavitt, Katy Johnson, Tess Saxton-Fox, Dan Skehan, Dan Minty, Matt McConnell, Stevey Poppe, Jenni Belanger, Michelle Wright, Jessica Leaf, and Katy Messenger. Since elementary school and college, you all have been such an inspiration to me. My time at Penn has been equally special. I am grateful to have met such wonderful people including Emmanuelle Genoyer, Chris Greer, and Sara Borst. You have made graduate school so much fun; I feel incredibly blessed to have met each of you and cannot wait to celebrate with you in the future.

Finally, I thank my family. To my parents, Ellen and Norton for your invaluable support and unconditional love. It's hard to properly acknowledge their contribution and convey how lucky I am: thank you for your encouragement of my creativity and curiosity. And to Lindsey especially, who supports me throughout my life in an infinite number of ways and inspires me to be a better person. And of course, for your editing expertise, from my emails to this acknowledgement page itself.

ABSTRACT

INTERPRETATION OF THE BMP MORPHOGEN GRADIENT DURING DORSAL-VENTRAL AXIAL PATTERNING

Hannah Greenfeld

Mary C. Mullins

Bone Morphogenetic Protein (BMP) patterns the dorsoventral (DV) embryonic axis in all vertebrates, but it is unknown how cells along the DV axis interpret and translate the gradient of BMP signaling into differential gene activation that will specify distinct cell fates. To determine the mechanism by which BMP signaling provides positional information to cells across the DV axis in the zebrafish embryo, we identified the genes that are directly regulated by BMP signaling during gastrulation. We identified 57 genes that are directly activated and 15 genes directly repressed by BMP signaling. By using Seurat analysis of single-cell RNA-seq data, we found that genes activated by BMP signaling are expressed in at least three distinct DV domains of the embryo. The expression boundaries of genes expressed in different domains correlate with both distinct BMP signaling levels and gradient slopes. The gradient is also highly dynamic during gradient formation from mid-blastula to early-gastrula stages, exposing cells to different signaling durations during gastrulation. The goal of this work is to distinguish between three models of BMP signal interpretation in which cells activate distinct gene expression through interpretation of thresholds of: 1. the BMP signaling gradient slope, 2. BMP signal duration, or 3. the level of BMP signal activation. We tested these three models

using quantitative measurements of phospho-Smad5 and by examining the spatial relationship between BMP signaling and activation of different target genes at single cell resolution across the embryo. We utilized mutants that have a modified phospho-Smad5 gradient shape and measured corresponding shifts in target gene expression to determine if the gradient slope provides positional information. To address the role of signal duration to pattern ventral cell fates, we tested the requirement of BMP ligand exposure to activate target gene expression. We found that BMP signaling gradient slope or BMP exposure duration did not account for the differential target gene expression domains. Instead we show that cells respond to three distinct levels of BMP signaling activity to activate and position target gene expression. Together, we demonstrate that distinct phospho-Smad5 threshold levels activate spatially-distinct target genes to pattern the DV axis.

TABLE OF CONTENTS

ACKNOWLEDGMENT ..... **III**

ABSTRACT ..... **V**

LIST OF TABLES ..... **IX**

LIST OF FIGURES ..... **X**

CHAPTER 1: INTERPRETATION OF BMP MORPHOGEN GRADIENTS **1**

1.1 Introduction: Morphogen patterning during development **2**

1.2 BMP signaling patterns the dorsal-ventral axis **4**
1.2.1 DV axis patterned by BMP signaling gradient 4
1.2.2 BMP signal transduction 7
1.2.3 Post-translational regulation of Smad transcription factors 8

1.3 Transcriptional regulation by Smads **11**
1.3.1 Smad interaction with DNA 11
1.3.2 Smad association with cofactors 13
1.3.3 Chromatin remodeling by Smads 15

1.4 Mechanisms of BMP morphogen gradient interpretation **16**
1.4.1 Concentration-dependent gene regulation 16
1.4.2 Temporal signal integration 20
1.4.3 Temporal signaling windows 23
1.4.4 Determining the mechanism of BMP signal interpretation that patterns the DV axis of the zebrafish embryo 24

CHAPTER 2: BMP SIGNALING GRADIENT INTERPRETED THROUGH CONCENTRATION THRESHOLDS IN DORSAL-VENTRAL AXIAL PATTERNING **26**

Summary **27**

2.1 Introduction **28**

2.2 Results **31**
2.2.1 Identification of target genes directly patterned by the BMP gradient 31
2.2.2 Ventral BMP target genes are expressed in at least three distinct domains 41
2.2.3 Distinct pSmad5 levels and gradient slopes correspond to different target gene expression boundaries 51
2.2.4 Test of gradient slope to position gene expression boundaries 55
2.2.5 Test of signal duration to position gene expression boundaries 60
2.2.6 Test of signal concentration to activate different target genes 67

2.3 Discussion **72**
2.3.1 BMP morphogen interpretation: multiple mechanisms for one signaling pathway 72
2.3.2 Multiple expression domains directly patterned by the BMP gradient 73
2.3.3 Concentration, not gradient shape or duration, positions expression boundaries 75

CHAPTER 3: MATERIALS AND METHODS **78**
Zebrafish 79
Genotyping 79
pSmad5 Immunostaining, Imaging, and Quantification 80
Fluorescent *in situ* Hybridization, Imaging, and Quantification 81
BMP2/7 Protein Injections 82
Cell disassociation cultures 82
RNA-sequencing and Analysis 83
Seurat Analysis of Single-cell RNA-sequencing Dataset 84
Statistical Analysis 84

CHAPTER 4: CONCLUSIONS AND FUTURE DIRECTIONS **85**

4.1 Summary of findings **86**

4.2 Translating gene expression domains into cell fates **87**
4.2.1 Identification of BMP target genes 87
4.2.2 Refinement of expression domains 88

4.3 Generation of different thresholds **93**
4.3.1 Differences in pSmad5 binding site affinity 93
4.3.2 Smad5 cofactors during DV patterning 94
4.3.3 Differences in pSmad5 threshold across the AV axis 95

4.4 Competency of BMP signaling during patterning **96**

4.5 Concluding Remarks **98**

BIBLIOGRAPHY **99**

LIST OF TABLES

Table 1: BMP upregulated target genes

Table 2: BMP downregulated target genes

LIST OF FIGURES

Figure 1.1: The French flag problem

Figure 1.2: BMP patterns the dorsal-ventral axis in zebrafish

Figure 1.3: Regulation of Smad transcription factors

Figure 1.4: Mechanisms of concentration-dependent gene expression

Figure 1.5: Duration-dependent patterning of the neural tube by Shh

Figure 2.1: Direct targets of BMP signaling in DV axial patterning

Figure 2.2: Identification of genes dependent on and directly regulated by BMP signaling

Figure 2.3: Three distinct expression domains of BMP direct target genes

Figure 2.4: Seurat predicted expression domains of 50 BMP directly upregulated target genes

Figure 2.5: Seurat predicted expression domains of 11 BMP directly downregulated target genes

Figure 2.6: Quantifying fluorescent in situ hybridization of three target genes.

Figure 2.7: pSmad5 gradient with distinct thresholds and slopes delineating expression domains

Figure 2.8: Expression profiles across the AV axis of the embryo

Figure 2.9: pSmad5 gradient thresholds versus slopes in positioning target gene expression in *chordin* mutant gradient

Figure 2.10: pSmad5 levels and target gene expression in *chordin* mutants

Figure 2.11: Thirty-minute duration of BMP2/7 sufficient for *sizzled, foxi1*, and *bambia* target gene expression

Figure 2.12: Differential target gene induction at 10, 20, and 30 minutes

Figure 2.13: Broadly expressed target gene *ved* rapidly activated following BMP exposure

Figure 2.14: Rapid activation of target genes does not require transcriptional feedback

Figure 2.15: Target genes *sizzled* and *bambia* respond to BMP in a concentration-dependent manner

Figure 2.16: Activation of different pSmad5 levels in BMP-treated disassociated cells

Figure 2.17: Differential response of *sizzled* and *bambia* to BMP concentrations

Figure 4.1: Variability of pSmad5 levels across the DV axis

Figure 4.2: Dynamic pSmad5 levels and target gene expression during gastrulation.

Figure 4.3: Response to BMP signaling across the animal-vegetal axis

Figure 4.4: Mid-gastrula embryos remain competent to BMP signaling

CHAPTER 1: Interpretation of BMP morphogen gradients

1.1 Introduction: Morphogen patterning during development

During the development of multicellular organisms, a single cell gives rise to a pool of pluripotent cells that are transformed into all the cell types and organs of the adult (Ashe and Briscoe, 2006; Briscoe and Small, 2015; Rogers and Schier, 2011). Pluripotent cells are patterned during the process of gastrulation to generate different organ progenitors. During gastrulation, the embryonic body plan is formed through the specification of the three germ layers and highly coordinated massive cell movements (Tuazon and Mullins, 2015). The number and position of different cell types are specified in a stereotyped fashion within the embryo. Different fates and cell movements are induced by localized signaling molecules, called morphogens. Morphogens are signaling molecules that form a gradient across multiple cell-lengths to induce different cells fates. The graded distribution of the morphogen exposes cells to different signaling levels at different locations within the tissue. The mechanism of how graded morphogen signaling controls cells fate specification remains a highly active area of research.

Morphogen gradients pattern the two primary body axes: the dorsal-ventral (DV) axis and the anterior-posterior (AP) axis, as well as multiple organ systems later during development, regeneration, and tissue homeostasis (Tuazon and Mullins, 2015). The DV axis is patterned by Bone Morphogenetic Proteins (BMP), while the AP is patterned by localized Nodal, Fibroblast Growth Factor (FGF), Wnt, and Retinoic Acid (RA) signaling (Dorey and Amaya, 2010;

Hikasa and Sokol, 2013; Langdon and Mullins, 2011; Schier and Talbot, 2005). Gradients of the morphogens are formed during gastrulation as the embryo is undergoing massive cell movements. Cells are therefore exposed to different signaling levels across both time and space. Misregulation of these signaling pathways within the early embryo affects the specification and relative proportion of cell types across the embryo (Nguyen et al., 1998; Schumacher et al., 2011). It is critical to understand how cells respond to morphogen gradients to determine how different cell fates are established within precise positions of the embryo.

The modern concept of morphogen gradients providing positional information to cells was proposed by Lewis Wolpert over 50 years ago (Wolpert, 1969) **(Figure 1.1)**. He proposed that cells within a field can gain information based on their location relative to each other as in a coordinate system. Differences in positional information are then converted to differences in cell fate. This concept of pattern regulation gave rise to the French Flag model that graded instructive cues can assign different cell fates in the correct order and proportion within a tissue. The French Flag problem requires cells to respond to different morphogen signaling thresholds, but how cells interpret graded morphogen signaling is not known for many biological systems. This chapter first discusses the Bone Morphogenetic Protein (BMP) signaling pathway and its role in dorsal-ventral axial patterning. This chapter next addresses how the BMP signal is transduced as well as the potential mechanisms by which BMP signaling regulates gene expression. Finally, the various mechanisms that have been

proposed to translate graded morphogen signaling into distinct domains of gene expression are addressed.

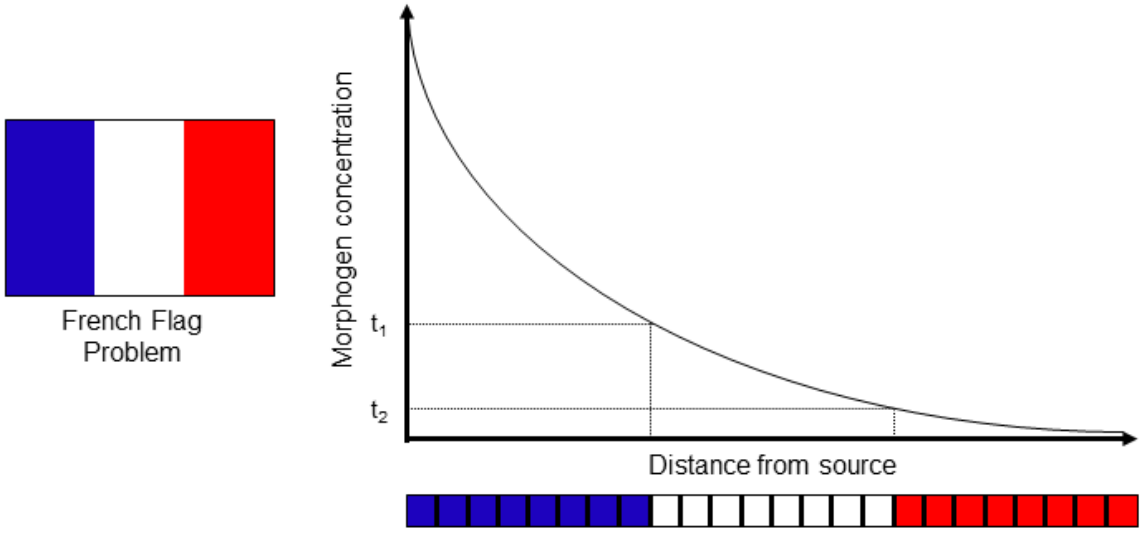

Figure 1.1 The French flag problem. Wolpert's French flag model represents a field of cells that has been divided into three regions of different cell fates depicted in blue, white and red. A graded distribution of a morphogen across a tissue exposes cells to different morphogen concentrations. Cells exposed to morphogen concentrations above the high threshold (t_1) differentiate into the blue fate, while cells exposed to morphogen concentrations between high and low thresholds (t_1 and t_2) will differentiate into the white fate. Cells exposed to morphogen levels below t_2 will form the red fate. Thus, a morphogen gradient can provide positional information and pattern multiple cell fates within a tissue.

1.2 BMP signaling patterns the dorsal-ventral axis

1.2.1 DV axis patterned by BMP signaling gradient

Bone Morphogenetic Proteins (BMP) are members of the TGF-β superfamily of secreted growth factors, which pattern multiple tissues that include the DV body axis, the neural tube, developing limb bud, and stem cell niches (Dutko and Mullins, 2011; Zinski et al., 2018). Misregulation of BMP signaling is associated with cancers, pulmonary hypertension, osteoporosis, and ectopic bone disease (Blanco Calvo et al., 2009; Lane et al., 2000; Shore et al., 2006;

Wu et al., 2003). Therefore, investigating BMP-mediated gene regulation is critical for understanding developmental patterning and cell fate specification, but also for understanding the progression and treatment of disease.

The DV axis is patterned in mice during E5.5-E8.5 (Beddington and Robertson, 1999) compared with 4 to 12 hours post fertilization (hpf) in zebrafish and Xenopus embryos (De Robertis and Kuroda, 2004; Tucker et al., 2008). BMP signaling is essential in the specification of ventral cell fates **(Figure 1.2A)**. The BMP ligands that are required during DV patterning are BMP 2, 4, and 7 (Ben-Haim et al., 2006; Nguyen et al., 1998; Reversade and De Robertis, 2005; Schmid et al., 2000; Stickney et al., 2007). In zebrafish, BMP2 and BMP7 are covalently linked to form a heterodimer that is required for ventral tissue specification (Little and Mullins, 2009). Loss of either *bmp2* or *bmp7* results in complete expansion of dorsal tissue specification across the axis and is embryonic lethal (Nguyen et al., 1998; Schmid et al., 2000) **(Figure 1.2B)**.

In the zebrafish early blastula, *bmp2* and *bmp7* are uniformly expressed across the embryo, but by the onset of gastrulation these transcripts are cleared from the dorsal region by factors induced by maternal Wnt and β-catenin signaling (Dal-Pra et al., 2006; Dick et al., 2000; Langdon and Mullins, 2011; Ramel and Hill, 2013). Signals emanating from the dorsal organizer activate the expression of the BMP antagonists: *chordin*, *noggin*, and *follistatin* (Fürthauer et al., 1999; Schulte-Merker et al., 1997; Stachel et al., 1993). These antagonists create and shape the gradient of BMP signaling activity across the DV axis,

which is highest on the ventral side of the embryo and lowest on the dorsal side **(Figure 1.2A)**.

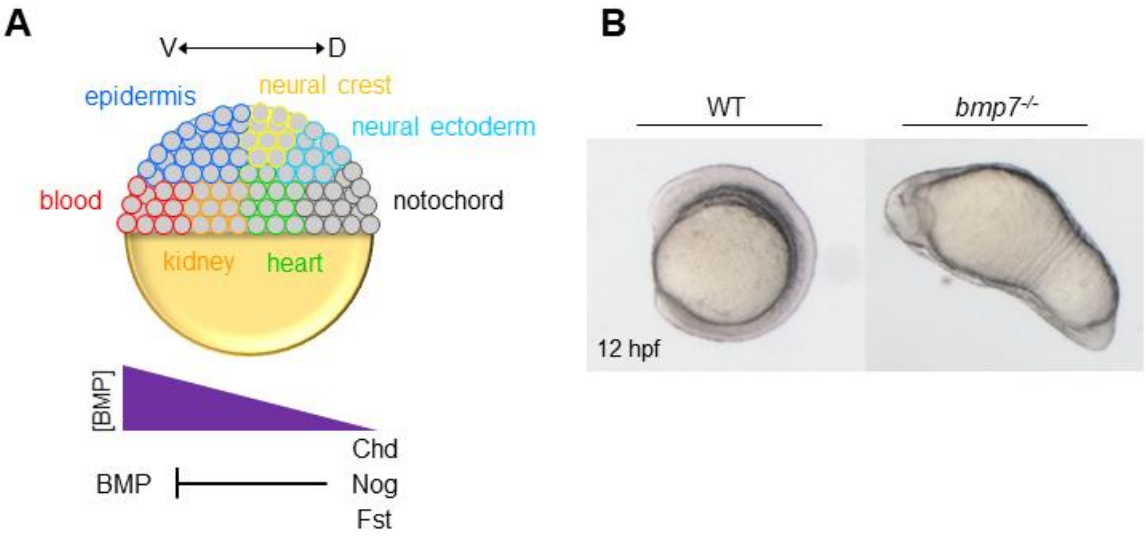

Figure 1.2 BMP patterns the dorsal-ventral axis in zebrafish. (A) Schematic of the fate map of the early zebrafish gastrula at 6 hours post fertilization (hpf). The BMP morphogen gradient specifies the cell fates that arise on the ventral side of the embryo. BMP signaling is inhibited by dorsally expressed antagonists Chordin (Chd), Noggin (Nog), and Follistatin (Fst). The ventral side is to the left. (B) A wild-type and *bmp7* mutant zebrafish embryo at 12 hpf. Loss of BMP signaling results in loss of all ventrally derived tissues and expansion of dorsal somites around the entire embryo. Photo taken by James Dutko.

Different levels of BMP activity specify the fate and relative abundance of ventral tissues. Null mutations of *bmp2b* in zebrafish eliminate epidermis, placodes, neural crest, and ventral mesendoderm and lead to expanded neural tissues (Nguyen et al., 1998). When BMP signaling is reduced in hypomorphic mutants or by moderate overexpression of *chordin*, there is loss of epidermal markers but an expansion of neural crest and placodal progenitor markers (Schumacher et al., 2011). Thus, epidermis is specified by high levels of BMP signaling while neural crest and placodal tissues are specified by intermediate

levels of BMP signaling. Changing the level of BMP signaling across the embryo shifts the position of gene expression patterns.

1.2.2 BMP signal transduction

The BMP2/7 heterodimer signals through a heterotetrameric receptor complex that is composed of two Type I and two Type II receptors (Armes and Smith, 1997; Graff et al., 1994; Shi and Massagué, 2003). The receptor complex must contain both Type I receptors, Bmpr1 and Acvr1l, however, the requirement of the different Type II receptors in the complex is not known (Little and Mullins, 2009). The expression of the Type I and Type II receptors is uniform across the DV axis of the zebrafish embryo (Hild et al., 1999). Once the BMP ligand binds to the complex, the Type II receptors phosphorylate the Type I receptors that in turn phosphorylate the Ser-X-Ser motif in the carboxy-terminus of Receptor-activated Smad (R-Smad) transcription factors (Massagué, 2012). Five of the 8 Smads found in vertebrates are R-Smads. Smad2 and Smad3 are activated by Nodal, Activin and TGF-β, while Smad1, 5, and 9 are activated by BMP and growth and differentiation factors (GDFs) (Miyazawa et al., 2002) **(Figure 1.3A)**. Smad2, 4, and 5 are maternally provided in the zebrafish, and Smad5 subsequently induces expression of Smad1 and 9 during gastrulation (Wei et al., 2014). All R-Smads share highly conserved Mad Homology 1 (MH1) and Mad Homology 2 (MH2) domains at the animo-terminus and carboxy-terminus respectively (Chaikuad and Bullock, 2016) **(Figure 1.3B)**. The sequence between the MH1 and MH2 domains is called the linker region that is highly variable between Smads.

Phosphorylated Smad (pSmad) forms homo- and heterotrimeric complexes with Smad4, a co-Smad that is shared with all R-Smads (Chacko et al., 2004; Qin et al., 2001) **(Figure 1.3A)**. Activation of R-Smads is blocked by the Inhibitory Smads (I-Smad), Smad6 and Smad7 (Miyazawa and Miyazono, 2017) **(Figure 1.3A)**. The I-Smads bind to the Type I receptor or Smad4 and block interaction with R-Smads. The activated Smad complex translocates into the nucleus where it accumulates (Massagué, 2012). Nuclear phosphatases, such as SCP2/Os4 in Xenopus, PDP in Drosophila, and PPM1A in zebrafish target BMP activated Smads for dephosphorylation of the C-terminus and result in the shuttling of the activated Smad complex out of the nucleus (Chen et al., 2006; Knockaert et al., 2006; Lin et al., 2006). Recycling and nuclear shuttling of Smads out of the nucleus is critical for the cells' ability to sense changing BMP levels.

1.2.3 Post-translational regulation of Smad transcription factors

Regulation of post-translational modification of sites within the linker region and N-terminal region of Smads provide additional layers of regulation of TGF-β signaling and is a source of integration with other signaling pathways. Because the linker regions are variable between Smads, post-translational modification of sites within this region are thought to provide pathway-specific regulation. The linker region of Smad1, 5, and 9 contains multiple phosphorylation sites for MAPK (4 PxSP motifs) and GSK-3β (2 S/TxxxS motifs) and a site for ubiquitination by Smurf ubiquitin ligases (PPXY motifs) (Sapkota et

al., 2007) **(Figure 1.3B)**. Phosphorylation of different sites within the linker region may induce conformational changes of Smad affecting the interaction with other proteins and DNA binding (Sapkota et al., 2007). In human cell lines (Kretzschmar et al., 1997), mouse (Aubin et al., 2004), and Xenopus embryos (Pera et al., 2003) phosphorylation of the linker region by MAPK leads to a decrease in Smad1 activity. FGF and IGF induces MAPK to phosphorylate Smad1 thereby inhibiting BMP signaling activity. Elimination of MAPK phosphorylation sites increases Smad1 potency resulting in strongly ventralized embryos and increased expression of the BMP target gene *sizzled,* while not increasing Smad1 protein levels (Pera et al., 2003).

Wnt signaling inhibits GSK-3β mediated linker phosphorylation and GSK-3β inhibition is required for epidermal differentiation by BMP signaling (Fuentealba et al., 2007) **(Figure 1.3B)**. CDK8/9 was also found to phosphorylate the linker region of Smad1 and phosphorylation of these sites induces the recruitment of Yap, the Hippo pathway effector in mouse embryonic stem cells (mESCS). Hippo signaling enhances BMP-mediated transcription and the suppression of neuronal fates in mESCs (Alarcón et al., 2009). Phosphorylation by both GSK-3β and CDK8/9 allows the PPXY motif within the Smad linker region to be recognized by Smad ubiquitin regulatory factor (Smurf1/2), an E3 ubiquitin ligase and leads to proteome-mediated degradation (Alarcón et al., 2009; Aragón et al., 2011) **(Figure 1.3B)**. Smurf1 specifically targets the BMP-responsive Smad1 and Smad5 (Zhu et al., 1999), while Smurf2 does not display

pathway specificity (Zhang et al., 2001). Smurf1 mutations in Drosophila lead to expansion of the DPP gradient and expanded domains of DPP target genes (Podos et al., 2001). However, Smurf1 knockouts in mice did not display developmental defects (Yamashita et al., 2005), but did have increased bone mass and osteoblast activity, indicating increased BMP signaling activity.

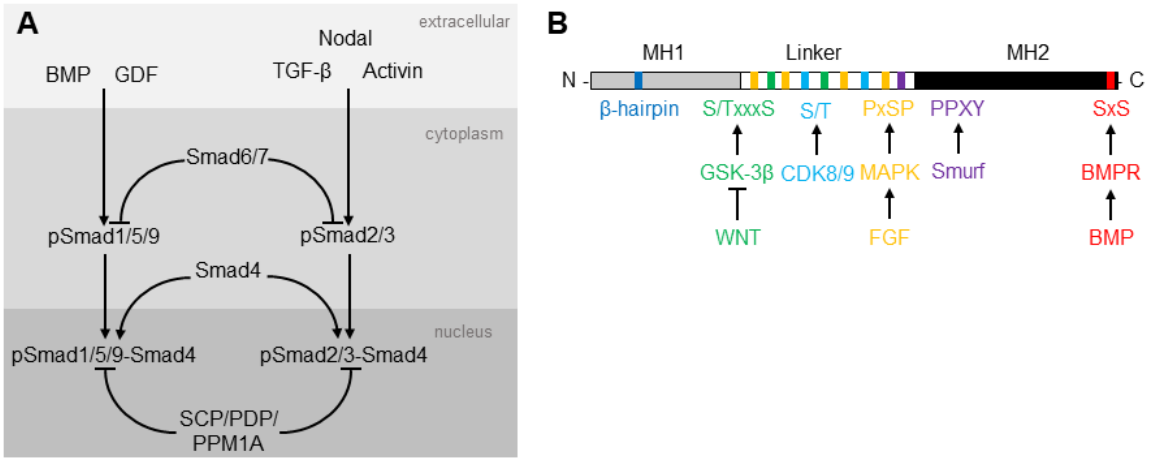

Figure 1.3 Regulation of Smad transcription factors. (A) Model of TGF-β signal transduction. R-Smad activation is inhibited by I-Smads. Activated R-Smads complex with Smad4 to enter the nucleus. Nuclear phosphatases dephosphorylate R-Smad-Smad4 complexes and inhibit signaling activity. (B) Schematic of Smad1 domains and motifs for posttranslational modification. The MH1 domain is conserved between R-Smads and Smad4 and contains the DNA-binding β-hairpin. The variable linker region is targeted by kinases (GSK-3β, CDK8/9, and MAPK) and ubiquitin ligases (Smurf). Motifs for phosphorylation and ubiquitination are indicated. The MH2 domain is conserved between all Smads and contains the domain that mediates association with the Type I receptor and SXS motif phosphorylated by the Type I receptor in response to BMP signaling.

Posttranslational modifications of Smad5 are essential for integration of BMP, FGF and Wnt to coordinate DV and AP patterning in zebrafish (Hashiguchi and Mullins, 2013). Both the AP and DV axis are patterned progressively from anterior to posterior (Hashiguchi and Mullins, 2013; Stern et al., 2006; Tucker et al., 2008). Inhibiting either FGF signaling or Wnt signaling expands the

expression of markers for anterior cell fates and modulates the temporal patterning of DV tissues. Marginal FGF and Wnt signaling restricts GSK-3β phosphorylated Smad1/5 to the ventral animal region of the embryo and MAPK phosphorylated Smad1/5 to the ventral margin. Mutations in the MAPK phosphorylation sites within the Smad1 linker region results in patterning of the DV tissues 30 minutes earlier than normal. This suggests that Smad inhibition by FGF signaling temporally regulates DV tissue patterning during gastrulation and allow cells to adopt both AP and DV identities simultaneously (Hashiguchi and Mullins, 2013).

1.3 Transcriptional regulation by Smads

1.3.1 Smad interaction with DNA

The co-Smad4 and all of the R-Smads, except for Smad2, bind directly to DNA (Massague et al., 2005). Smads bind to DNA through a highly conserved 11-residue β-hairpin loop in the MH1 domain **(Figure 1.3B)**. Crystal structures of Smad1 and Smad3 MH1 domains revealed direct binding to a minimal 4 base pair sequences GTCT or AGAC (BabuRajendran et al., 2010; Shi et al., 1998b). This is consistent with the consensus Smad-binding element (SBE) identified by PCR-based screening of random sequences (Zawel et al., 1998). The Smad3 MH1 domain binds DNA with relatively weak affinity, 1.14×10^{-7} M (Shi et al., 1998b). Palindromic repeats of the SBE have been found within the regulatory region of Nodal, Activin, and TGF-β target genes by chromatin-

immunoprecipitation (ChIP)-sequencing or promoter sequence analysis (Dennler et al., 1998; Liu et al., 2011; Wong et al., 1999).

While the DNA-contact amino acids are invariant between Smad1 and Smad3, the MH1 domain of Smad1 preferentially binds to a GC-rich sequence (GCCGnCGC) that was first identified in Drosophila (Kim et al., 1997) and subsequently found at the regulatory region of BMP target genes identified in mammals, Xenopus, and zebrafish (Brugger et al., 2004; Collery and Link, 2011; Ishida et al., 2000; Karaulanov et al., 2004; Morikawa et al., 2011). The crystal structure of the Smad1 MH1 domain bound to the SBE displayed a rearranged DNA contact interface compared to the Smad3 MH1 domain and results in fewer interactions with the phosphate backbone (BabuRajendran et al., 2010). The reduction of contact sites between Smad1 and DNA further reduced the overall affinity to DNA compared to Smad3.

Comparison of Smad3 and Smad5 MH1 domains binding to palindromic SBE or GC-rich sequences confirmed that while Smad3 MH1 binds additively to both the SBE and GC-rich motifs, Smad5 MH1 dimerized cooperatively on the palindromic sequences (Chai et al., 2015). Smad5 MH1 displayed stronger cooperative binding to the GC-rich sequence than the SBE where it formed a constitutive dimer on the GC-rich palindrome sequence. The crystal structures of both Smad1 and Smad5 MH1 domains displayed a less compacted confirmation and more “open” structure compared to Smad3 MH1 allowing for the potential to homodimerize on DNA (BabuRajendran et al., 2010; Chai et al., 2015). Together,

comparing the structure of MH1 domains of different Smads bound to DNA revealed that BMP-responsive Smads bind DNA in a different mode than Smads activated by other TGF-β signaling and may underlie differences in the transcriptional response.

Comparison of genome-wide analyses of Smad binding sites between different cells types has revealed how TGF-β signaling can elicit cell-type specific responses. ChIP-seq of Smad1/5 in endothelial cells (ECs) and pulmonary arterial smooth muscle cells (PASMCs) identified binding sites within enhancer regions of target genes and was associated with the upregulation of target gene expression (Morikawa et al., 2011). Approximately 20% of Smad1/5 binding sites overlapped between ECs and PASMCs and differences in the binding patterning between the two cell types were proposed to be determined by differences in chromatin accessibility. Genome-wide mapping of Smad3 binding sites in embryonic stem cells (ESCs), myotubes, and pro-B cells identified that unique association with transcription factors directed cell-type specific binding (Mullen et al., 2011). Smad3 interacts with Oct4 in ESCs, Myod1 in Myotubes, and PU.1 in pro-B cells. Ectopic expression of Myod1 in ESCs redirected Smad3 to new sites occupied by Myod1, highlighting the importance of interaction with cofactors for Smads targeting of specific DNA sequences.

1.3.2 Smad association with cofactors

Interaction with additional DNA binding transcription factors is crucial for Smads to increase their affinity and specificity for target gene regulatory

sequence. The cooperation between Smads with other transcription factors allows Smads to have relatively low DNA binding sequence specificity, binding only 3 or 4 base pairs, while achieving specific responses to a wide range of signals. The first Smad-interacting transcription factor identified is Foxh1 in Xenopus (Chen et al., 1996). Foxh1 is required for the Smad2-Smad4 complex binding of the activin-response element of the Nodal target gene *mix.2*. Zebrafish and Xenopus embryos deficient for Foxh1 display a reduction in Nodal signaling and loss of the organizer and axial mesendoderm structures (Sirotkin et al., 2000; Slagle et al., 2011). However, the Foxh1 loss of function phenotype in zebrafish is less serve than the Nodal mutant phenotype suggesting additional Smad2 interacting cofactors (Kunwar et al., 2003). Cofactor association has also been found to induce transcriptional repression. Smad3 was found to form a complex with Snail1 to inhibit expression of genes driving the epithelial-to-mesenchymal transition in breast epithelial cells (Vincent et al., 2009).

While many cofactors of Smad2/3 have been identified, only a few endogenous interactions between BMP responsive Smads and cofactors have been identified *in vivo*. The Smad1 homolog in Drosophila, Mad interacts with the transcriptional repressor Schnurri (Arora et al., 1995). The Mad-Schnurri complex binds to a well characterized site (GGCGCC-AN_4-GNCV) to repress *brinker* expression (Pyrowolakis et al., 2004). The Schnurri homlog in vertebrates was found to have an activating role in transcriptional regulation with BMP activated Smads (Yao et al., 2006). Another transcription factor that interacts with BMP

activated Smads is Oct4. ChIP-seq of Smad1 in mouse ESCs has uncovered the Oct4 sequence-binding motif enriched in Smad1 binding sites and depletion of Oct4 led to reduced Smad1 binding (Morikawa et al., 2011). Maternal-zygotic mutants for the zebrafish homolog of Oct4, Pou5f3 have DV patterning defects and lack *p63* expression, a BMP target gene (Belting et al., 2011). This suggests that pSmad1/5 and Oct4/Pou5f3 may cooperate to induce ventral gene expression during DV patterning. Similarly, cooperativity between Smad5 and Sox5 was found to be required for neural crest specification and *msx1* expression in Xenopus (Nordin and LaBonne, 2014).

1.3.3 Chromatin remodeling by Smads

In addition to sequence-specific DNA-binding transcription factors, Smad proteins have been found to interact with coregulators that can modify chromatin structure. Smad1, 3, and 4 bind to the histone acetyl transferase (HAT) p300 (Feng et al., 1998; Pouponnot et al., 1998). HATs activate transcription by acetylating specific lysine residues on histones (Ogryzko et al., 1996). Interestingly, association of p300 is essential for Smad2-mediated transcription, and this suggests that chromatin remodeling is required for Smad transcriptional activation (Hill, 2016; Ross et al., 2006). Both Smad1/5 and Smad2/3 can recruit histone demethylase, KDM6B to remove the repressive mark histone H3 lysine-27 trimethylation (H3K27me3) in mESCs (Akizu et al., 2010; Dahle et al., 2010). Recruitment of the histone demethylase by Smad1/5 and Smad2/3 results in a loss of H3K27me3 at the Noggin and Nodal promoters, respectively, thereby

counteracting Polycomb repression. Smads repress transcription via recruitment of transcriptional corepressors that remove activating histone acetylation or induce repressive histone marks. Smad proteins can recruit the histone deacetylases (HDACs) directly, such as Smad3 recruitment of HDAC4/5 (Kang et al., 2005), or indirectly through other corepressors (Wotton et al., 1999).

1.4 Mechanisms of BMP morphogen gradient interpretation

Understanding how graded morphogen signaling is transformed into gene expression programs is essential to determine how these signals correctly pattern cell specification during development. The mechanism of gene regulation by a morphogen must translate small differences in morphogen signaling into discrete changes in gene expression. The patterning of gene expression in time and space depends on how the graded information is interpreted. Different morphogen gradients have been proposed to be translated by: i) the steady state amount of morphogen signaling, ii) the steepness of the gradient, or iii) the total amount of signaling a cell is exposed to over time. Here we explore how gradients of BMP signaling are interpreted to pattern gene expression within developing tissues.

1.4.1 Concentration-dependent gene regulation

The first extracellular signaling molecule found to behave as a morphogen was the TGF-β family member, Activin (Green and Smith, 1990). Disassociated cells from the animal cap of Xenopus embryos responded in a concentration-dependent manner to Activin. Different doses of Activin were found to induce five

different cell states in Xenopus explants within 2 hours of exposure (Green et al., 1992; Gurdon et al., 1995). Xenopus cells express low (*Xbra*) and high threshold (*Xgsc*) target genes in response to absolute receptor occupancy, 100 and 300 receptors per cell, respectively, and the response does not depend on the ratio of bound to unbound receptors (Dyson and Gurdon, 1998). Similarly, Xenopus animal cap explants were found to respond to BMP4 in a concentration-dependent manner (Wilson et al., 1997). Different concentrations of Smad1 were able to recapitulate the graded activity of BMP4. The BMP Drosophila homolog, Decapentaplegic (Dpp) gradient specifies three thresholds of gene expression in the dorsal ectoderm (Ashe et al., 2000). Modulating the gene dose of *dpp* alters the position of target gene expression.

Recent development of human and mouse *in vitro* stem cell models has allowed for the study of morphogen patterning within simplified mammalian systems. Incubation of mouse and human stem cells grown in circular colonies with BMP4 for 42 hours results in the discrete radial patterning of markers associated with the three germ layers (Morgani et al., 2018; Warmflash et al., 2014). Although BMP4 is added uniformly to the micropatterned colonies, expression of Noggin at the center of the colony is thought to form the BMP signaling activity gradient. The response of micropatterned colonies of human embryonic stem cells to BMP4 was concentration dependent, while the response to Nodal depended on the rate of concentration change (Heemskerk et al., 2019). BMP4 was also able to specify two cell fates within the dorsal telencephalic

midline at different concentrations in mouse embryonic stem cells (Watanabe et al., 2016).

Differences in transcription factor binding site affinity at the regulatory region of target genes have been proposed to underly concentration-dependent transcriptional regulation (Ashe and Briscoe, 2006). In this model, low threshold target genes would be regulated by high affinity cis-regulatory elements, while high threshold targets regulated by lower affinity elements **(Figure 1.4A)**. Consistent with this model, the enhancer for a high threshold Dpp target gene *Race* contains a low affinity binding site for Mad (Wharton et al., 2004). Increasing the affinity of the Mad binding sites in the *Race* enhancer increases the expression domain, essentially lowering the threshold required for expression.

However, differences in DNA-binding affinities alone cannot predict expression domains patterned by other morphogens, such as Bicoid (Ochoa-Espinosa et al., 2005). Furthermore, a subset of target genes remain correctly positioned even when the Bicoid gradient is flattened (Ochoa-Espinosa et al., 2009). Reading out of concentration thresholds has also been found to depend on chromatin accessibility and Bcd-mediated chromatin remodeling (Hannon et al., 2017). High threshold target genes are inaccessible to low levels of Bcd at the posterior nuclei **(Figure 1.4B)**. Proper positioning of target gene expression by Bcd has been found to rely on the integration of repressive signaling inputs in

combination with binding site affinity (Dunipace et al., 2011; Löhr et al., 2009; Reeves and Stathopoulos, 2009) **(Figure 1.4C)**.

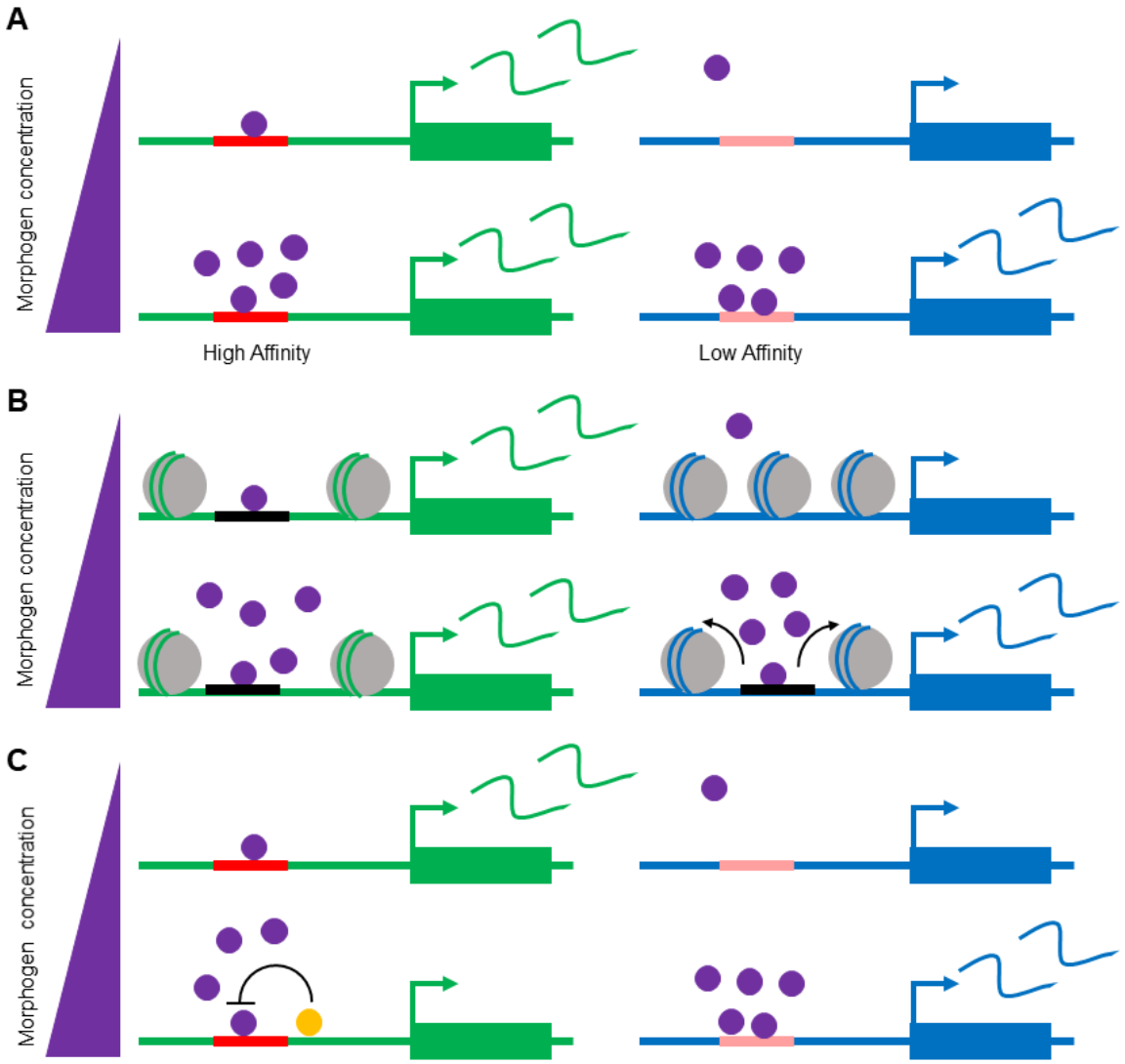

Figure 1.4 Mechanisms of concentration-dependent gene expression. (A) Target genes have different binding site affinity for the transcriptional effector within the cis-regulatory element. Target genes that can be activated by low levels of a morphogen contain high affinity elements. Genes that require high levels of signal have low affinity elements. (B) Target genes activated by different morphogen levels have different chromatin confirmation. Genes activated by lower levels of signal have more accessible binding sites than high threshold genes. High levels of morphogen may open chromatin directly or through recruitment of chromatin modifying enzymes. (C) Repressive interactions with other inputs can establish discrete expression domains.

Recently, spatially distinct BMP target genes in the Drosophila embryo have been found to have different transcriptional bursting frequencies (Hoppe et al., 2020). The transcriptional bursts for a high threshold target gene *hnt* were more frequent and shorter than the transcriptional bursts of a lower threshold target gene *ush*. The differences in burst frequency were modulated by differences in k_{on} of the enhancer. Low levels of BMP signaling activity are unable to maintain an active promoter state for *hnt* and result in the narrower domain of expression. Differences in transcriptional burst kinetics are an exciting mechanism that may underlie concentration-dependent gene regulation within other systems and for other morphogens.

1.4.2 Temporal signal integration

Studies of morphogen interpretation have increasingly found signal duration playing a role in target gene patterning (Economou and Hill, 2020). Sonic Hedgehog (Shh) is one of the best studied morphogens that encodes positional information based on signal duration in specifying the digit identities in the limb bud and DV patterning of the chick neural tube (Dessaud et al., 2007; Harfe et al., 2004). In the neural tube, Shh is produced at the ventral midline and specifies the ventral neural progenitor domains: the p3 domain marked by Nkx2.2, pMN domain marked by Olig2, and the p2 domain marked by Pax6 (Briscoe and Small, 2015). However, the neural progenitor domains do not correlate with absolute concentration of Gli activity, the downstream effector of Shh (Balaskas et al., 2012). Instead, the progenitor domains are established

sequentially with “high threshold” domains requiring longer durations of signaling (Dessaud et al., 2007).

Cells in the neural tube become progressively “desensitized” to Shh signaling over time after extended signal exposure (Ribes et al., 2010). The desensitization of cells to Shh occurs through negative feedback via the upregulation of the receptor Patched (Ptc) which inhibits signaling (Marigo and Tabin, 1996). At the onset of patterning, cells closest to the source remain sensitive to Shh signaling and can immediately activate *olig2* expression, the motor neuron marker. However, these cells cannot express the interneuron maker *nkx2.2* because its expression is inhibited by Pax6. Over time Olig2 accumulates and in turn represses *pax6* expression removing the *nkx2.2* inhibition, but due to the temporal adaptation, cells are less sensitive to Shh and require higher levels of signal to induce *nkx2.2* expression (Dessaud et al., 2010). Thus the temporal adaption in combination with a gene regulatory network allows cells to integrate Shh signaling level and duration to pattern the neural tube (Balaskas et al., 2012; Zagorski et al., 2017).

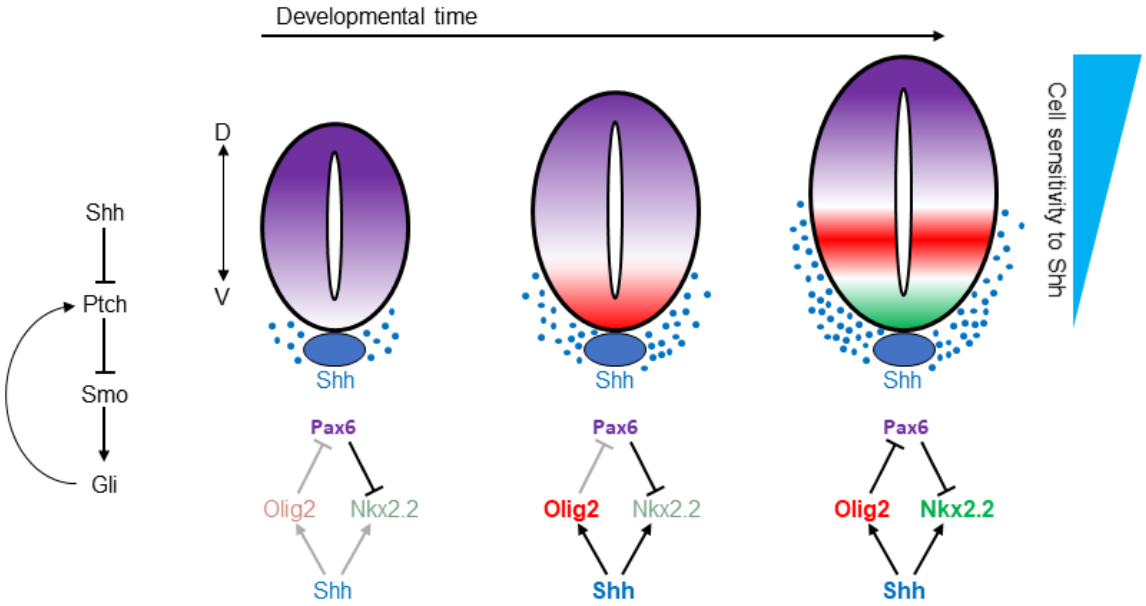

Figure 1.5 Duration-dependent patterning of the neural tube by Shh. Binding of the Shh ligand to the transmembrane receptor Ptch relieves repression of another transmembrane protein Smo. De-repression of Smo initiates the signal transduction that activates the transcriptional effector Gli which regulates transcription activity. Shh activates Ptch expression generating a negative feedback loop. Shh is produced from the floor plate at the ventral side of the neural tube (NT) forming a ventral to dorsal gradient. At the onset of patterning, Pax6 is expressed across the entire NT. As the gradient increases over time, cells closest to the source of Shh express *olig2*, but are unable to express *nkx2.2* due to inhibition by Pax6. Olig2 then negatively regulates *pax6* expression, releasing repression of *nkx2.2*. Because of the negative feedback loop of Ptch activation by Shh, cells closest to the source become desensitized to Shh signaling over time. Therefore, higher levels of Shh signaling are required to activate expression of *nkx2.2*.

Mechanisms other than gene regulatory networks have been found to underlie duration-dependent patterning. Differences in the transcriptional kinetics of target gene induction by Nodal signaling have been proposed to pattern gene expression in the zebrafish embryo (Dubrulle et al., 2015). Distinct levels of nuclear Smad2 did not correlate with the boundaries of target gene expression. Instead, exposing cells to high levels of Nodal signaling for 1 hour was sufficient to activate the expression of a long-range gene *ntl*, but insufficient for expression

of the short-range gene *gsc*. The expression of *gsc* requires 2 hours of Nodal exposure and the difference in the signal duration requirement could be explained by differences in the transcription rate of the two genes.

Differences in signal duration have been proposed to pattern BMP target genes. In chick ectodermal explants, BMP signaling is required for olfactory and lens placodal cell differentiation (Sjödal et al., 2007). Different concentration of BMP4 (10-50 ng/ml) did not affect the relative proportion of these cell types specified. However, markers for olfactory placodal cells are expressed after 12-15 hours of BMP4 exposure, while lens cell markers require 30 hours of BMP4 exposure. Differences in BMP signal duration (1 and 24 hours) has also been found to specify different dorsal interneuron subtypes in chick explants (Tozer et al., 2013) and mouse spinal organoids (Duval et al., 2019). While the mechanisms of how genes respond to different durations of BMP signaling are currently not known, because of the prolonged patterning, it is speculated that a transcriptional network downstream of BMP underlies the duration-dependent morphogen interpretation in the neural tube (Tozer et al., 2013).

1.4.3 Temporal signaling windows

Studies of BMP-mediated patterning have revealed that in addition to the importance of signal duration, the timing of when cells are exposed to morphogen signal is also essential. In the zebrafish embryo, cells are exposed to a gradient of BMP signaling from mid-blastula stages and throughout gastrula stages and beyond, from 4 to 12 hours post fertilization (hpf) (Tucker et al.,

2008). However, BMP signaling before the onset of gastrulation at 6 hpf and after mid-gastrulation at 8 hpf is not required for DV patterning of the head and anterior trunk. Reinitiating expression of Alk8, a BMP receptor, in a maternal-zygtoic Alk8 mutant using a heat-shock transgene at 6 hpf, completely rescued patterning. Loss of BMP signaling after 8 hpf caused dorsalization that was restricted to the tail, and embryos are completely wild-type when BMP signaling is inhibited after 12 hpf. Together, these data show that head and trunk axial tissues are patterned within a 2-hour window from 6 to 8 hpf. Critical temporal windows of competency to BMP signaling during patterning were also found in the neural tube. A marker for the dorsal interneuron domain dP1, Ath1 requires 24 hours of BMP signaling for expression at both low (2 ng/ml) or high (8 ng/ml) levels of BMP4 (Tozer et al., 2013). Explants that were grown in media for 24 hours before BMP was added expressed Ath1 6 hours earlier. This may suggest that cells are not competent to respond to BMP signaling until a later window of time.

1.4.4 Determining the mechanism of BMP signal interpretation that patterns the DV axis of the zebrafish embryo

How the gradient of BMP signaling is interpreted during DV axial patterning has not been studied in vertebrates. The zebrafish embryo is an amenable genetic model to study DV axial patterning. BMP has additional functions in earlier embryonic stages of mouse development making the study of BMP signaling in DV patterning challenging. The development of a novel

quantitative imaging assay by the Mullins lab has enabled refined measurements of spatially graded pSmad5 levels across the entire zebrafish embryo at a single cell resolution (Zinski et al., 2017; Zinski et al., 2019). This assay allows us to investigate how the pSmad5 gradient patterns gene expression domains that will give rise to different ventral cell fates. Gradients of BMP signaling have been proposed to pattern gene expression by different mechanisms in different contexts. Differences in BMP signal concentration (Heemskerk et al., 2019; Watanabe et al., 2016), signal duration (Tozer et al., 2013), gradient slope (Rogulja and Irvine, 2005) have been suggested to provide positional information during tissue patterning. The focus of this dissertation is to distinguish between these different models of BMP morphogen interpretation during DV axial patterning. By modulating the BMP gradient slope, signaling duration, and signaling level within the embryo, we can decipher how cells interpret the BMP gradient to activate expression of target genes and pattern the DV axis.

CHAPTER 2: BMP signaling gradient interpreted through concentration thresholds in dorsal-ventral axial patterning

The contents of this chapter have been submitted for publication as:

Greenfeld H, Lin J, Mullins MC. 2020. BMP signaling gradient interpreted through concentration thresholds in dorsal-ventral axial patterning.

Summary

Bone Morphogenetic Protein (BMP) patterns the dorsoventral (DV) embryonic axis in all vertebrates, but it is unknown how cells along the DV axis interpret and translate the gradient of BMP signaling into differential gene activation to specify distinct cell fates. To determine the mechanism of BMP morphogen interpretation in the zebrafish gastrula, we identified 57 genes that are directly activated by BMP signaling. By using Seurat analysis of single-cell RNA-seq data, we found that these genes are expressed in at least three distinct DV domains of the embryo. We distinguished between three models of BMP signal interpretation in which cells activate distinct gene expression through interpretation of thresholds of: 1. the BMP signaling gradient slope, 2. BMP signal duration, or 3. the level of BMP signal activation. We tested these three models using quantitative measurements of phospho-Smad5 and by examining the spatial relationship between BMP signaling and activation of different target genes at single cell resolution across the embryo. We found that BMP signaling gradient slope or BMP exposure duration did not account for the differential target gene expression domains. Instead we show that cells respond to three distinct levels of BMP signaling activity to activate and position target gene expression. Together, we demonstrate that distinct phospho-Smad5 threshold levels activate spatially-distinct target genes to pattern the DV axis.

2.1 Introduction

During embryonic patterning, the molecular identity of unspecified cells is determined by the location of each cell within the embryo (Wolpert, 1969). Thereby, a cell's position becomes translated into a specific cell fate. This positional information is provided by gradients of secreted signaling molecules called morphogens, which induce the specification of multiple cell fates (Ashe and Briscoe, 2006; Briscoe and Small, 2015; Rogers and Schier, 2011; Sagner and Briscoe, 2017). The genetic programs underlying different cell fates are activated in distinct regions of tissue within the morphogen gradient. The proper position of gene expression boundaries is essential during development because these domains determine the differentiation and relative abundance of distinct cell types. A fundamental question in developmental biology is how a graded morphogen signal is translated into discrete gene expression domains to specify cell fate.

Multiple mechanisms have been proposed for how morphogen gradients provide positional information to pattern a tissue. Cells in different positions along the gradient may respond to: 1) different signaling concentrations, 2) different lengths of signal exposure, or 3) different spatial slopes of the signaling gradient. There is evidence that cells can read out each of these aspects of a morphogen gradient to activate different genes in different contexts. For example, the Bicoid transcription factor morphogen gradient activates target genes through different concentration thresholds to pattern the anterior-posterior (AP) axis of *Drosophila*

(Hannon et al., 2017; Huang et al., 2017). In contrast, the duration of Sonic Hedgehog (Shh) ligand exposure has been shown to pattern gene expression in the vertebrate neural tube and in the limb bud (Dessaud et al., 2007; Harfe et al., 2004). There is conflicting evidence for the mechanism of Bone Morphogenetic Protein (BMP) morphogen interpretation. Both the duration of BMP signaling (Tozer et al., 2013) and different BMP ligands (Andrews et al., 2017) have been suggested as mechanisms responsible for establishing dorsal interneuron identities in the neural tube, while BMP has been shown to pattern gene expression in a concentration-dependent manner in human and mouse embryonic stem cells (Heemskerk et al., 2019; Watanabe et al., 2016). While in *Drosophila*, there is evidence that cells read out the spatial slope of the Dpp (the BMP homolog) gradient to regulate cell proliferation in the imaginal wing disc (Rogulja and Irvine, 2005). Dpp signaling was shown to regulate the activity of the intercellular Fat signaling pathway, allowing cells to sense differences in signaling activity between neighboring cells (Rogulja et al., 2008).

A BMP morphogen signaling gradient is required early in embryonic development to pattern the dorsal-ventral (DV) embryonic axis in vertebrates and invertebrates (Bier and De Robertis, 2015; Tuazon and Mullins, 2015; Zinski et al., 2018). Despite its fundamental role to pattern tissues along the DV axis in all metazoans, the mechanism by which the BMP signaling gradient is interpreted into positional information and multiple cell fates along the axis is not known. In zebrafish, loss of BMP signaling eliminates epidermis, placodes, neural crest,

and ventral mesendoderm and leads to a massive expansion of neural tissues (Mullins et al., 1996; Nguyen et al., 1998; Schmid et al., 2000). A gradient of BMP2/7 signaling activity across the embryo forms during gastrulation, with the highest level of signaling ventrally and the lowest levels dorsally (Tucker et al., 2008; Zinski et al., 2017). This signaling gradient is transduced through a heterotetrameric receptor complex that phosphorylates and activates the transcription factor, Smad5 (Little and Mullins, 2009). BMP signaling activity is thus interpreted by cells through nuclear accumulation of phosphorylated Smad5 (pSmad5) to specify different ventral cell fates (Kramer et al., 2002). pSmad5 in complex with co-Smad4 in turn activates gene expression (Massague et al., 2005; Schmierer and Hill, 2007).

Changing the level of BMP signaling across the embryo shifts the position and relative proportion of ventral cell fates, demonstrating that the gradient shape is important for patterning (Neave et al., 1997; Nguyen et al., 1998; Nguyen et al., 2000; Schumacher et al., 2011; Tribulo et al., 2003; Wagner and Mullins, 2002). The shape of the BMP signaling gradient depends on the extracellular antagonist Chordin, which binds the BMP ligand and blocks signaling in the dorsal region of the embryo (Piccolo et al., 1996; Schumacher et al., 2011; Troilo et al., 2014; Tuazon et al., 2020; Zinski et al., 2017). The BMP signaling gradient is dynamic during late-blastula to mid-gastrula stages, thus pSmad5 nuclear levels differ across the embryo both in space and time (Tucker et al., 2008; Zinski et al., 2017). However, it remains unknown if gradient shape or gradient

dynamics play a role in positioning gene expression domains that specify ventral cell fates along the DV axis.

Here we investigated the mechanism by which BMP signaling provides positional information to cells across the DV embryonic axis. We identified greater than 50 genes that directly read out the BMP signaling gradient to specify distinct ventral-lateral cell fates along the DV axis. We tested three prominent mechanisms of morphogen gradient interpretation: interpretation by signaling gradient slope, by BMP signal duration, and by signaling gradient concentration thresholds. By using quantitative measurements of pSmad5 in all nuclei of the embryo to investigate the spatial relationship between BMP signaling activity levels and the activation of different target genes, we eliminated BMP gradient slope and BMP signal duration as mechanisms positioning target gene expression. We determined that cells respond to at least three distinct levels of pSmad5 to activate different target genes, and these threshold levels of pSmad5 can precisely position gene expression boundaries in the embryo.

2.2 Results

2.2.1 Identification of target genes directly patterned by the BMP gradient

BMP signaling is essential for ventral tissue specification, but it remains unknown how graded BMP signaling is interpreted by cells of the embryo to generate the distinct gene expression domains that pattern the DV axis. Only a limited number of genes directly regulated by BMP signaling have been identified

in the zebrafish gastrula. To identify the genes responding to the BMP gradient, we determined which genes are directly activated by pSmad5 from all BMP-dependent gene expression during gastrulation. BMP-dependent gene expression was determined by performing RNA-sequencing (RNA-seq) on wild-type and *bmp7* mutant embryos (*bmp7a*^{sb1aub}) at two time points when the BMP signaling gradient patterns ventral tissues: early- (shield) and mid-gastrula (70% epiboly) stages (Hashiguchi and Mullins, 2013; Kwon et al., 2010; Tucker et al., 2008). All ventral tissue specification is absent in *bmp7* mutants and activation of Smad5 is abolished **(Figure 2.1A and 2.2A-B)** (Dick et al., 2000; Nguyen et al., 1998; Schmid et al., 2000). We identified 1559 genes that were differentially expressed (FDR < 0.05) in *bmp7* mutant compared to wild-type embryos at an early-gastrula stage **(Figure 2.2C)** and 852 genes that were differentially expressed at mid-gastrulation. **(Figure 2.1B)**. Most differentially-expressed genes were downregulated in *bmp7* mutants compared to wild-type embryos at both early- and mid-gastrula stages, including many known markers of ventral tissues reflecting a loss of ventral cell fates **(Figure 2.1B and 2.2C)**.

To identify the subset of BMP-dependent genes that are directly regulated by BMP signaling, we treated *bmp7* mutant embryos at 4 hours post fertilization (hpf) with cycloheximide (CHX), a translation inhibitor, and then injected BMP2/7 recombinant protein into the intercellular space of the blastula **(Figure 2.1C)**. First, we chose 4 hpf because the zygotic genome has been activated by this timepoint (Lee et al., 2013; Schier and Talbot, 2005; Vastenhouw et al., 2010),

but the DV axis has yet to be patterned and all cells of the embryo remain competent to respond to BMP signaling (Tucker et al., 2008). Second, translation was inhibited with CHX to prevent the expression of secondary targets but not direct targets of BMP signaling. Finally, embryos were injected with BMP2/7 protein to activate BMP signaling and induce robust phosphorylation of Smad5 in *bmp7* mutant embryos **(Figure 2.1D)**.

Total RNA was isolated 1.5 hours post injection from *bmp7* mutant embryos treated with CHX with or without BMP2/7 protein injection for RNA-seq analysis. We identified 363 genes that were differentially expressed (FDR < 0.05) in embryos injected with BMP2/7 protein **(Figure 2.1E)**. In BMP2/7 injected and CHX treated embryos, a known direct target of BMP signaling, *foxi1* (Hans et al., 2007), was confirmed to be expressed by *in situ* hybridization 1.5 hours after injection **(Figure 2.2D)**. We compared the 274 genes that were upregulated by BMP signaling after CHX treatment to the genes that were BMP-dependent during gastrulation. We found 57 genes that are both directly upregulated by BMP signaling and endogenously expressed during gastrulation when ventral tissues are specified **(Table 1)**. Gene Ontology (GO) analysis of the 57 target genes found enrichment of terms for cell fate specification and tissue differentiation **(Figure 2.1F)**. The BMP target genes were also enriched for GO terms for DNA-binding transcription factor activity **(Figure 2.2E)**, which together are consistent with roles in specifying ventral cell fates. Fifteen genes were found to be both downregulated by BMP signaling after CHX treatment and

downregulated in wild-type embryos compared to *bmp7* mutants indicating that pSmad5 can directly inhibit gene expression **(Table 2)**. There is evidence that BMP-activated Smad transcription factors directly repress transcription via recruitment of repressors and chromatin modifiers (Blitz and Cho, 2009; Pyrowolakis et al., 2004; Stevens et al., 2017). Ten of these downregulated target genes are known to be expressed within dorsal ectodermal tissue, which is consistent with a role in direct downregulation by BMP signaling (Cechmanek and McFarlane, 2017; Ceinos et al., 2013; Goudevenou et al., 2011; Lee et al., 2014; Lyons et al., 2010; Rinner et al., 2005; Sarmah and Wente, 2010; Webb et al., 2011; Yamakawa et al., 2018; Zinski et al., 2017). Thus, we identified genes that directly read out the BMP signaling gradient to initiate the genetic cascade that specifies different ventral cell fates (Bhat et al., 2013; Hans et al., 2007; Kwon et al., 2010; Mills et al., 1999; Santos-Pereira et al., 2019). We now have a comprehensive list of genes directly responding to the BMP gradient during DV patterning.

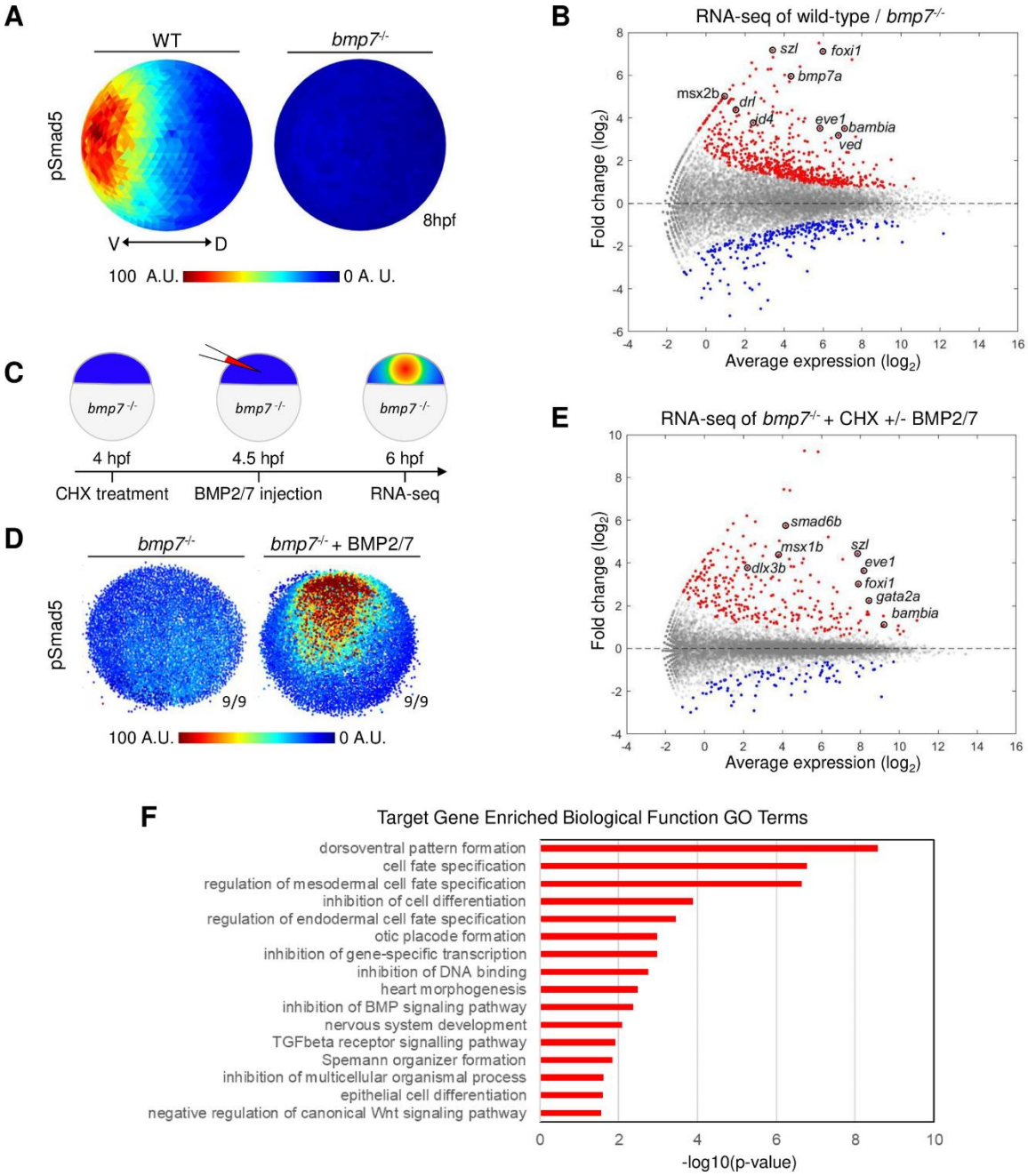

Figure 2.1 Direct targets of BMP signaling in DV axial patterning (A) Animal view, dorsal to right of mean pSmad5 intensities at mid-gastrula stage (8 hpf) wild-type (n=4) and *bmp7* mutant (n=3) embryos. A.U. is arbitrary units. (B) Differential gene expression in wild-type and *bmp7* mutants at 8 hpf using RNA-seq. Significantly upregulated genes in wild-type compared to *bmp7* mutants are shown in red, significantly downregulated genes are shown in blue. All other genes shown in gray. A subset of known BMP-dependent genes is highlighted. (C) Schematic of method to isolate RNA for sequencing from cycloheximide (CHX) treated *bmp7* mutant embryos injected with BMP2/7 protein. (D)

Representative image of pSmad5 intensities of all nuclei of an individual *bmp7* mutant and *bmp7* mutant injected with 10 pg of BMP2/7 protein. Animal pole facing up. A.U. is arbitrary units. (E) Differential gene expression using RNA-seq of CHX-treated *bmp7* mutants versus CHX-treated *bmp7* mutants injected with BMP2/7 protein. Significantly upregulated genes with BMP2/7 protein injection are shown in red, significantly downregulated genes are shown in blue. All other genes are shown in gray. A subset of BMP direct target genes is highlighted. (F) Gene Ontology (GO) term analysis for biological processes of the 57 direct target genes.

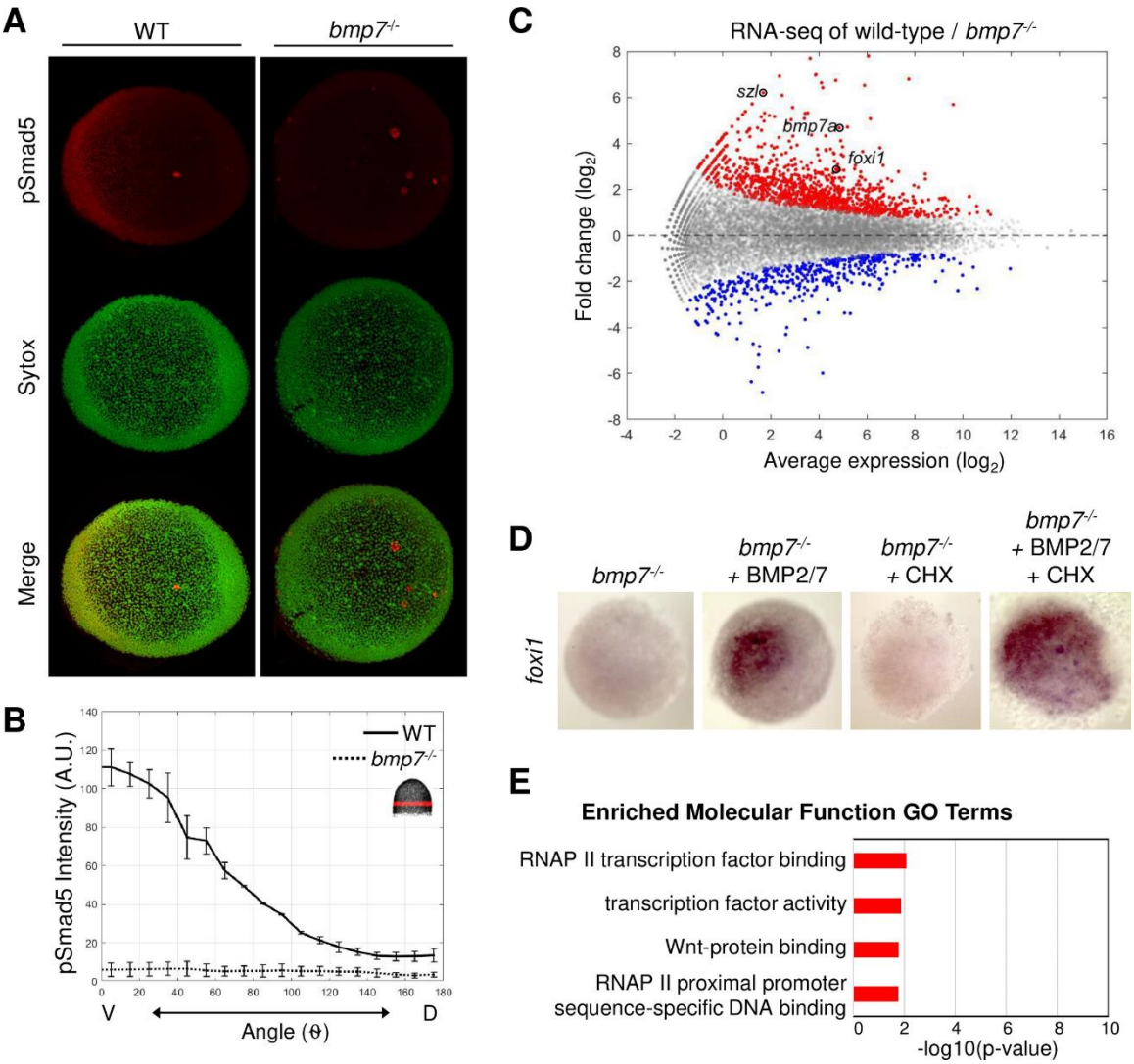

Figure 2.2 Identification of genes dependent on and directly regulated by BMP signaling Related to Figure 2.1. (A) Animal view of the maximum projection of pSmad5 immunofluorescence of a wild-type and *bmp7* mutant mid-gastrula stage (8 hpf) embryo. Nuclei are stained with Sytox Green. (B) Mean pSmad5 profiles of wild-type (n=4) (solid line) and *bmp7* mutants (n=3) (dotted

line) across the DV axis. Location of the 40 µm band of cells (red) that was averaged is indicated on the embryo in top right corner. A.U. is arbitrary units. (C) Differential gene expression of wild-type and *bmp7* mutants at early gastrulation (6 hpf) using RNA-seq. Significantly upregulated genes in wild-type compared to *bmp7* mutants shown in red; significantly downregulated genes shown in blue. All other genes shown in gray. A subset of known BMP-dependent genes is highlighted. (D) Animal view of *in situ hybridization* of *foxi1*, a known direct target of BMP signaling, in the conditions shown. CHX = cycloheximide. **(E)** Gene Ontology (GO) term analysis for molecular functions of the 57 direct target genes.

Table 1 BMP upregulated target genes. Related to Figure 2.1 and 2.2. List of names and RefSeq accession numbers of genes directly activated by BMP signaling during gastrulation, as well as the corresponding cluster number based on the Seurat predicted expression profile. Clusters 1, 2, 3 are genes with predicted ventrally enriched expression. Cluster 4 contains the genes with predicted uniform profiles or significant dorsal expression. NS indicates genes that were not sequenced in the Farrell et al., 2018 scRNA-seq dataset.

Gene	**Transcript**	**Cluster #**
dlx2a	NM_131311	1
smtnl1	NM_001013321	1
szl	NM_181663	1
tbx3a	NM_001101670	1
tp63	NM_152987	1
bmp4	NM_131342	2
foxi1	NM_181735	2
gata2a	NM_131233	2
smad6b	NM_001045051	2
smad7	NM_175082	2
smad9	NM_001328499	2
atp1b3a	NM_131221	3
bambia	NM_131784	3

crabp2b	NM_001320394	3
dlx3b	NM_131322	3
eve1	NM_131114	3
fam212ab	NM_199788	3
foxh1	NM_131502	3
id2a	NM_201291	3
klf2b	NM_131857	3
msx1a	NM_131273	3
msx3	NM_131272	3
smad6a	NM_001024810	3
tfap2c	NM_001008576	3
tle3a	NM_131012	3
tll1	NM_131010	3
ube2e2	NM_001003494	3
ved	NM_183074	3
vent	NM_131700	3
vox	NM_131698	3
cbx7a	NM_001017853	4
csad	NM_001007348	4
foxi3a	NM_198917	4
fzd4	NM_001305469	4
fzd5	NM_131134	4
hsd3b2	NM_212797	4
id3	NM_152967	4
id4	NM_001039990	4

lats1	NM_001020510	4
msx2b	NM_131276	4
mthfd1l	NM_001242996	4
nkd1	NM_001043333	4
nkx2.7	NM_131419	4
nrarpb	NM_181496	4
nudt4b	NM_001004648	4
pcdh18a	NM_001115058	4
ppp1r14c	NM_001029963	4
skilb	NM_001130669	4
wwtr1	NM_001037696	4
zfp36l1b	NM_199649	4
cdx1a	NM_212836	NS
dram1	NM_001006049	NS
kcnh6a	NM_212837	NS
neu4	NM_001020548	NS
si:ch211-107n13.1	NM_001082926	NS
slc14a2	NM_001020519	NS
tdrd7b	NM_001353929	NS

Table 2. BMP downregulated target genes. Related to Figure 2.1 and 2.2. List of names and RefSeq accession numbers of genes directly inhibited by BMP signaling during gastrulation, as well as the expression domain predicted by Seurat. NE indicates predicted expression is not enriched along the DV axis. NS indicates genes that were not sequenced in the Farrell et al., 2018 scRNA-seq dataset.

Gene	**Transcript**	**Predicted Domain**
chrd	NM_130973	dorsal
her11	NM_001003886	dorsal
sparc	NM_001001942	dorsal
st8sia1	NM_001327841	dorsal
zgc:113314	NM_001033753	dorsal
def6a	NM_201040	NE
grk7b	NM_001033090	NE
ip6k2a	NM_201470	NE
mhc1lia	NM_001327882	NE
pmela	NM_001045330	NE
si:ch211-133n4.4	NM_001077376	NE
cpa4	NM_001002217	NS
cyp2p9	NM_200620	NS
zgc:86896	NM_001002100	NS

2.2.2 Ventral BMP target genes are expressed in at least three distinct domains

Next, we determined where the genes reading out the BMP signaling gradient are expressed along the DV axis of the embryo. Target genes responding to different aspects of the gradient would be predicted to be expressed in different domains of the embryo. To sort the target genes based on their expression pattern, we analyzed a previously published single-cell RNA-seq (scRNA-seq) dataset of mid-gastrula zebrafish embryos using the Seurat method, which predicts the spatial position of individual cell transcriptomes (Farrell et al., 2018; Satija et al., 2015). Locations of single-cell transcriptomes were inferred by Seurat based on the co-expression of known landmark genes and mapped onto an embryonic grid that was divided into 64 bins: 8 bins across the DV axis and 8 bins across the AV (animal-vegetal) axis **(Figure 2.3D)**. The predicted expression patterns of the BMP direct target genes within the 64 bins across the embryo are shown as a heatmap **(Figure 2.3A-D, 2.4A-D)**. To visualize the predicted expression profiles across the DV axis, we summed expression in all bins within each of the 8 positions along the DV axis **(Figure 2.3A''-C'', 2.4A-D)**.

Genes were then clustered based on their predicted expression profiles across the DV axis. Fifty of the 57 upregulated target genes were found in the scRNA-seq dataset, and 27 genes showed predicted ventrally-restricted expression **(Figure 2.4A-C)**. These ventrally-restricted target genes were further sorted based on the bins where they were predicted to be expressed in across

the DV axis. Five genes had predicted expression enriched within the first 3 to 4 bins, 6 genes were predicted to be expressed within the first 5 bins, and 19 genes within the first 6 to 7 bins **(Figure 2.3D and 2.4A)**. Target genes with uniform expression or that also included dorsal expression were assumed to have multiple signaling inputs and excluded from our analysis **(Figure 2.4D) (Table 1)**. The downregulated target genes that were sequenced in the scRNA-seq dataset displayed either dorsal enrichment or were not enriched along the DV axis **(Figure 2.5) (Table 2)**. To further investigate how the pSmad5 gradient is interpreted into spatially-distinct gene expression domains, we focused on genes that are induced exclusively by BMP signaling. Some of the BMP target genes are known to have multiple signaling pathways contributing to the total expression pattern. For example, the expression of *eve1* is known to be activated by both BMP as well as by FGF signaling (Joly et al., 1993; Kudoh et al., 2004; Pyati et al., 2005). Similarly, we also avoided examining genes that have significant expression remaining in *bmp7* mutant embryos **(Table 1)**.

investigate how the gradient of BMP signaling directs target gene expression: *sizzled* in cluster 1, *foxi1* in cluster 2, and *bambia* in cluster 3. To validate the predicted expression patterns of the three target genes, we performed fluorescent *in situ* hybridization (FISH) for each gene on early-gastrula (7 hpf) wild-type embryos **(Figure 2.6A)**, when the BMP gradient is patterning ventral fates (Kwon et al., 2010; Tucker et al., 2008). Each embryo was subdivided into 128 bins equally spaced across the AV and DV axes **(Figure**

2.6B). Expression intensity for each lateral half of the embryo was averaged into 64 bins, normalized, and displayed similarly as the Seurat heatmap **(Figure 2.3A'-C')**. The measured and predicted expression profiles of the three target genes are similar across the DV axis **(Figure 2.3A''-C'')** validating this approach for examining the DV expression domain. While Seurat accurately predicted differences in expression patterns of the three genes across the DV axis, *sizzled* and *bambia* were incorrectly predicted to be uniformly expressed along the AV axis. Using the quantified FISH for these target genes and other landmark genes will improve accuracy of Seurat's predicted expression pattern across the AV axis of the embryo.

To more precisely determine where the three target genes are expressed across the DV axis, we quantified the FISH expression intensity **(Figure 2.3E-G, 2.6A)**. The expression of *sizzled*, *foxi1*, and *bambia* was quantified around the DV axis of the embryo at the AV location of highest intensity **(Figure 2.6C-E)**. While *sizzled* and *bambia* are expressed more broadly along the AV axis, *foxi1* is a marker for non-neural ectoderm and only expressed in an animal-ventral domain of the embryo (Kwon et al., 2010). We measured target gene expression boundaries in individual embryos **(Figure 2.6C-E)**. We found that the boundaries of the target genes are located in distinct positions along the DV axis **(Figure 2.3H-J)**, with each target gene expressed in a significantly different domain of the embryo **(Figure 2.3K)**. These results together with the Seurat analysis of 27

direct target genes indicate that the BMP signaling gradient can pattern the embryo into at least three distinct gene expression domains.

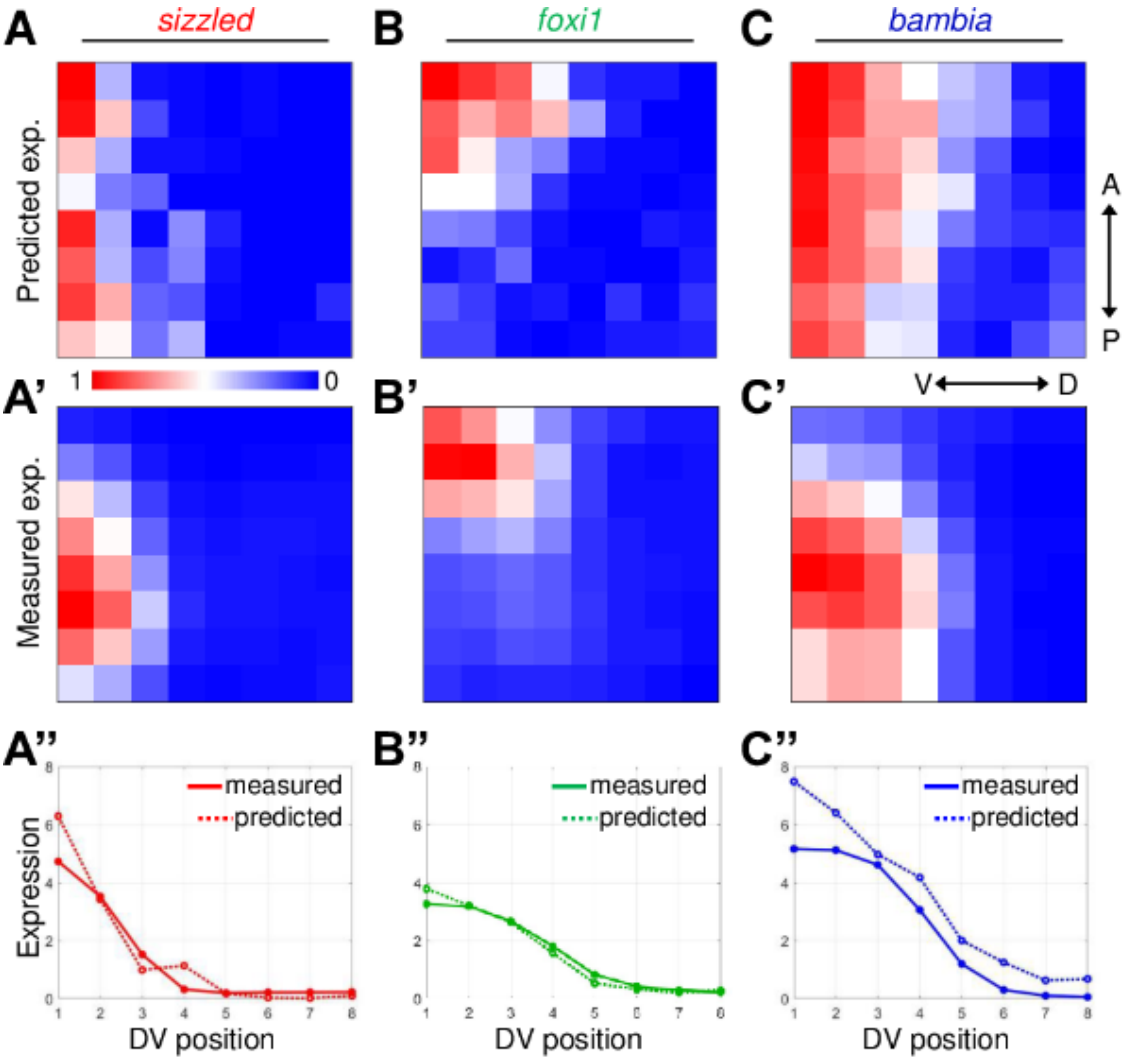

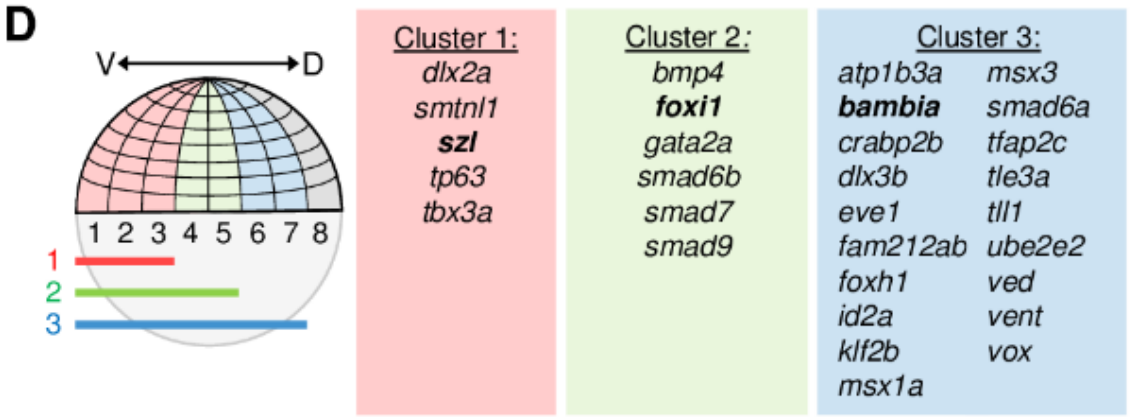

Cluster 1:	Cluster 2:	Cluster 3:	
dlx2a	*bmp4*	*atp1b3a*	*msx3*
smtnl1	***foxi1***	***bambia***	*smad6a*
szl	*gata2a*	*crabp2b*	*tfap2c*
tp63	*smad6b*	*dlx3b*	*tle3a*
tbx3a	*smad7*	*eve1*	*tll1*
	smad9	*fam212ab*	*ube2e2*
		foxh1	*ved*
		id2a	*vent*
		klf2b	*vox*
		msx1a	

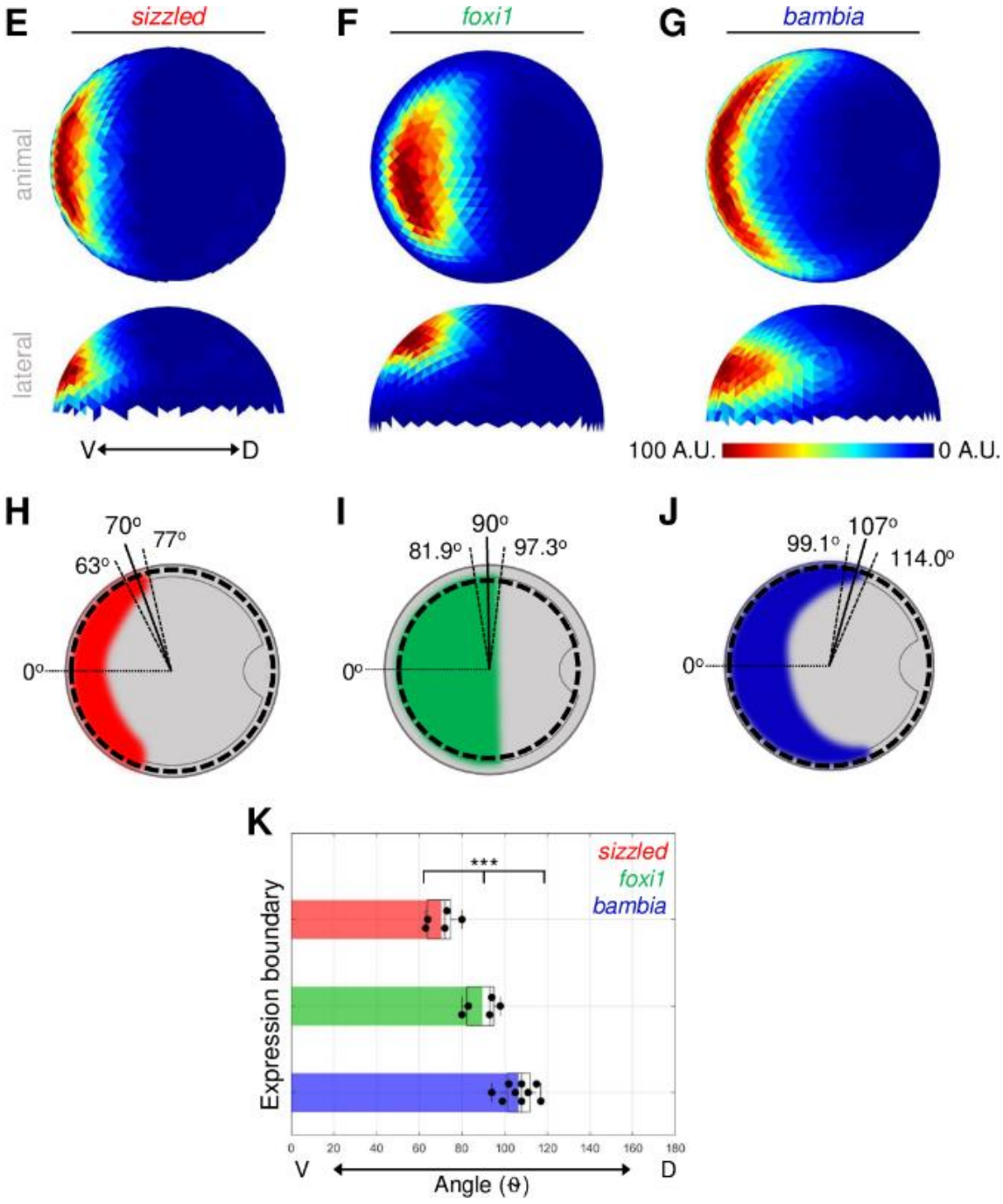

Figure 2.3 Three distinct expression domains of BMP direct target genes
(A-C) Heat map of gene expression patterns from Seurat analysis of mid-gastrula (8 hpf) scRNA-seq dataset. Predicted expression normalized across all bins of *sizzled* (A), *foxi1* (B), and *bambia* (C). (A'-C') Average fluorescent *in situ* hybridization intensity measured in early-gastrula (7 hpf) wild-type embryos divided into 64 equally-spaced bins. (A''-C'') Measured and Seurat predicted

expression profiles across the DV axis. Each point is the sum of the expression intensity from all bins at one DV position. (D) Schematic of embryonic grid divided into 64 bins and the three nested expression domains. Table of 27 ventrally-expressed target genes divided into three clusters based on their Seurat expression profiles. (E-G) Animal and lateral views of average fluorescent *in situ* hybridization signal in wild-type embryos at early-gastrula (7 hpf) of *sizzled* (n=5) (E), *foxi1* (n=5) (F), and *bambia* (n=9) (G). A.U. is arbitrary units. (H-J) Schematic of animal view (dorsal to right) of expression domains in early gastrula embryos of *sizzled* (H), *foxi1* (I), and *bambia* (J). The mean (solid line) and standard deviation (dotted lines) of expression boundaries shown as degrees across the DV axis. Position of domain boundary measured from the average intensity from a 40 µm band of cells across the DV axis at the location indicated by the dotted circle. (K) DV position of the expression boundaries of individual wild-type embryos. ***$P < 0.001$ in comparing three expression domains using one-way ANOVA.

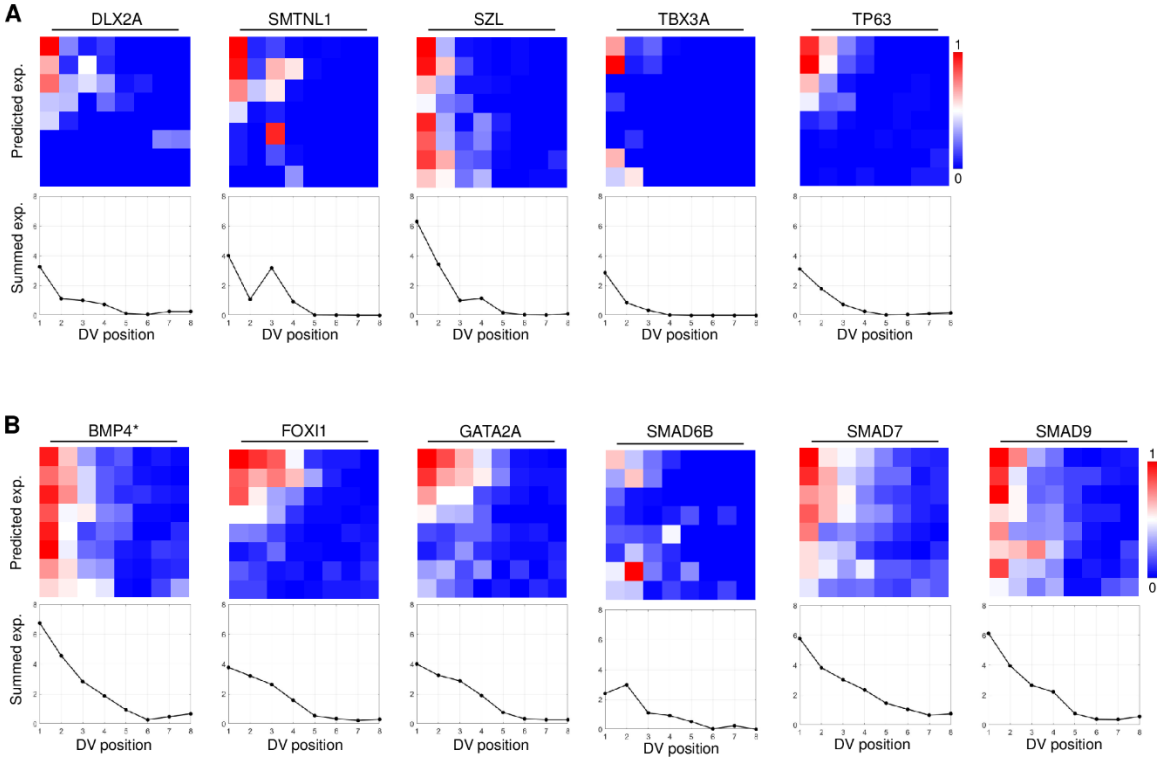

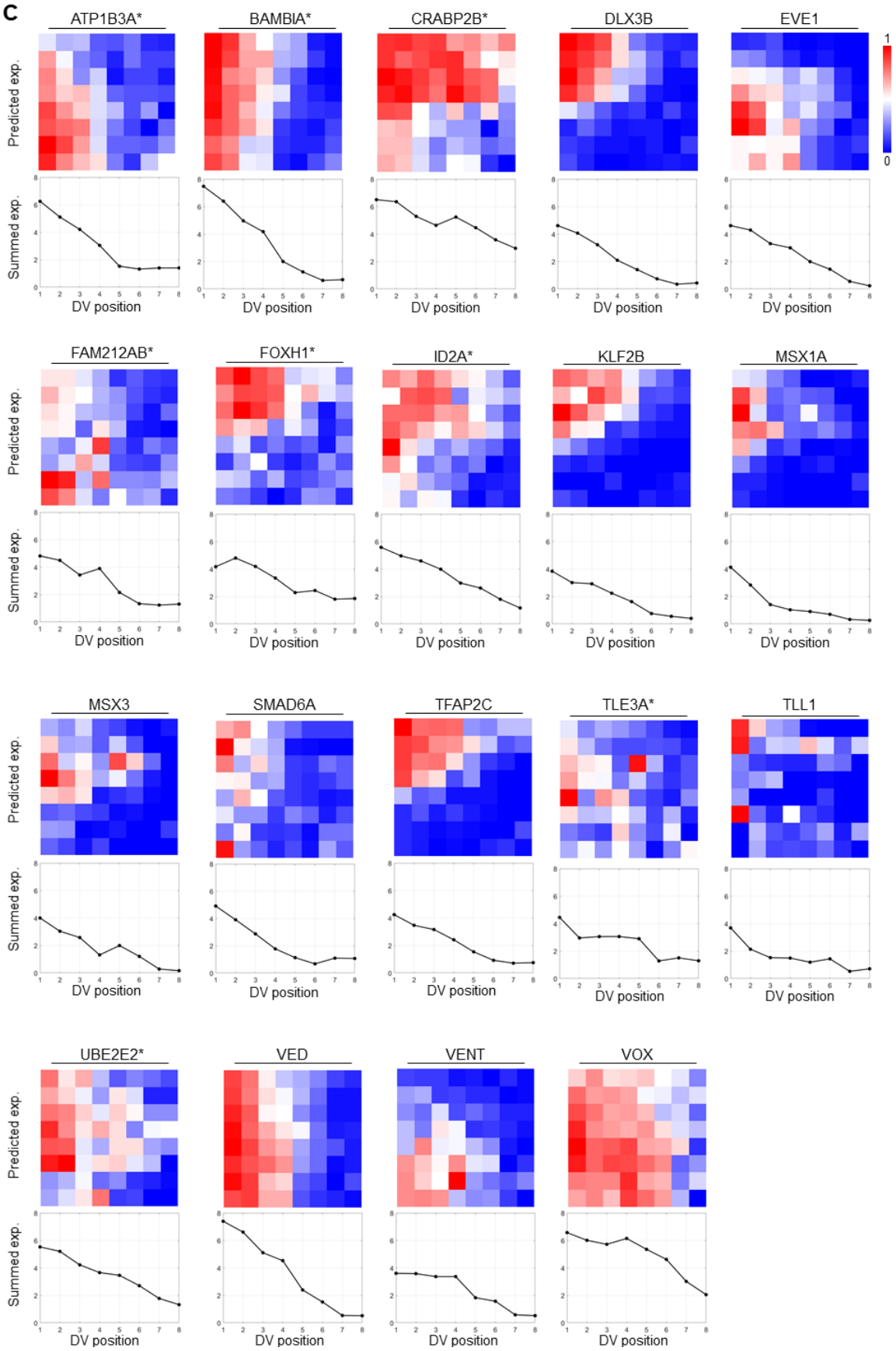
C
ATP1B3A*
BAMBIA*
CRABP2B*
DLX3B
EVE1
FAM212AB*
FOXH1*
ID2A*
KLF2B
MSX1A
MSX3
SMAD6A
TFAP2C
TLE3A*
TLL1
UBE2E2*
VED
VENT
VOX
Predicted exp.
Summed exp.
DV position
1
0

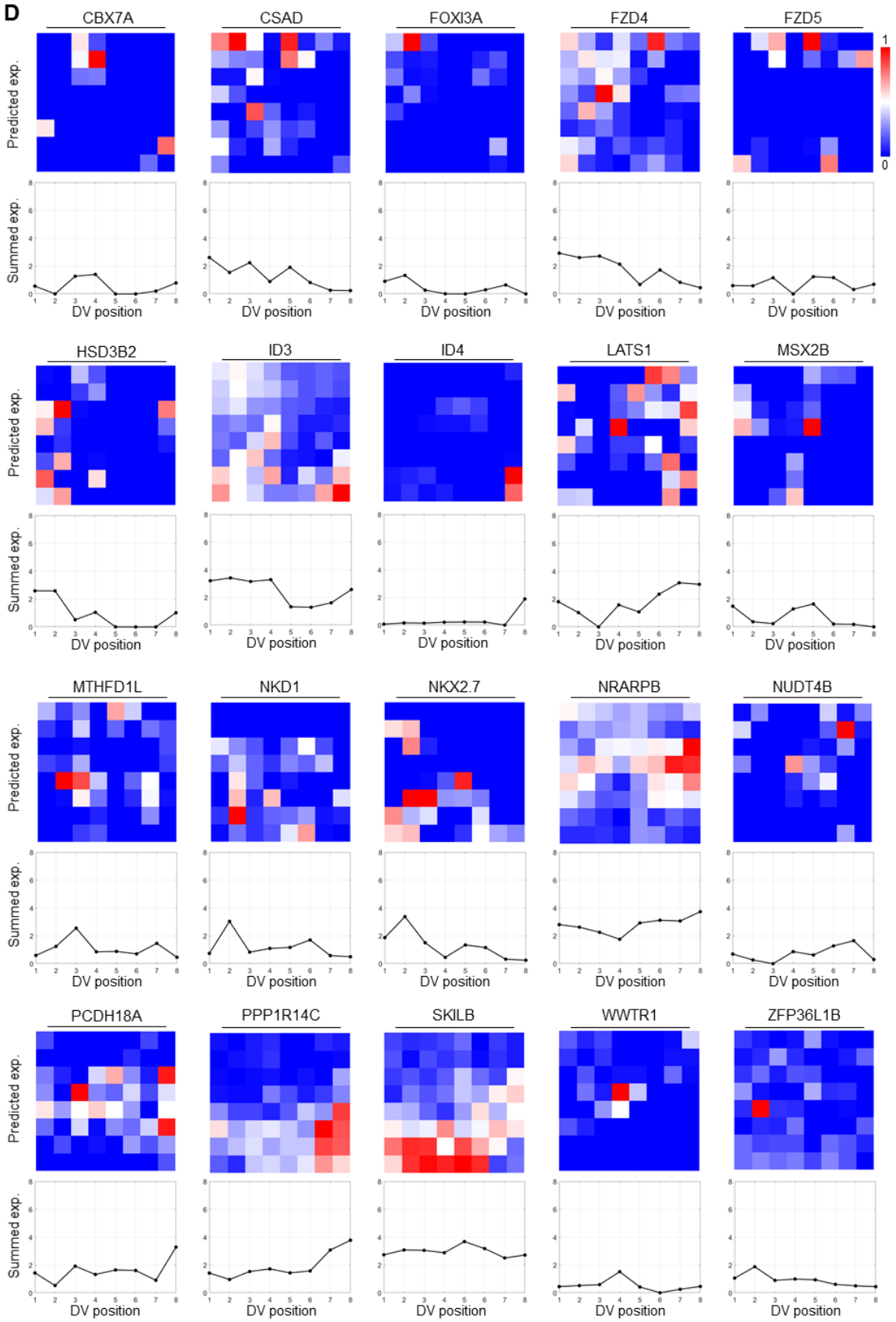
D
CBX7A
CSAD
FOXI3A
FZD4
FZD5
HSD3B2
ID3
ID4
LATS1
MSX2B
MTHFD1L
NKD1
NKX2.7
NRARPB
NUDT4B
PCDH18A
PPP1R14C
SKILB
WWTR1
ZFP36L1B
Predicted exp.
Summed exp.
DV position
1
0

Figure 2.4 Seurat predicted expression domains of 50 BMP directly upregulated target genes. Related to Figure 2.3. (A-D) Heat map of gene expression patterns from Seurat analysis for 50 target genes directly upregulated by BMP signaling and sequenced in scRNA-seq dataset of mid-gastrula (8 hpf) embryos. Predicted expression normalized across all bins. Below are Seurat predicted expression profiles across the DV axis. Each point is the sum of the expression intensity from all bins at one DV position. Genes are considered expressed in a bin with greater than 0.5 A.U. (arbitrary unit) of predicted expression. (A-C) Target genes with ventrally enriched expression. The genes known to expressed dorsally or in the prechordal plate are indicated by asterisks. (A) Cluster 1 target genes that are expressed within the first 3 or 4 bins. (B) Cluster 2 target genes that are expressed within the first 5 bins. (C) Cluster 3 target genes that are expressed within the first 6 or 7 bins. (D) The remaining target genes that have random or uniform expression across the DV axis.

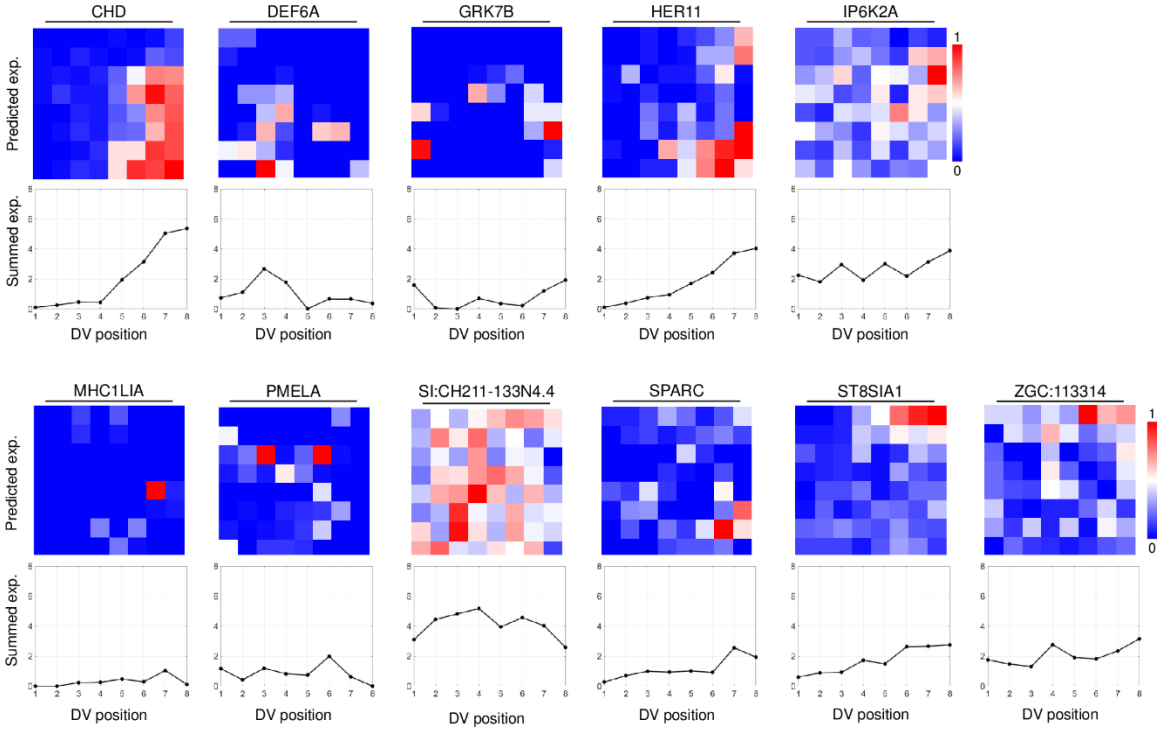

Figure 2.5 Seurat predicted expression domains of 11 BMP directly downregulated target genes. Related to Figure 2.3. Heat map of gene expression patterns from Seurat analysis for 11 target genes directly downregulated by BMP signaling that were sequenced in a scRNA-seq dataset of mid-gastrula (8 hpf) embryos. Predicted expression was normalized across all bins. Below are Seurat-predicted expression profiles across the DV axis. Each point is the sum of the expression intensity from all bins at one DV position. Genes are considered expressed in a bin with greater than 0.5 A.U. (arbitrary

unit) of predicted expression. Genes with higher predicted expression in bins 5-8 than bins 1-4 are considered to be dorsally enriched.

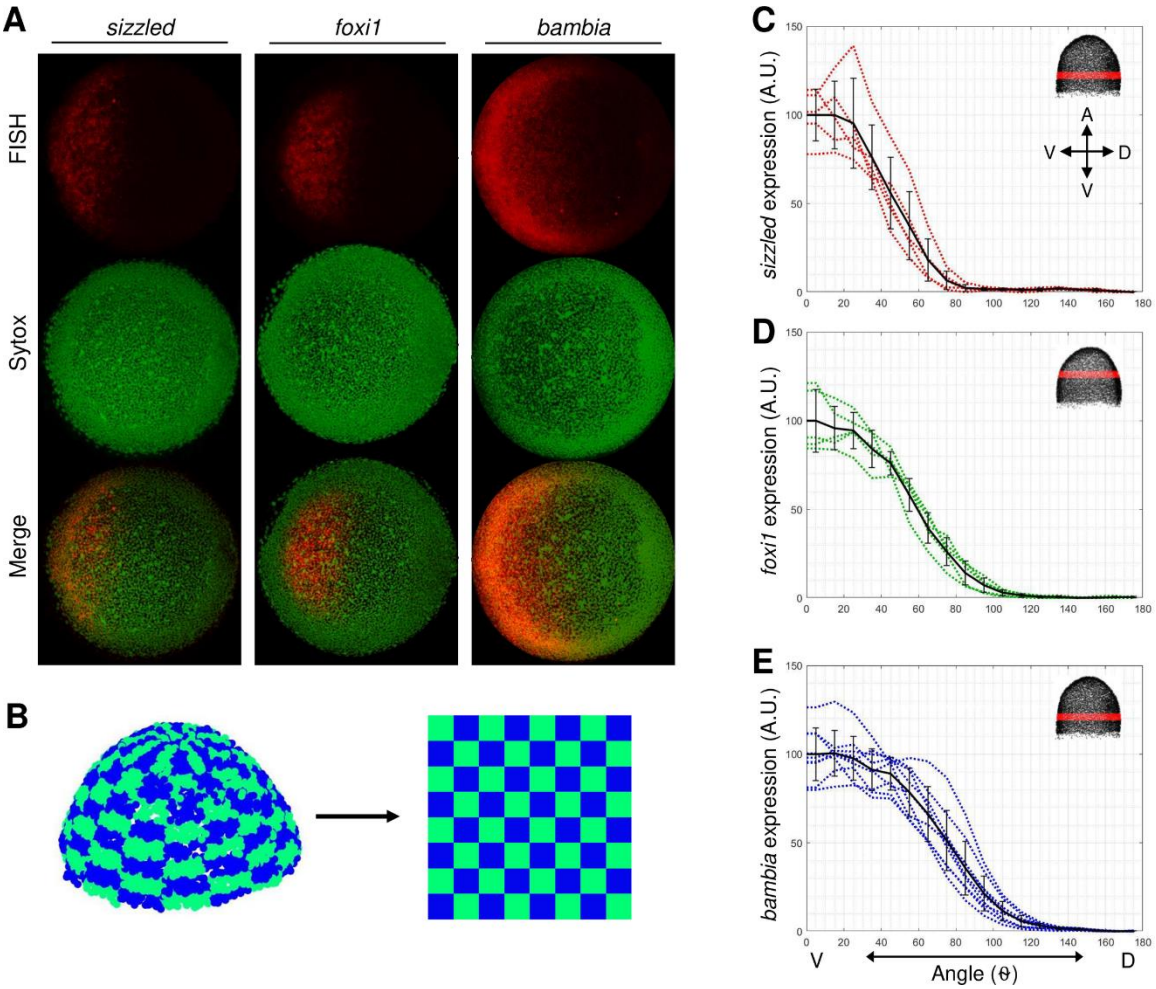

Figure 2.6 Quantifying fluorescent in situ hybridization of three target genes. Related to Figure 2.3. (A) Animal view of a maximum projection of fluorescent *in situ* hybridization for *sizzled*, *foxi1*, and *bambia* of individual wild-type embryos at an early-gastrula stage (7 hpf). Nuclei are stained with Sytox Green. (B) Schematic of cells of individual embryo partitioned into 128 equally-spaced bins. Expression intensity within each bin is averaged. Both halves of the embryo are averaged together into 64 bins, and the expression intensity is normalized across all bins. Expression intensity is displayed as an 8 by 8 heatmap. (C-E) Individual (colored) and averaged (black) expression profiles of *sizzled* (n=5) (C), *foxi1* (n=5) (D), and *bambia* (n=9) (E) across the DV axis of wild-type embryos at 7 hpf. Location of the 40 µm band of cells that was averaged is indicated on the embryo in the top right corner. The boundary of the expression domain was measured in individual embryos at the position of 10% maximum expression intensity. A.U. is arbitrary units.

2.2.3 Distinct pSmad5 levels and gradient slopes correspond to different target gene expression boundaries

Next, we determined where the boundaries of the three BMP target genes are located along the pSmad5 gradient. We took sibling embryos of those stained for FISH and quantified pSmad5 immunostaining at an early-gastrula (7 hpf) stage **(Figure 2.7A)**. To identify the pSmad5 position that corresponds to each target gene expression boundary, we overlaid the DV position of the target gene boundaries onto the pSmad5 gradient profile of the sibling embryos. The pSmad5 gradient position at each expression boundary could indicate a distinct pSmad5 gradient slope or threshold that cells need to reach to induce differential expression of each gene. If gene expression is determined by a pSmad5 threshold level, then cells will not express a target gene until they reach the particular threshold level of pSmad5. Alternatively, if gene expression boundaries are positioned by distinct gradient slopes, then cells will activate target genes in response to a particular steep or shallow slope of the gradient independent of specific pSmad5 levels. It is also possible that one gene may respond to slope, while the others respond to distinct thresholds, for example. The same mechanism need not apply to all three target genes.

We found that expression of the three target genes correlates with significantly distinct pSmad5 gradient levels **(Figure 2.7B)**. The expression boundary of *sizzled* corresponds to 60% of maximum pSmad5 intensity **(Figure 2.7D)**. While the expression boundary of *foxi1* corresponds to 25% of maximum

pSmad5 intensity **(Figure 2.7E)**, that of *bambia* is very low at only 7% of pSmad5 maximum intensity **(Figure 2.7F)**. The slope of the gradient changes across the DV axis in addition to the level of pSmad5. To determine if the expression boundaries correlate with distinct slopes of the pSmad5 gradient, we overlaid the boundaries of the target gene domains onto the slope of the pSmad5 gradient. The three target gene domains also correspond to three significantly distinct pSmad5 gradient slopes **(Figure 2.7C)**. The expression boundary of *sizzled* corresponds to a gradient slope of 1.4 (A.U./degree), *foxi1* corresponds to a slope of 0.76 (A.U./degree), and *bambia* to a slope of 0.35 (A.U./degree) **(Figure 2.7G-I)**. To determine if cells along the AV axis show a differential responsiveness to BMP signaling, we analyzed the expression profiles of the three target genes over the top of the AV axis of the embryo **(Figure 2.8A)**. The three targets are also expressed in significantly distinct profiles across the AV axis **(Figure 2.8B-D)**, which correlates with significantly distinct pSmad5 levels **(Figure 2.8E-H)**. The expression domain of *sizzled* corresponds to a distinct gradient slope, while the slopes at the *foxi1* and *bambia* boundaries are not significantly distinct over the AV axis **(Figure 2.8I-L)**.

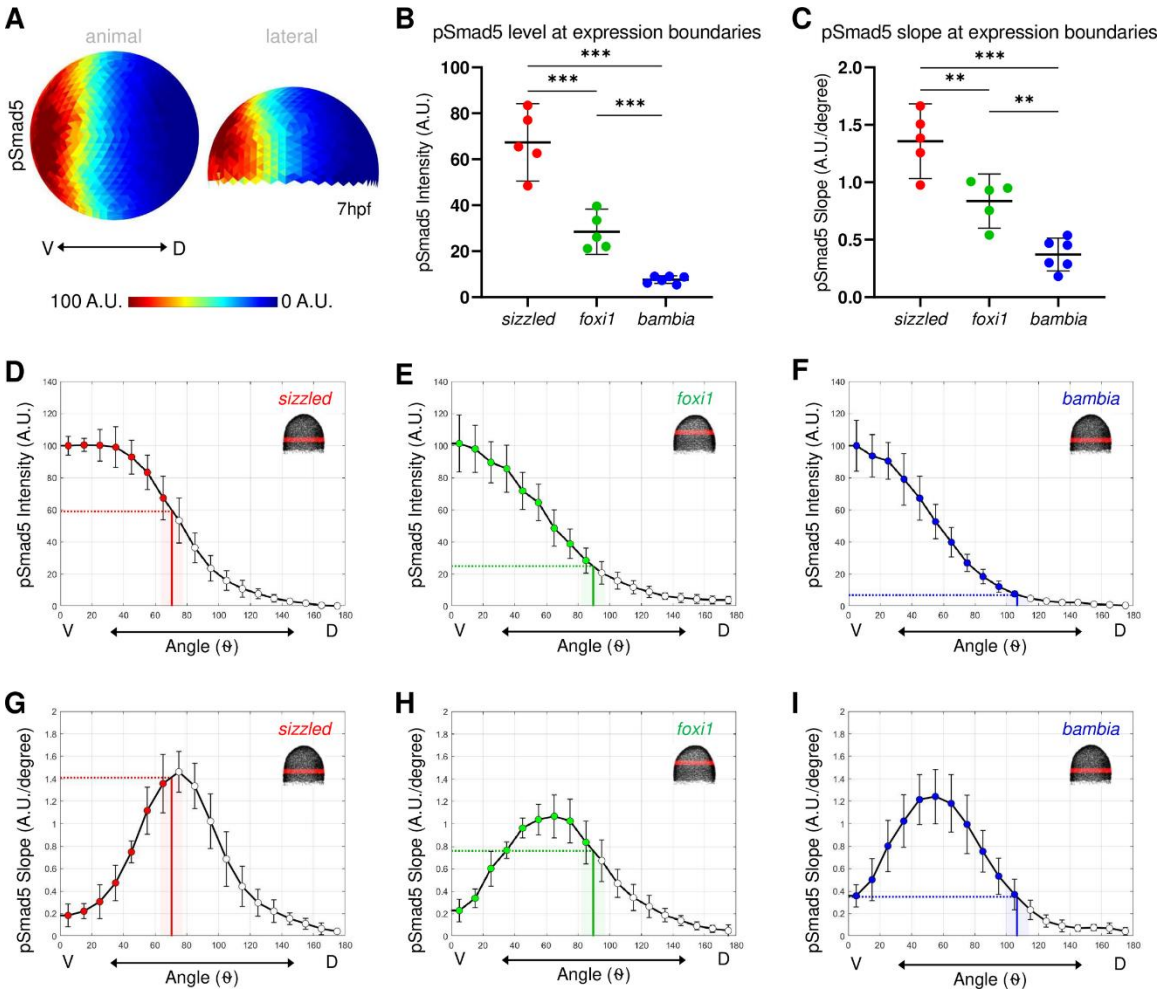

Figure 2.7 pSmad5 gradient with distinct thresholds and slopes delineating expression domains. (A) Animal and lateral view of average pSmad5 intensities in early-gastrula (7 hpf) wild-type embryos (n=5). A.U. is arbitrary units. (B) Measurement of pSmad5 intensity at the expression boundaries of *sizzled* (red), *foxi1* (green), and *bambia* (blue) across the DV axis of wild-type embryos at 7 hpf. ***$P < 0.0001$ in comparing pSmad5 levels using unpaired two-tailed Students *t* tests. (C) Measurement of pSmad5 gradient slope at the expression boundaries of *sizzled* (red), *foxi1* (green), and *bambia* (blue) across the DV axis of wild-type embryos at 7 hpf. ** $P < 0.01$, ***$P < 0.0001$ in comparing pSmad5 slopes using unpaired two-tailed Students *t* tests. (D-F) Wild-type pSmad5 profiles across the DV axis. The intensity is averaged from a 40 μm band of cells around the DV axis at the location shown in red in the right corner embryo schematic of each panel. One wild-type clutch was used for (D,E,G,H) (n=5), another wild-type clutch was used for (F,I) (n=6). Positions of expression boundaries for *sizzled* (D), *foxi1* (E), and *bambia* (F) shown as vertical solid lines. Level of pSmad5 at the boundary is indicated as a horizontal dotted line. Colored dots indicate positions where target genes are expressed. Standard deviations of expression boundaries are shaded. (G-I) Slopes of pSmad5 profiles shown in (D-

F). Positions of expression boundaries for *sizzled* (G), *foxi1* (H), and *bambia* (I) are shown as vertical solid lines. Slope of pSmad5 at the boundary is indicated as a horizontal dotted line. Colored dots indicate positions where target genes are expressed. Standard deviations of expression boundaries are shaded.

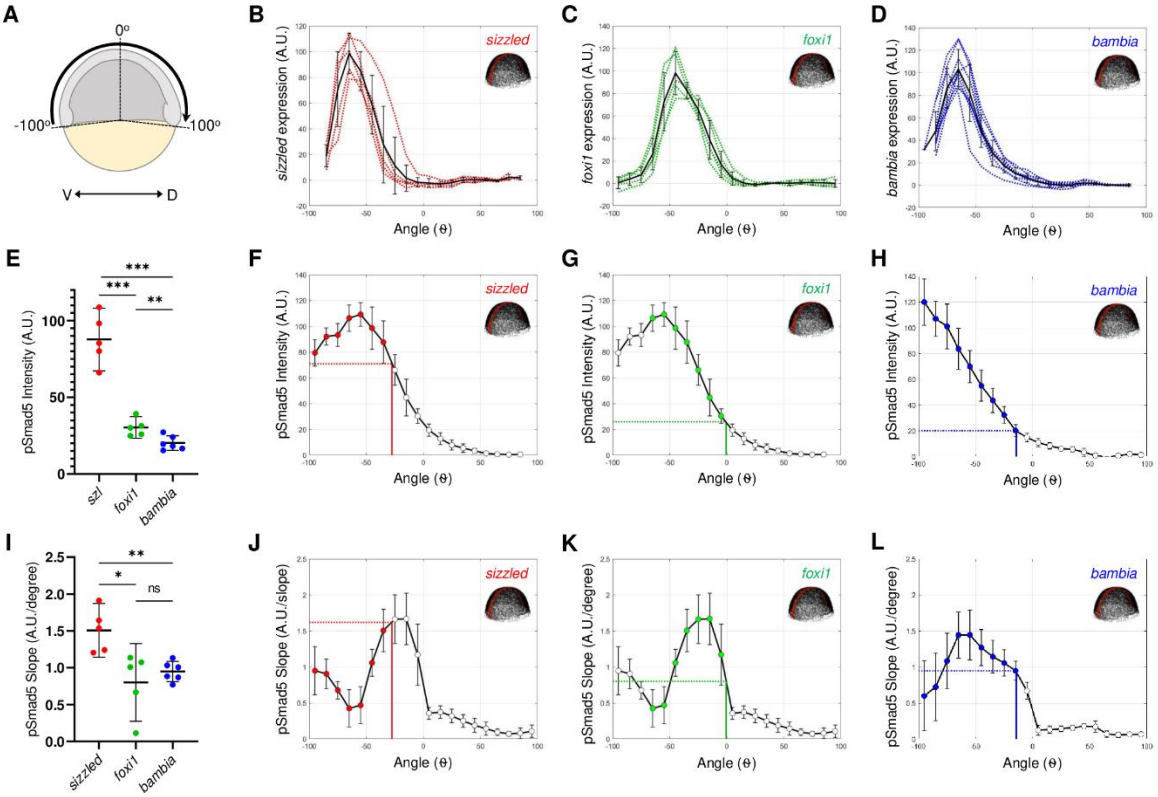

Figure 2.8 Expression profiles across the AV axis of the embryo. Related to Figure 2.7. (A) Schematic showing the location where a band of cells over the top of the embryo was averaged, beginning at the ventral margin (-100º) and ending at the dorsal margin (100º). (B-D) Individual (colored) and averaged (black) expression profiles of *sizzled* (n=5) (B), *foxi1* (n=5) (C), and *bambia* (n=9) (D) across the AV axis of wild-type embryos at 7 hpf. Location of the 40 µm band of cells that was averaged is indicated in red on the embryo in the top right corner. The boundary of the expression domain was measured in individual embryos at the position of 10% maximum expression intensity. A.U. is arbitrary units. (E) Measurement of pSmad5 intensity at the location of expression boundaries for *sizzled* (red), *foxi1* (green), and *bambia* (blue) across the AV axis of wild-type embryos at 7 hpf. $^{**}P < 0.01$, $^{***}P < 0.0001$ in comparing pSmad5 levels using unpaired two-tailed Students *t* tests. (F-H) pSmad5 profiles across the AV axis. The intensity is averaged from a 40 µm band of cells around the AV axis at the location shown in red in the right corner embryo schematic of each panel. One wild-type clutch was used for (F, G) (n=5), another clutch was used for (H) (n=6).

Positions of expression boundaries for *sizzled* (F), *foxi1* (G), and *bambia* (H) shown as vertical solid lines. Level of pSmad5 at the boundary is indicated as a horizontal dotted line. Colored dots indicate positions where target genes are expressed. (I) Measurement of pSmad5 slope at the location of expression boundaries for *sizzled* (red), *foxi1* (green), and *bambia* (blue) across the AV axis of wild-type embryos at 7 hpf. **P* < 0.05 , ***P* < 0.01 in comparing pSmad5 slopes using unpaired two-tailed Students *t* tests. NS is not significant. (J-L) Slopes of pSmad5 profiles shown in (F-H). Positions of expression boundaries for *sizzled* (J), *foxi1* (K), and *bambia* (L) are shown as vertical solid lines. Slope of pSmad5 at the boundary is indicated as a horizontal dotted line. Colored dots indicate positions where target genes are expressed.

2.2.4 Test of gradient slope to position gene expression boundaries

The boundaries of target gene expression across the DV axis correspond to both distinct pSmad5 concentrations and pSmad5 gradient slopes. To directly test the ability of either pSmad5 concentration thresholds or gradient slope to position gene expression in the gastrula embryo, we utilized mutants that have a modified pSmad5 gradient shape and measured corresponding shifts in target gene expression **(Figure 2.9A, B)**. If cells across the DV axis respond to distinct levels of pSmad5 to activate target gene expression, the boundaries of target gene expression will correlate with the same pSmad5 levels even if the gradient shape is altered **(Figure 2.9B)**. Alternatively, if cells respond to the shape of the gradient, the target gene boundaries will correlate with the same gradient slope regardless of pSmad5 level **(Figure 2.9B)**.

To investigate the spatial shifts in target gene expression when the pSmad5 gradient shape is altered, we used *chordin* mutant early-gastrula embryos. Chordin is a BMP ligand antagonist that acts as a dorsal sink for BMP, thus shaping BMP signaling activity during gastrulation (Pomreinke et al., 2017;

Tuazon et al., 2020; Zinski et al., 2017). In *chordin* mutant embryos, the shape of the BMP signaling gradient is altered where the highest levels of BMP signaling activity expand laterally and the slope of the gradient is shallower in the lateral regions **(Figure 2.9C, G-L, 2.10A)**. While maximum pSmad5 levels are similar in wild-type and *chordin* mutant embryos during gradient formation, from 4.7 to 6.3 hpf (Zinski et al., 2017), a broader region of cells express the highest pSmad5 levels in *chordin* mutants **(Figure 2.9C, G-I)**.

Embryos from crosses between *chordin-/-* and +/- fish were immunostained at an early-gastrula stage (7 hpf) for pSmad5, while siblings were assayed by FISH for the three target genes **(Figure 2.10C-E)**. The pSmad5 gradient and FISH domains were quantitated blindly, followed by genotyping for the *chordin* mutation. The gradient of pSmad5 is expanded laterally in *chordin* mutants compared to the wild-type siblings **(Figure 2.9C**), as previously shown (Zinski et al., 2017)**.** The expression domains of the three target genes were also significantly expanded laterally in *chordin* mutants **(Figure 2.9D-F, 2.10B).**

To test whether a similar pSmad5 level delineated the boundary of the expression domains, possibly acting as a concentration threshold to provide positional information to cells, we determined the position of the target gene expression boundary on the pSmad5 gradients of wild-type and *chordin* mutant siblings. We found that a similar pSmad5 level corresponds to the boundary of *sizzled*, *foxi1*, and *bambia* expression in both wild-type and *chordin* mutants **(Figure 2.9G-I, 2.10F)**. The *sizzled* boundary corresponds to 56.8% and 56.5%

of the maximum pSmad5 intensity in wild-type and *chordin* mutants, respectively. The *foxi1* boundary corresponds to 16.5% and 20.8% in wild-type and *chordin* mutants. The *bambia* boundary corresponds to 7.2% and 8% in wild-type and *chordin* mutants. The similar levels of pSmad5 delineating the expression boundaries of these three target genes in wild-type and *chordin* mutants provides strong support for a concentration threshold model but does not eliminate the other models.

We also determined the pSmad5 gradient slope at the boundaries of the three target genes in both wild-type and *chordin* mutants. We did not find a consistent pSmad5 gradient slope at the expression boundaries for *sizzled* and *bambia* **(Figure 2.9J, L, 2.10G)**. The *sizzled* boundary corresponds to gradient slopes of 1.1 and 0.52 (A.U./degree) in wild-type and *chordin* mutants, respectively. The *bambia* boundary corresponds to 0.35 and 1.0 slopes (A.U./degree) in wild-type and *chordin* mutants. The boundary of *foxi1* expression corresponds to 0.61 and 0.83 slopes (A.U./degree) in wild-type and *chordin* mutants which is not significantly distinct **(Figure 2.9K, 2.10G)**. However, multiple positions across the DV axis have similar pSmad5 gradient slopes, so gradient shape alone would be unable to provide specific positional information. In contrast, the concentration threshold model does provide unique positional information across the DV axis.

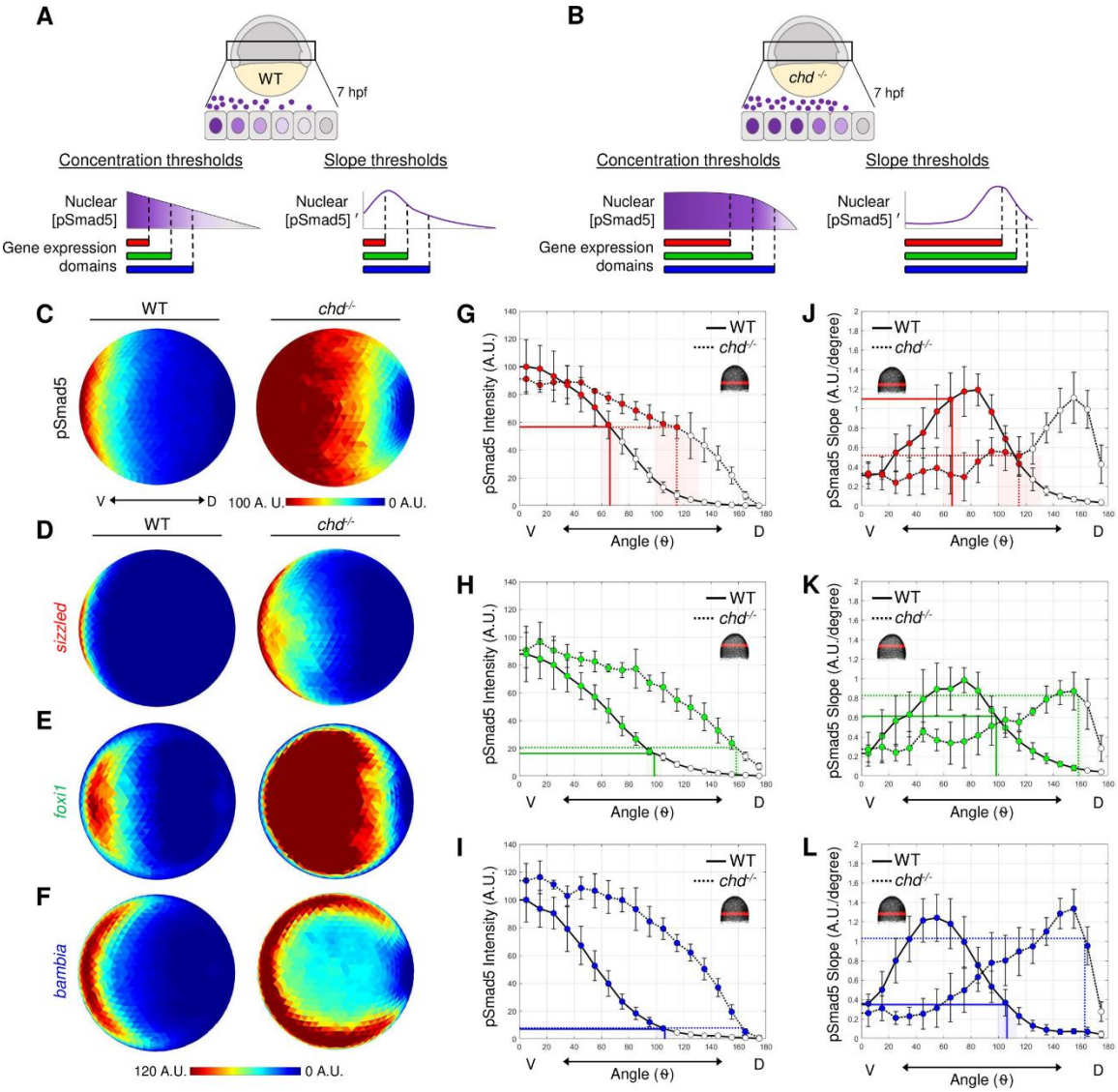

Figure 2.9 pSmad5 gradient thresholds versus slopes in positioning target gene expression in *chordin* mutant gradient. (A) Model of three target gene expression domains in wild-type gastrula embryos positioned by either distinct pSmad5 levels or distinct pSmad5 gradient slopes. (B) Model of predicted target gene expression boundaries in *chordin* mutant gastrula embryos corresponding to distinct pSmad5 levels or gradient slopes if cells are interpreting pSmad5 concentration or shape, respectively. (C) Animal view of average pSmad5 intensities of early-gastrula (7 hpf) wild-type (n=6) and *chordin* mutants (n=5). (D-F) Animal view of average fluorescent *in situ* hybridization intensities of wild-type and *chordin* mutants for *sizzled* (D) (wild-type n=8, *chd-/-* n=8); *foxi1* (E) (wild-type n=6, *chd-/-* n=7); and *bambia* (F) (wild-type n=9, *chd-/-* n=4). A.U. is arbitrary units. (G-I) pSmad5 profiles of wild-type (black solid line) and *chordin*

mutants (black dotted line). Location of 40 µm band of cells that was averaged is indicated on embryo in top right corner. Expression boundaries of *sizzled* (G), *foxi1* (H), and *bambia* (I) in wild-type (solid colored line) and *chordin* mutants (dotted colored line). Standard deviations of expression boundaries are shaded. (J-L) Slope of pSmad5 profiles shown in (G-I) of wild-type (black solid line) and *chordin* mutants (black dotted line). Expression boundaries of *sizzled* (J), *foxi1* (K), and *bambia* (L) in wild-type (solid colored line) and *chordin* mutants (dotted colored line). Standard deviations of expression boundaries are shaded. A.U. is arbitrary units.

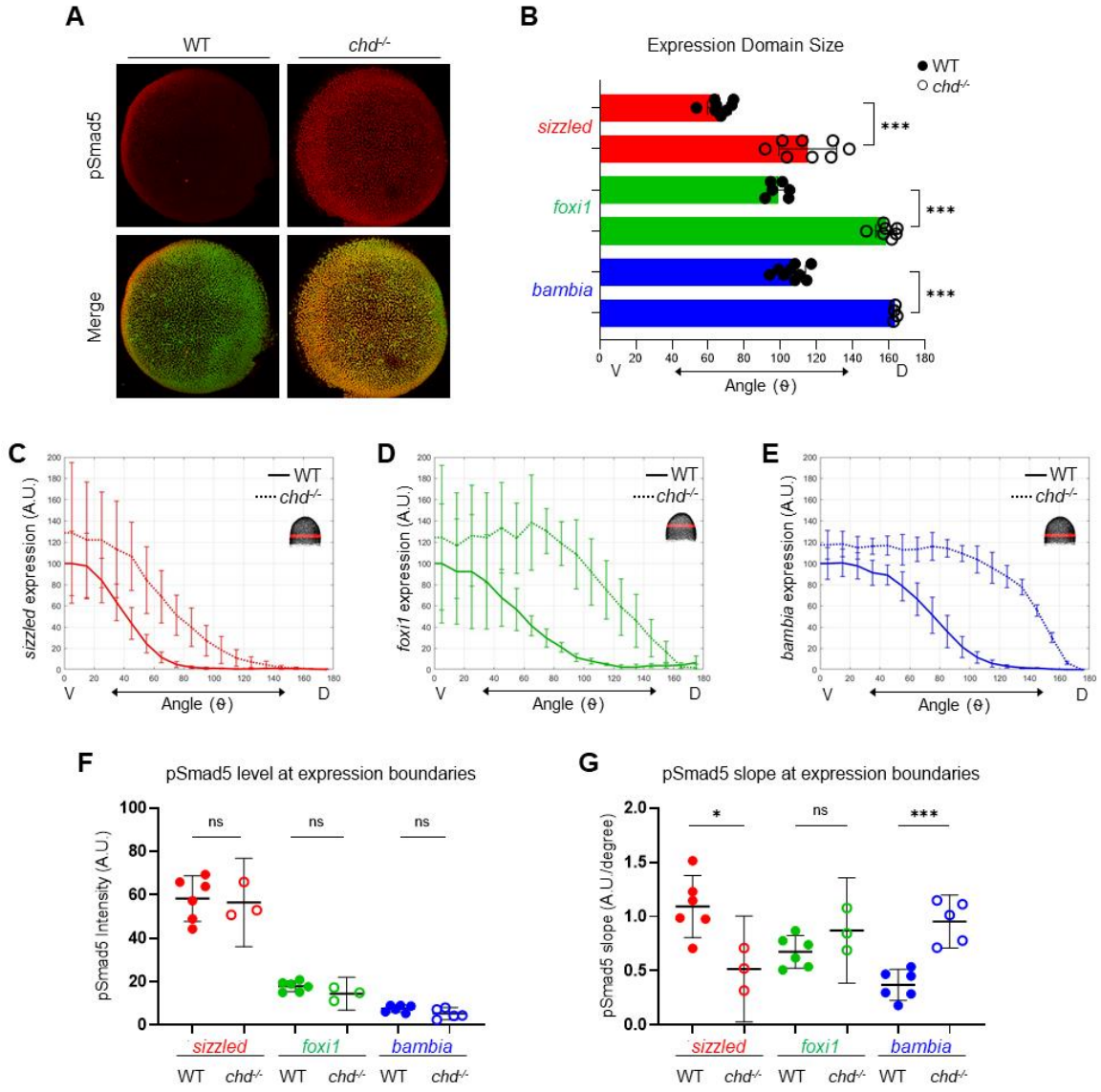

Figure 2.10 pSmad5 levels and target gene expression in *chordin* mutants. Related to Figure 2.9. (A) Animal view of the maximum projection of pSmad5 immunofluorescence in an individual wild-type and *chordin* mutant at an early-

gastrula stage (7 hpf). Merged image with Sytox Green staining nuclei. Because the *chordin* mutant displays high pSmad5 levels throughout the embryo, a lower confocal laser intensity gain was used in imaging the wild-type and *chordin* mutant embryos in this experiment compared to other pSmad5 imaging experiments. (B) Position of expression boundaries for *sizzled* (red), *foxi1* (green) and *bambia* (blue) in individual wild-type (filled) and *chordin* mutant (opened) embryos. ***$P < 0.001$ in comparing WT to *chd*-/- in an unpaired two-tailed Students *t* test. (C-E) Average expression profiles of *sizzled* (C), *foxi1* (D), and *bambia* (E) across the DV axis of wild-type (solid line) and *chordin* mutant (dotted line) embryos. Location of the 40 µm band of cells that was averaged is indicated on the embryo in the top right corner. (F) Measurement of pSmad5 intensity at the location of expression boundaries for *sizzled* (red), *foxi1* (green), and *bambia* (blue) across the DV axis of wild-type (filled) and *chordin* mutant (opened) embryos at 7 hpf. NS is not significant in comparing pSmad5 levels using unpaired two-tailed Students *t* tests. (G) Measurement of pSmad5 gradient slope at the location of expression boundaries for *sizzled* (red), *foxi1* (green), and *bambia* (blue) across the DV axis of wild-type (filled) and *chordin* mutant (opened) embryos at 7 hpf. *$P < 0.05$, ***$P < 0.001$ in comparing pSmad5 slopes using unpaired two-tailed Students *t* tests. NS is not significant. A.U. is arbitrary units.

2.2.5 Test of signal duration to position gene expression boundaries

The gradient of BMP signaling forms from mid-blastula to early-gastrula stages (Hashiguchi and Mullins, 2013; Tucker et al., 2008; Zinski et al., 2017). Embryonic cells are exposed to the BMP2/7 ligand for over 4 hours during this time period. It is not known if activation of target genes requires differential duration to BMP signaling activity, or if cells activate target gene expression once the pSmad5 threshold level is reached **(Figure 2.11A)**. In a signal duration model that determines ventral target gene expression boundaries, the most ventrally-restricted genes would require the longest signal duration (e.g. *sizzled*), whereas the most broadly expressed ventrolateral target genes would require the shortest signal duration (e.g. *bambia*) **(Figure 2.11A)**. To address the role of signal duration to pattern ventral cell fates, we tested the requirement of BMP ligand

exposure to activate target gene expression. If cells respond to different durations of signal, then genes that require longer signal exposure will not be expressed after a pulse of BMP signaling. If cells respond to concentration thresholds, then a pulse of a high BMP2/7 concentration will activate all three target genes **(Figure 2.11B)**.

To test the role of signal duration on the immediate response of gene expression, we injected BMP2/7 protein into *bmp7* mutant embryos at 4 hpf and fixed embryos 30 minutes after injection for FISH and pSmad5 immunostaining **(Figure 2.11C)**. We detected robust pSmad5 activation after 30 minutes of BMP2/7 ligand exposure **(Figure 2.11D)**. Strikingly, expression of *sizzled* **(Figure 2.11E)**, *foxi1* **(Figure 2.11F)**, and *bambia* **(Figure 2.11G)** was also observed 30-minutes post injection. This suggests that spatially-distinct target genes can be rapidly activated following exposure to BMP ligand. Specifically, activation of these target genes does not require the full 4 hours of BMP signaling that cells are exposed to endogenously.

While even shorter signal durations would be unlikely to be physiologically relevant, we nevertheless investigated gene expression responses at shorter durations of 10, 20, and 30 minutes in this assay. We found that *sizzled* is expressed within 10 minutes of activating BMP signaling in *bmp7* mutant embryos **(Figure 2.12A, B)**. The expression of *foxi1* and *bambia* was first observed 20 and 30 minutes after BMP2/7 injection, respectively **(Figure 2.12C, D)**. While *bambia* with the broadest expression domain would be expected to

require the shortest signal duration, we found that it was expressed latest among the three genes at 30 minutes in response to BMP signaling **(Figure 2.12)**.

To determine if genes in the same domain share the same transcriptional kinetics, we measured the expression of another broadly-expressed target gene, *ved* **(Figure 2.13A)**. The expression profiles of *ved* closely resemble *bambia* in both wild-type and *chordin* mutant embryos indicating that *ved* is activated by the same low pSmad5 threshold level **(Figure 2.13B)**. However, unlike *bambia*, *ved* is rapidly activated in response to BMP signaling **(Figure 2.12D, 2.13C)**. While differences in transcriptional kinetics have been suggested to underly target genes activated by Nodal in zebrafish patterning (Dubrulle et al., 2015), differences in the transcriptional kinetics of these BMP target genes do not correlate with domain size.

The mechanism of duration-dependent signaling can also include a genetic regulatory network that creates spatially distinct domains of expression (Balaskas et al., 2012). To determine the role of secondary transcriptional regulation in defining the expression domains, we treated *bmp7* mutant embryos with CHX at 4 hpf before injecting BMP2/7 protein **(Figure 2.14A)**. Again, all three target genes were rapidly activated with the CHX treatment after 30 minutes of BMP ligand exposure **(Figure 2.14B-D)**. Thus, BMP target genes can be expressed in distinct domains of the embryo independent of distinct durations of BMP signaling or feedback through genetic regulatory networks. Therefore, we

conclude that different durations of BMP signaling activity are not directly positioning the expression of these target genes within the embryo.

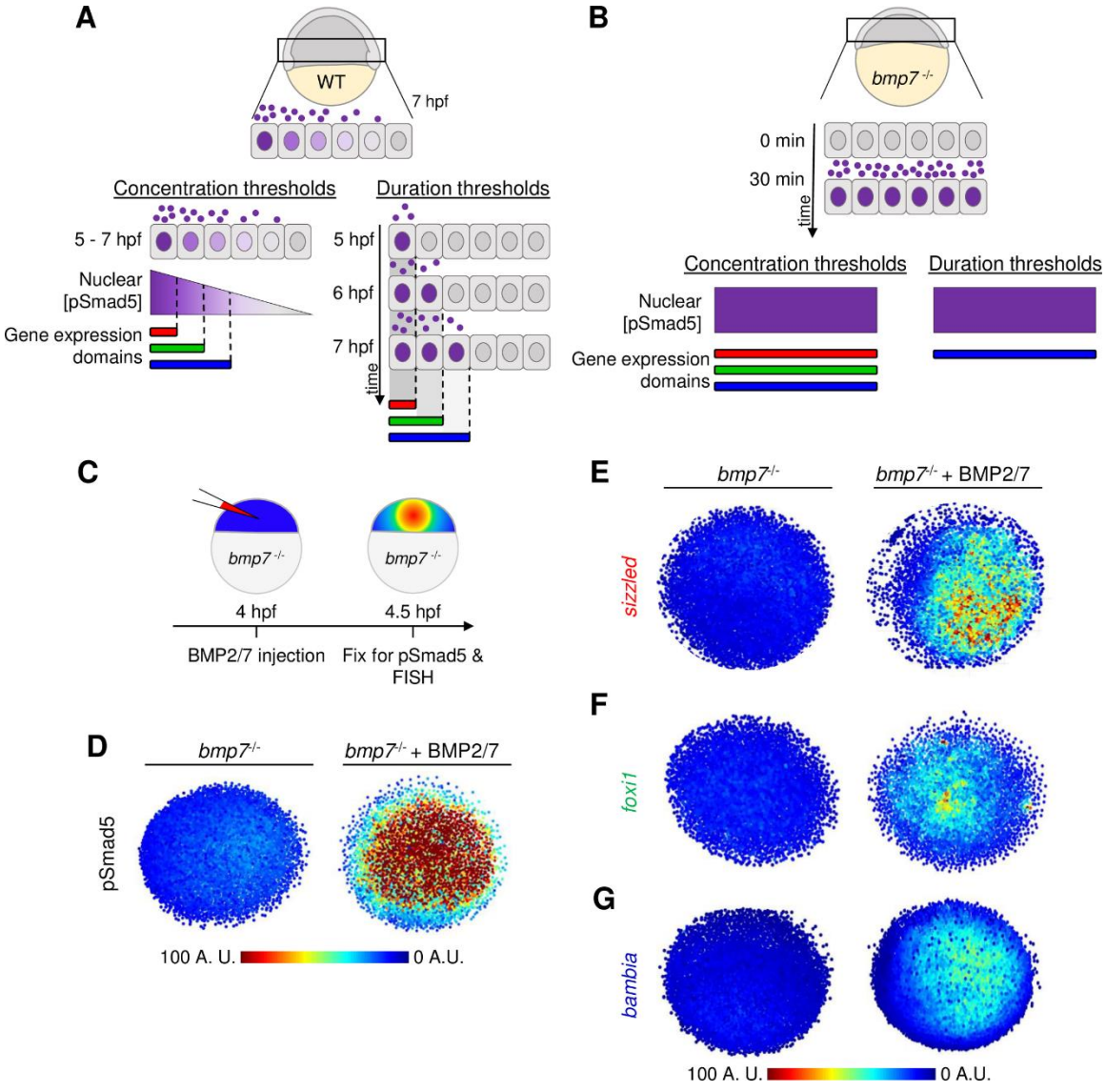

Figure 2.11 Thirty-minute duration of BMP2/7 sufficient for *sizzled, foxi1*, and *bambia* target gene expression. (A) Model of target gene expression regulated by distinct pSmad5 levels or distinct durations of BMP signaling. (B) Model of target gene activation after a 30-minute pulse of BMP ligand exposure. If target genes are activated by different pSmad5 levels, then all three target genes will be expressed following exposure to high levels of BMP signaling. If differences in signal duration activate BMP target gene expression, then a gene

that requires a short signal duration will be expressed, but genes requiring longer signal durations will not be expressed. (C) Experimental schematic of a *bmp7* mutant embryo injected with 5 pg of BMP2/7 protein that is fixed 30 minutes post-injection for pSmad5 immunostaining or FISH. (D) Representative immunostaining of pSmad5 intensities of an uninjected *bmp7* mutant (n=8) and a *bmp7* mutant injected with 5 pg of BMP2/7 protein (n=9). Animal pole is facing up. (E-G) Representative FISH in *bmp7* mutants uninjected or injected with 5 pg of BMP2/7 protein for *sizzled* (E) (n=11 uninjected, n=11 injected), *foxi1* (F) (n=10, n=11), and *bambia* (G) (n=10, n=11). Animal pole is facing up. A.U. is arbitrary units.

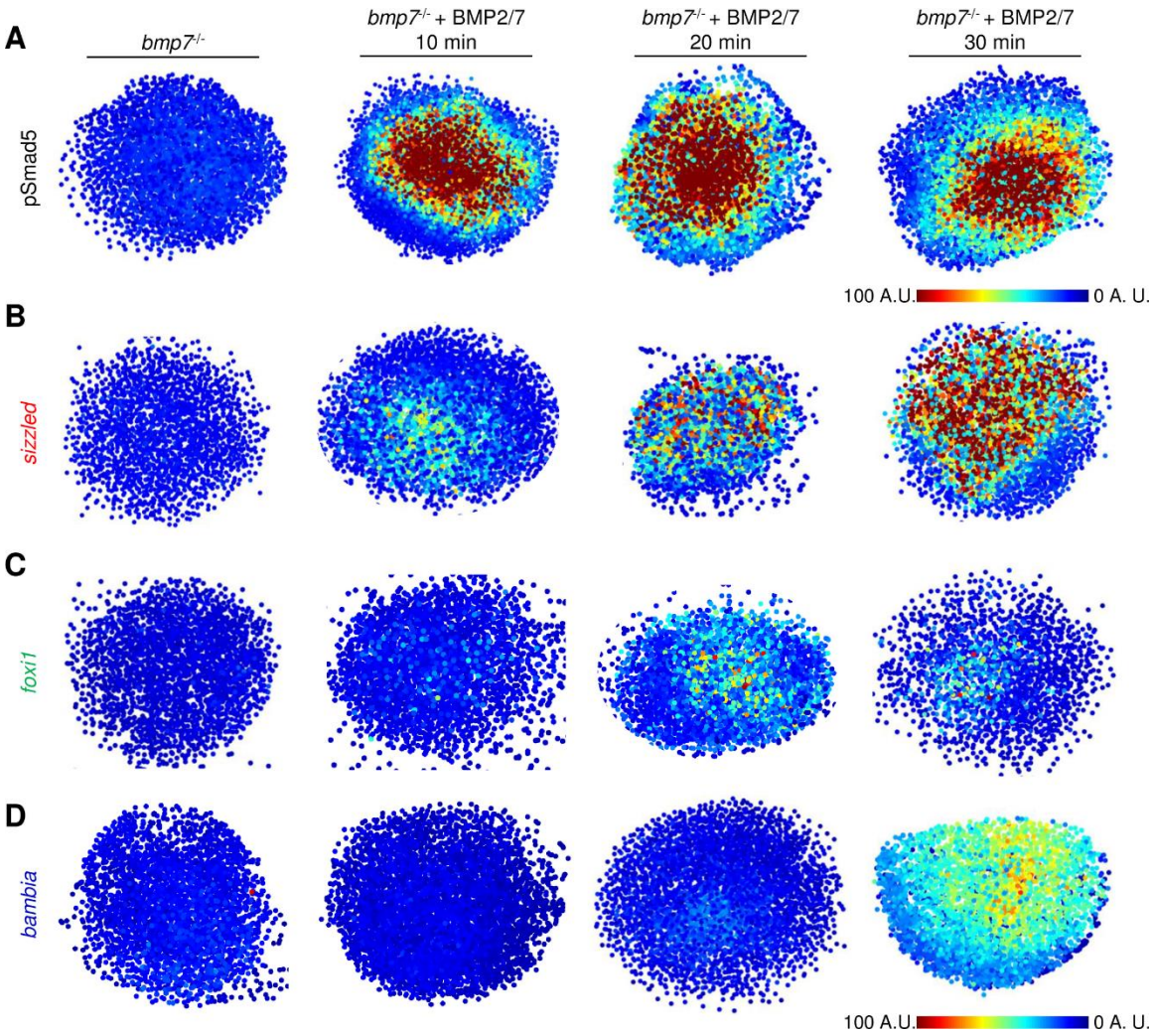

Figure 2.12 Differential target gene induction at 10, 20, and 30 minutes. Related to Figure 2.11. (A) Representative immunostaining of pSmad5 intensities of an uninjected *bmp7* mutant (n=10) and *bmp7* mutants injected with 5 pg of

BMP2/7 protein and fixed after 10, 20, and 30 minutes after injection (n=10, n=10, n=10). Animal pole is facing up. (B-D) Representative FISH for *sizzled* (E) (n=10, n=11, n=10, n=10), *foxi1* (F) (n=5, n=5, n=5, n=5), and *bambia* (G) (n=5, n=5, n=5, n=5) in uninjected *bmp7* mutants and *bmp7* mutants injected with 5 pg of BMP2/7 protein and fixed 10, 20, and 30 minutes after injection. Animal pole is facing up. A.U. is arbitrary units.

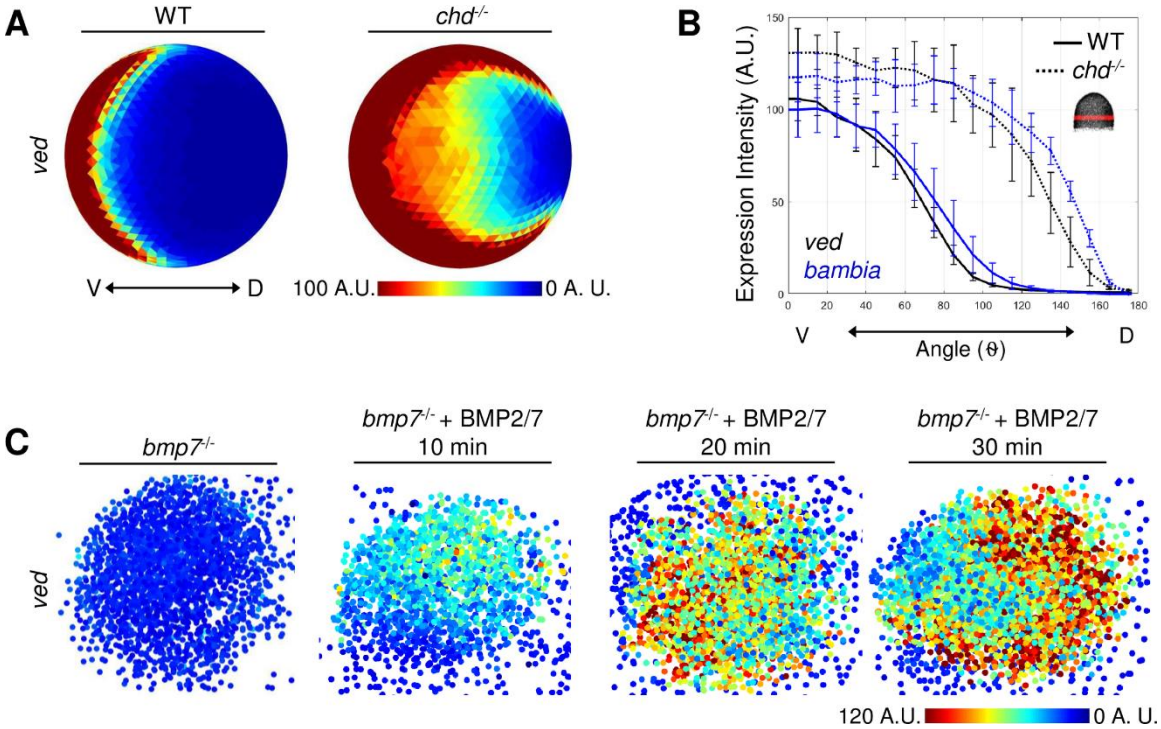

Figure 2.13 Broadly expressed target gene *ved* rapidly activated following BMP exposure. Related to Figure 2.11. (A) Animal views of average fluorescent *in situ* hybridization signal (FISH) of *ved* in wild-type embryos (n=6) and *chordin* mutants (n=5) at an early-gastrula stage (7 hpf). (B) Average expression profiles of *ved* (black) and *bambia* (blue) in wild-type (solid line) and *chordin* mutants (dotted line). Location of 40 µm band of cells that was averaged is indicated on embryo in right corner. (C) Representative FISH for *ved* in *bmp7* mutants uninjected or injected with 5 pg of BMP2/7 protein and fixed 10, 20, and 30 minutes after injection (n=5, n=5, n=5, n=5). Animal pole is facing up. A.U. is arbitrary units.

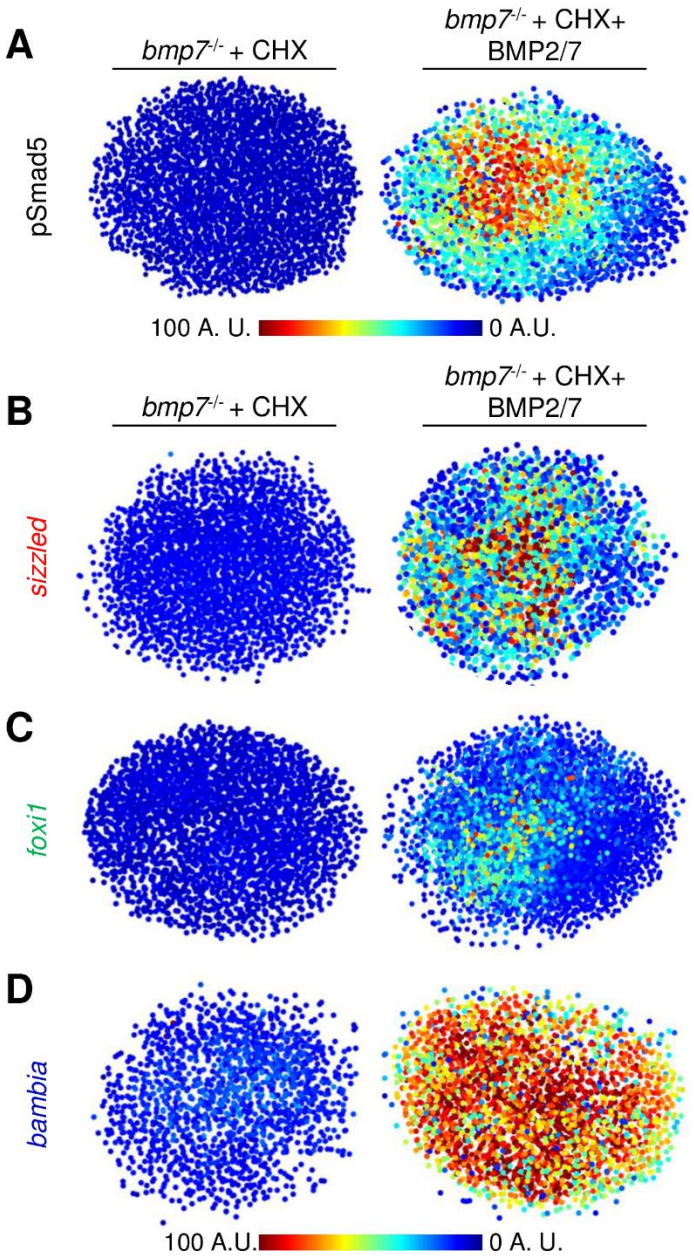

Figure 2.14 Rapid activation of target genes does not require transcriptional feedback. Related to Figure 2.11. (A) Representative immunostaining of pSmad5 intensities of an uninjected *bmp7* mutant treated with CHX (n=15) and a *bmp7* mutant treated with CHX and then injected with 5 pg of BMP2/7 protein (n=15). Animal pole is facing up. (B-D) Representative FISH in CHX treated *bmp7* mutants that were either uninjected or injected with 5 pg of BMP2/7 protein for *sizzled* (E) (n=10 uninjected, n=11 injected), *foxi1* (F) (n=10, n=10), and *bambia* (G) (n=10, n=11). Animal pole is facing up. CHX = cycloheximide. A.U. is arbitrary units.

2.2.6 Test of signal concentration to activate different target genes

We have shown the three target genes are expressed rapidly upon exposure to high levels of BMP **(Figure 2.11)**. If the target genes are responding to concentration thresholds alone, then exposing cells to different levels of BMP should activate target genes expressed in distinct domains regardless of signal duration or gradient shape. To expose cells to more stable and uniform levels of BMP, we manually disassociated cells from *bmp7* mutant animal caps at 4 hpf and incubated the disassociated cells with 20 ng/ml or 5 ng/ml BMP2/7 protein for two hours. Incubation of 20 ng/ml and 5 ng/ml BMP2/7 recapitulated endogenous high and low levels of BMP signaling, respectively, found in wild-type embryos **(Figure 2.15A, 2.16)**. Cells from *bmp7* mutants expressed *sizzled* when incubated with the high level of BMP2/7 protein but not the lower level **(Figure 2.15B, 2.17A)**, as predicted in the concentration threshold model. While *bambia* is expressed in response to both high and low levels of BMP2/7 protein **(Figure 2.15C, 2.17B)**, also consistent with the concentration threshold model.

We further quantitated in this assay system the number of cells above each predicted pSmad5 threshold for *sizzled* and *bambia* expression and the number of cells expressing each gene **(Figure 2.7D-F, 2.9G-I)**. The predicted pSmad5 threshold for *sizzled* is 60 A.U. and the predicted pSmad5 threshold is 7 A.U. for *bambia*. There is a similar proportion of cells with pSmad5 levels above the predicted *sizzled* threshold (60 A.U.) and cells expressing *sizzled* in *bmp7* mutants treated with 5ng/ml and 20ng/ml BMP2/7 **(Figure 2.15D)**. Also, similar

proportions of cells are above the predicted pSmad5 threshold level for *bambia* (7 A.U.) and are expressing *bambia* in the *bmp7* mutants treated with 5ng/ml and 20ng/ml BMP2/7 **(Figure 2.15E)**. Together, our data support a model where distinct concentration thresholds of BMP signaling activate spatially-distinct target genes in DV axial patterning during gastrulation.

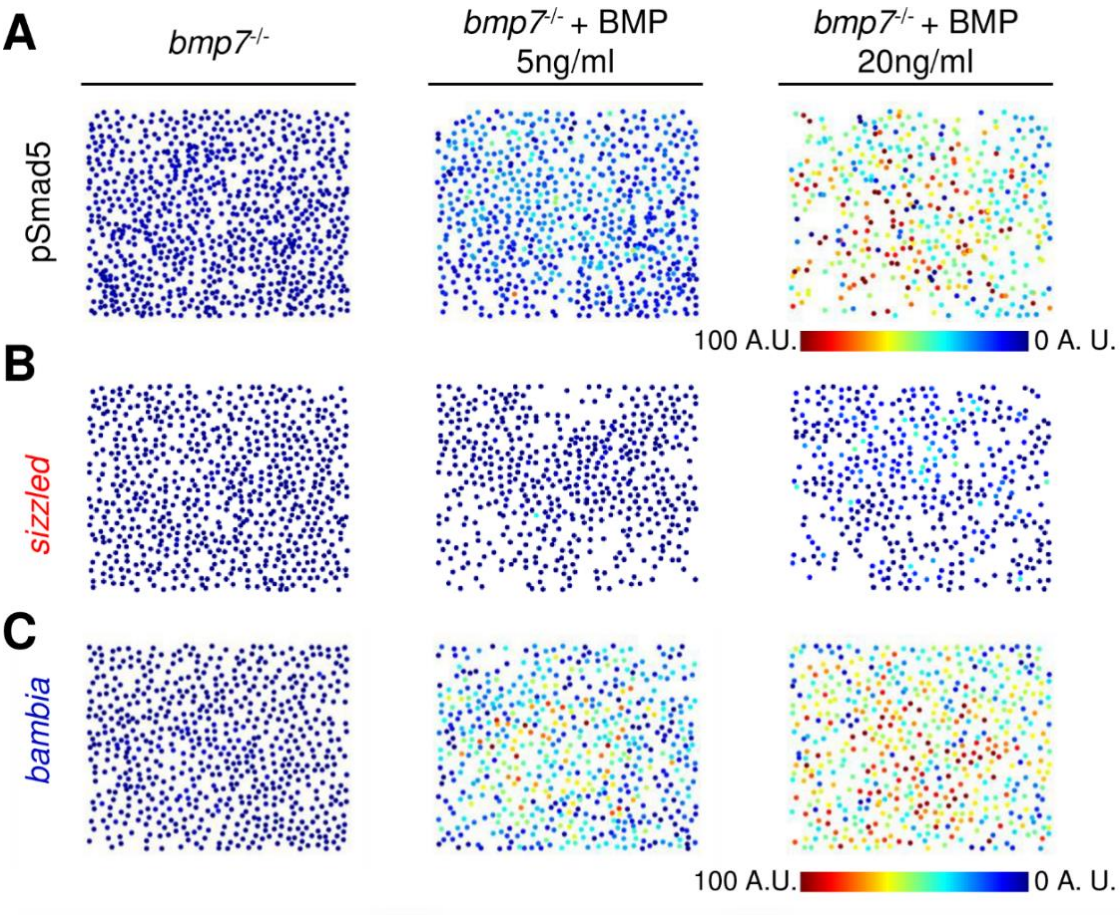

D

	bmp7$^{-/-}$	*bmp7*$^{-/-}$ + BMP 5ng/ml	*bmp7*$^{-/-}$ + BMP 20ng/ml
Proportion of cells above 60 A.U. pSmad5	0%	0.3%	28%
Proportion of *sizzled* expressing cells	0%	0.7%	26%

E

	bmp7$^{-/-}$	*bmp7*$^{-/-}$ + BMP 5ng/ml	*bmp7*$^{-/-}$ + BMP 20ng/ml
Proportion of cells above 7 A.U. pSmad5	2%	90%	97%
Proportion of *bambia* expressing cells	0.8%	78%	98%

Figure 2.15 Target genes *sizzled* and *bambia* respond to BMP in a concentration-dependent manner. (A) Representative pSmad5 immunostaining intensities of disassociated cells from *bmp7* mutants and *bmp7*

mutants treated with 5 or 20 ng/ml BMP2/7 protein. (B,C) Representative FISH for *sizzled* (B) and *bambia* (C) in *bmp7* mutants and *bmp7* mutants treated with 5 or 20ng/ml BMP2/7 protein. (D) Table displaying the proportion of cells above the predicted pSmad5 threshold for *sizzled* (60 A.U.) in each condition, and the proportion of cells expressing *sizzled* in each condition. Cells with greater than 10% of maximum signal intensity are considered to be expressing *sizzled*. (E) Table displaying the proportion of cells above the predicted pSmad5 threshold for *bambia* (7 A.U.) in each condition, and the proportion of cells expressing *bambia* in each condition. Cells with greater than 10% of maximum signal intensity are considered to be expressing *bambia*. A.U. is arbitrary units.

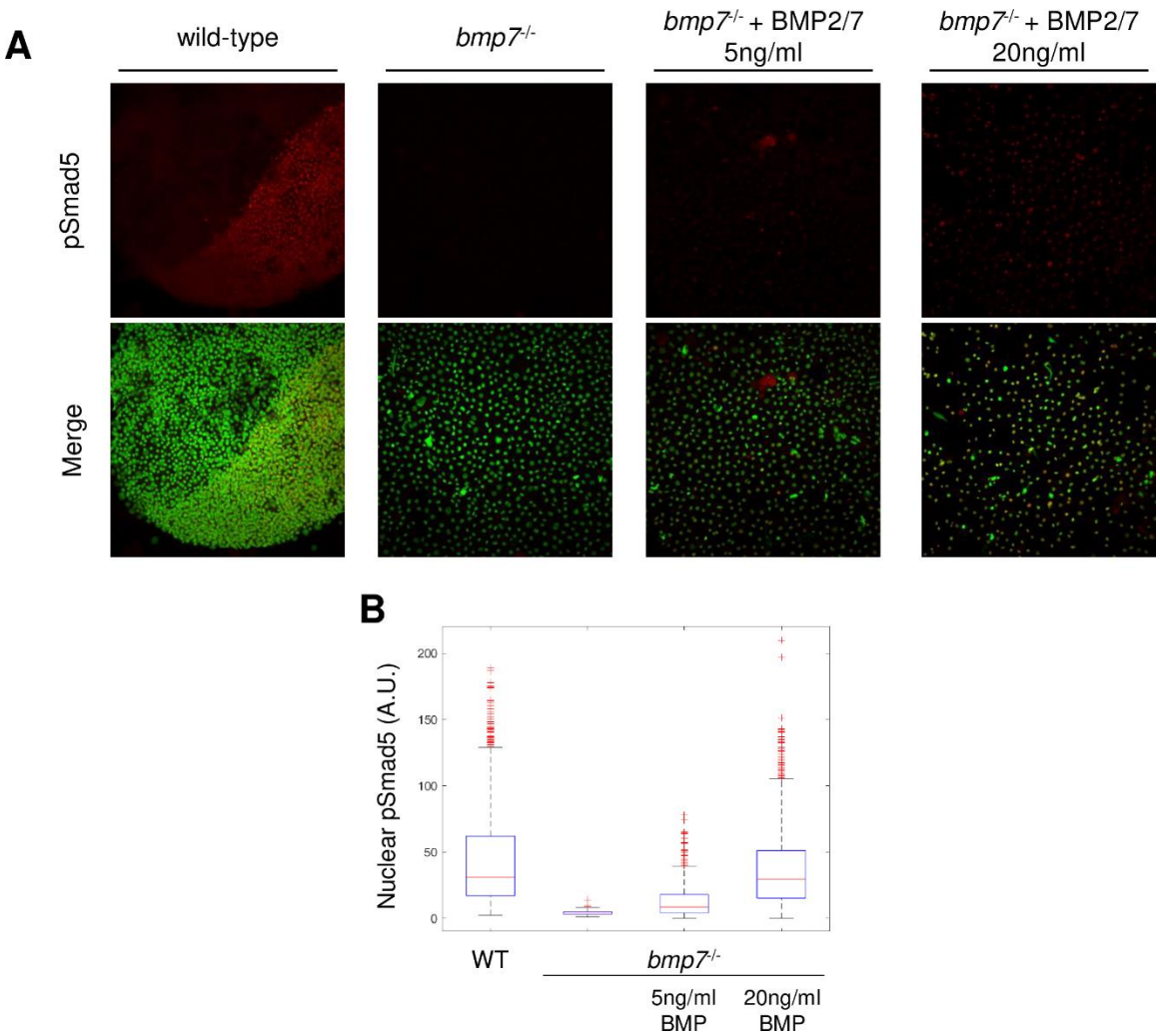

Figure 2.16 Activation of different pSmad5 levels in BMP-treated disassociated cells. Related to Figure 2.15. (A) Representative maximum projection of pSmad5 immunofluorescence in whole-mount wild-type embryo, disassociated cells from *bmp7* mutants and disassociated cells from *bmp7* mutants treated with 5 or 20 ng/ml BMP2/7 protein. Merged image with Sytox

Green stained nuclei. (B) Quantification of nuclear pSmad5 intensities of individual cells in whole-mount wild-type embryos, disassociated cells from *bmp7* mutants and disassociated cells from *bmp7* mutants treated with 5 or 20 ng/ml BMP2/7 protein.

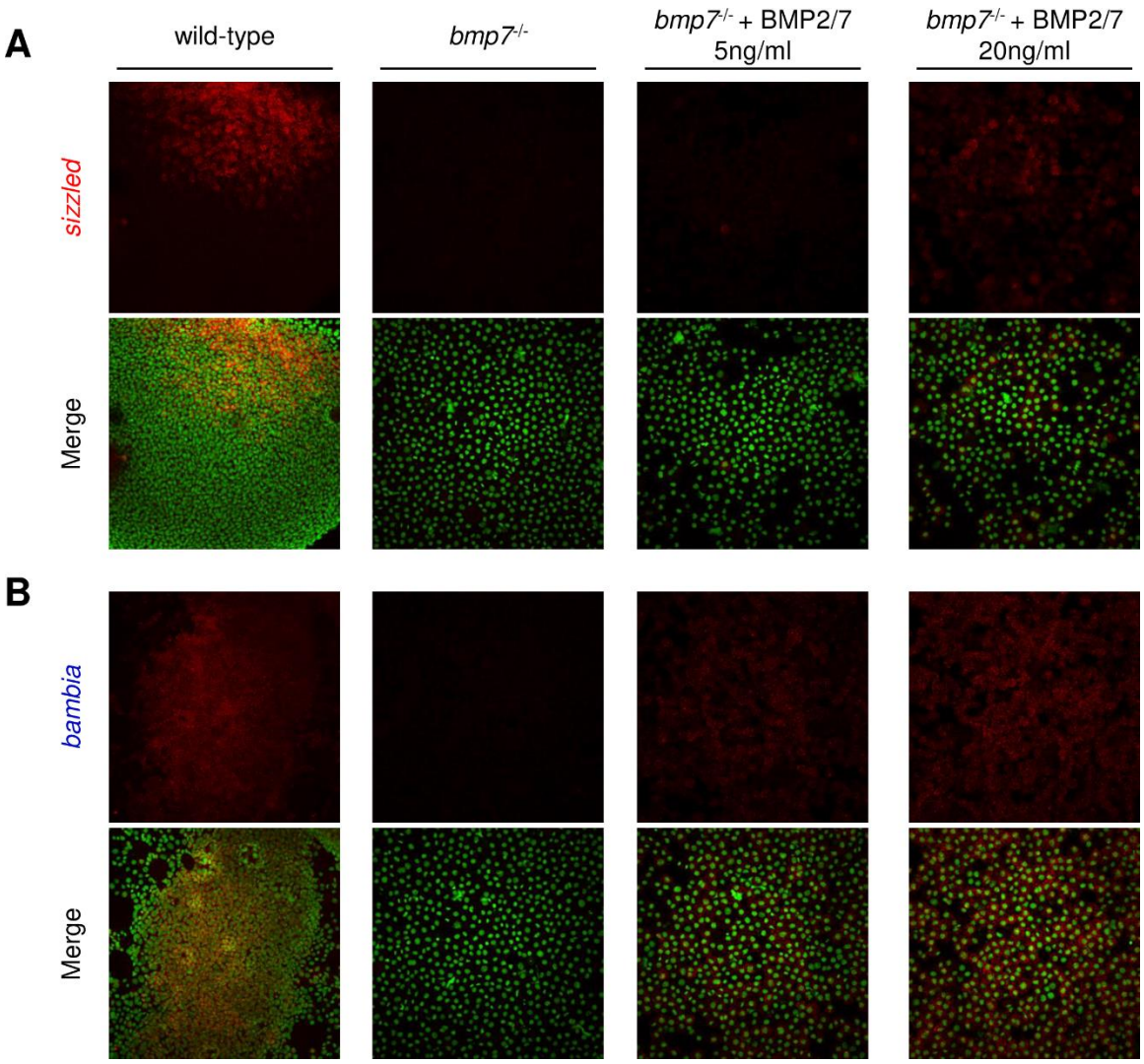

Figure 2.17 Differential response of *sizzled* and *bambia* to BMP concentrations. Related to Figure 2.15. (A) Representative maximum projection of *sizzled* fluorescent *in situ* hybridization in whole-mount wild-type embryos, disassociated cells from *bmp7* mutants and disassociated cells from *bmp7* mutants treated with 5 or 20 ng/ml BMP2/7 protein. Merged image with Sytox Green stained nuclei. (B) Representative maximum projection of *bambia* fluorescent *in situ* hybridization in whole-mount wild-type embryos, disassociated cells from *bmp7* mutants and disassociated cells from *bmp7* mutants treated with 5 or 20ng/ml BMP2/7 protein. Merged image with Sytox Green stained nuclei.

2.3 Discussion

2.3.1 BMP morphogen interpretation: multiple mechanisms for one signaling pathway

Multiple mechanisms have been reported for how a gradient of BMP signaling activity can provide positional information to pattern a tissue. In fact, there is conflicting evidence for how cells perceive gradients of BMP signaling depending on the context. In *Drosophila*, Dpp (the BMP homolog) is required for patterning and proliferation of the wing imaginal disc (Affolter and Basler, 2007; Restrepo et al., 2014). Cells in the wing disc have been suggested to sense the shape of the Dpp gradient (Rogulja and Irvine, 2005) and the relative temporal change of Dpp signaling (Wartlick et al., 2011). There is similar conflicting evidence for BMP patterning the dorsal neural tube. Both signal duration (Tozer et al., 2013) and ligand identity (Andrews et al., 2017) have been proposed to pattern neuronal identities. The mechanisms responsible for cellular interpretation of the BMP signaling gradient could vary in different contexts or by individual target genes. Understanding the mechanism of BMP morphogen interpretation in DV patterning will allow us to compare mechanisms across species and systems.

Here, we provide evidence that the BMP morphogen gradient acting to pattern dorsoventral axial tissues is interpreted in a concentration-dependent manner to activate three target genes underlying ventral cell fate specification. We precisely measured endogenous pSmad5 levels and gene expression

activation within the embryo at a single-cell resolution. We found that the genes directly patterned by the BMP signaling gradient are expressed in at least three distinct domains of the embryo, which correspond to at least three different pSmad5 gradient levels that are required to activate representative target genes from each domain. Further, these pSmad5 levels act as thresholds that cells must reach to activate target gene expression and position gene expression boundaries in the embryo, regardless of gradient shape or exposure time. Together, our data support a model whereby the BMP signaling gradient is interpreted as a concentration-dependent morphogen providing positional information to pattern gene expression along the embryonic DV axis.

2.3.2 Multiple expression domains directly patterned by the BMP gradient

The genes directly patterned by the BMP signaling gradient remained unknown prior to this work. Identification of the genes reading out the BMP gradient during DV patterning is not only critical to study the mechanism of morphogen patterning we report here, it is also valuable for investigations of the ventral cell types specified by this morphogen gradient. Known markers of ventrally derived tissues were found to be directly regulated by BMP signaling such as *tp63* specifying epidermis (Mills et al., 1999; Santos-Pereira et al., 2019), *foxi1* specifying otic placode (Hans et al., 2007; Kwon et al., 2010), and *tfap2c* specifying neural crest precursors (Bhat et al., 2013), as well as genes with unknown roles in cell fate specification. We identified many genes encoding components of BMP and other signaling pathways. Interestingly, BMP signaling

directly activates the canonical Wnt receptors *fzd4/5*, the Nodal signaling cofactor *foxh1*, and the Retinoic Acid binding protein *crabp2b*. This pathway specific feedback may be critical for robust gradient formation and integration of multiple signaling pathways during embryonic patterning. While our analysis identified the initial gene expression read-out of the BMP gradient, further work is needed to resolve the genetic regulatory network committing progenitors to specific ventral cell fates.

To determine the number of positional values established by the BMP signaling gradient, we reanalyzed a scRNA-seq dataset (Farrell et al., 2018) using the Seurat analysis algorithm (Satija et al., 2015) to infer the DV expression domains of the 57 direct targets identified. Based on these results, the target genes were sorted into three DV clusters and validated by analysis of a representative of each cluster as expressed in three distinct embryonic domains. Though we identified three distinct domains, the remaining target genes could further partition into additional domains across the DV axis. These broad overlapping domains will undergo further refinement through regulatory feedback and interaction with other signaling pathways later in development to specify cell fates. For example, the BMP target gene and preplacodal ectodermal marker *dlx3b* is initially broadly expressed in cluster 3 **(Figure 2.4C)**. By late-gastrulation (9 hpf), expression of *dlx3b* is restricted by factors also induced by BMP signaling, *tfap2a/c*, *foxi1* and *gata3* to form bilateral stripes that separate specification of epidermis and preplacodal ectoderm (Kwon et al., 2010). Future

studies will have to address how other broadly expressed domains are refined into sharp, spatially discrete domains.

2.3.3 Concentration, not gradient shape or duration, positions expression boundaries

Our mutant analysis demonstrates that cells do not interpret the pSmad5 gradient slope to activate three spatially distinct target genes. The slope of the pSmad5 gradient undergoes a 2-fold decrease in *chordin* mutants compared to wild-type embryos in the ventral-lateral region (25-75 degrees) and a 2-fold increase in the dorsal-lateral region (125-155 degrees) **(Figure 2.9J-L)**, but the boundaries of target gene expression remain strongly correlated with specific pSmad5 levels **(Figure 2.9G-I)**. Previous analysis of the BMP signaling gradient over time has revealed that the gradient is highly dynamic from mid-blastula to mid-gastrula stages (Tucker et al., 2008; Zinski et al., 2017). Nuclear pSmad5 levels rapidly increase at the most ventral positions (0-25 degrees) from 4.7 to 6.7 hpf. However, the pSmad5 gradient region that we determined patterns target gene expression (70-110 degrees) is remarkably stable during this time (Zinski et al., 2017). Our lab previously found no significant difference in pSmad5 levels in this region during this time period, although the gradient slope undergoes a 2-fold increase (Zinski et al., 2017). Stable pSmad5 levels over time may allow cells to continually read out the gradient to reduce cell-to-cell variability, and steepening of the slope could allow for sharper gene expression boundaries to form.

We also showed that cells do not require integration of BMP signaling over a prolonged duration to pattern the DV axis. We found that cells rapidly activate multiple, distinctly-expressed target genes upon a 30-minute exposure to the BMP ligand. This is consistent with previous studies from our lab showing that BMP signaling prior to gastrulation is not required for DV patterning (Tucker et al., 2008). Specifically, reinitiating BMP signaling activity at 6 hpf in a BMP-deficient embryo rescues DV patterning. However, reinitiating BMP signaling activity at 6.5 hpf in a BMP-deficient embryo failed to rescue. Therefore, while cells do not require integration of BMP signaling before gastrulation, there is a critical window of time in early gastrulation during which cells are responding to BMP signaling. Furthermore, all cells across the DV axis are exposed to BMP signaling for the same amount of time as the gradient forms (Tucker et al., 2008; Zinski et al., 2017). During mid-blastula stages (before 4 hpf), BMP signaling is activated at low levels everywhere, before signaling is cleared from the dorsal side and the gradient steepens (Tucker et al., 2008). Together, these data show that cells do not require differences in BMP signal duration to activate spatially-distinct target genes.

While BMP signal duration or gradient slope has been shown to pattern tissues in other contexts, we find that distinct pSmad5 threshold levels pattern the embryonic DV axis. It will be important to investigate the molecular mechanism by which these thresholds activate target genes to compare BMP interpretation across contexts. The molecular mechanisms that establish different

pSmad5 thresholds will be particularly interesting because BMP-responsive Smad transcription factors bind DNA with weak affinity (BabuRajendran et al., 2010; Shi et al., 1998a). Therefore, the classic model where differential affinity of transcription factors to regulatory elements produces spatially-distinct target gene expression patterns alone cannot underlie BMP interpretation. To increase affinity and selectivity for DNA, Smad proteins bind to other high affinity DNA-binding transcription factors (Hill, 2016). Differential DNA-binding of Smad to target gene regulatory elements may be mediated by interactions with these cofactors. In *Drosophila*, the cofactor Zelda is required for BMP target genes to be expressed in the correct domain (Deignan et al., 2016) and may represent such a Smad co-factor. However, a Zelda ortholog is not present in vertebrates, so other co-factors may play this role. Future studies on the association of Smad5 with cofactors or chromatin modifiers will be essential to further uncover the mechanism establishing concentration-dependent morphogen interpretation.

CHAPTER 3: Materials and Methods

Zebrafish

Adult zebrafish were kept at 28°C in a 13-hr light/11-hr dark cycle and procedures were approved by the University of Pennsylvania IACUC. All zebrafish husbandry was performed in accordance with institutional, national ethical and animal welfare guidelines. The embryos used for experiments were between 0-8 hours post fertilization, with some phenotypes tracked 1-2 days post fertilization. Embryos were collected and raised at 28°C in E3 solution. In this study, sex/gender is not relevant since zebrafish sex determination takes place after 25 days post fertilization (Santos et al., 2017). Adult *chordin*^{tt250} homozygous fish were generated by injecting *chordin* mRNA into 1-cell stage *chordin*-/- embryos to rescue the embryonic ventralization and then raised to adulthood.

Wild-type (TU)	RRID: ZIRC_ ZL57
chordin^{tt250}	RRID: ZDB-ALT-980413-523, ZIRC_ZL61
bmp7a^{sb1aub}	RRID: ZFIN_ZDB-ALT-050216-2, ZIRC_ZL1390

Genotyping

Adult and embryonic genomic DNA was obtained using HotShot DNA isolation. Genotyping of adults and embryos for the *chordin* mutation was performed using KASPar genotyping (Smith and Maughan, 2015). Primers were

designed and generated by LGC Bioscience Technologies to the following sequences flanking the [WT/mutant] nucleotide:

chordin^{tt250}	GTTTGGTGTGATGCACTGCGTTATGTGTCATTGTGAGCCG[G/A] TGAGTTGTGCACAGTTCAGTTTGAAATCCATATTGAATCT

pSmad5 Immunostaining, Imaging, and Quantification

pSmad5 immunostaining, imaging, and quantification were performed as previously described (Zinski et al., 2017; Zinski et al., 2019). Embryos were fixed in 4% paraformaldehyde at 4°C, blocked in NCS-PBST, and probed overnight with a 1:100 dilution of anti-phosphoSmad1/5/9 antibody (Cell Signaling Technology Cat# 13820, RRID:AB_2493181), followed by a 1:500 dilution of goat anti-rabbit Alexa Fluor 647 (Molecular Probes Cat# A-21244, RRID:AB_141663) and a 1:1000 dilution of Sytox Green (ThermoFisher Scientific Cat# S7020). Embryos were gradually dehydrated into methanol, then cleared and mounted in BABB, a 1:2 ratio of benzyl alcohol (Sigma B-1042) and benzyl benzoate (Sigma B-6630). Mounted embryos were imaged on a Zeiss LSM880 confocal microscope with an LD LCI Plan-Achromat 25X/0.8 Imm Corr DIC M27 multi-immersion lens in the oil-immersion setting. The same single bead from a calibration slide (ThermoFisher Scientific Cat#F369009, well A1) was imaged between slides to account for any fluctuations in laser power.

Images were analyzed with a custom MATLAB algorithm to identify individual nuclei center-points and extract pSmad5 intensities from within each nucleus (Zinski et al., 2017; Zinski et al., 2019), which were normalized based on the standard calibration bead intensity. Resulting embryos were aligned across the DV axis and conformed using Coherent Point Drift. Population means were generated after genotyping for wild-type and heterozygous sibling controls, since all imaging and analysis was performed blinded. Mean profiles were generated by averaging pSmad5 intensities of cells in a 30μm band. 3-D embryo-wide displays of mean pSmad5 were generated by projecting all nuclei on a sphere divided into 4800 equilateral triangles and nuclei within each triangle averaged together. The pSmad5 gradient slopes were obtained by fitting a lowess fit to the average 3-D data's spherical coordinates phi and theta using the 'fit' function in MATLAB.

Fluorescent *in situ* Hybridization, Imaging, and Quantification

Embryos were fixed in 4% paraformaldehyde at 4°C and gradually dehydrated in methanol. Whole-mount *in situ* hybridizations were performed using DIG-labeled anti-sense RNA probes (made with labeling kit: Roche 11175033910) to *sizzled* (Muraoka et al., 2006)*, foxi1* (Kwon et al., 2010)*,* and *bambia.* Probes were visualized with anti-DIG-Horseradish Peroxidase (Roche 11207733910) developed with TSA Plus Cyanine 3 kits using a 1:50 dilution (Perkin Elmer NEL744001KT) and nuclei were stained with 1:1000 dilution of Sytox Green. Embryos were cleared, mounted, and imaged as described for

immunofluorescence. Images were analyzed using the same MATLAB algorithm, except fluorescent intensity was extracted from a 25 pixel sphere from the center-point of each nucleus to include the cytoplasmic staining.

BMP2/7 Protein Injections

For cycloheximide (CHX) assays, embryos were dechorionated and treated with 10 ug/ml of cycloheximide (Sigma #C4859) at 4 hours post fertilization for 30 minutes. For both the CHX assay and time-course, the embryos were injected with a 3 nl solution containing KCL (0.1 M), bovine serum albumin (BSA; 0.1%), rhodamine-dextran (0.5%) and either 120 or 60 nM of hBMP2-hBMP7 heterodimer (R&D Systems 2339-BM) into the extracellular space. Embryos were allowed to develop for the time indicated, then fixed in 4% paraformaldehyde and processed for RNA extraction, whole-mount pSmad5 immunostaining or fluorescent in situ hybridization.

Cell disassociation cultures

At 4 hpf, *bmp7* mutant embryos were dechorionated and placed into 1X Modified Barth's Saline (MBS) as previously described (Sagerström et al., 2005). One hundred animal caps were removed with forceps, and the collected cells were diluted to a final concentration of 5×10^5 in 1X MBS containing Gentamicin (50 ug/ml; Gibco). The cells were disassociated by quickly vortexing and 5 or 20 ng/ml of hBMP2-hBMP7 heterodimer (R&D Systems 2339-BM) was added to the tube for 2 hours before fixing with 4% paraformaldehyde. To perform

immunofluorescence and FISH, cells were transferred to glass slides by cytospin at 750 rpm for 5 minutes. The pSmad5 immunostaining was performed and analyzed as described above with the slides mounted in Fluoromount-G (Southern Biotechnology Associates) for imaging. For FISH, cells were fixed in 4% paraformaldehyde for 10 min and allowed to air-dry for 1 hour before performing the fluorescent *in situ* hybridization and analyzed as described above with the slides mounted in Vectashield mounting medium (Vector Labs) for imaging. Fluorescent signal was normalized to the median of the top and bottom 5% of cells in wild-type embryos imaged on slides.

RNA-sequencing and Analysis

Two replicates of 40 wild-type and *bmp7* mutants were collected at early gastrula (shield, 6 hpf) and mid-gastrula (70% epiboly, 8 hpf). Three replicates of 50 *bmp7* mutant embryos treated with cycloheximide with or without injected BMP2/7 protein were collected 90 minutes after injection. Total RNA was extracted from dechorionated embryos with Trizol and purified with phenol-chloroform. Libraries were prepared with Illumina TruSeq stranded polyA-selection mRNA kit by the Next-Generation Sequencing Core at the University of Pennsylvania. Libraries were analyzed using the Agilgent BioAnalyzer and Kapa Biosystems library quantitation kit before sequencing on a HiSeq4000. Sequence reads were aligned to the zebrafish GRCz11 genome assembly with RNA-seq Unified Mapper (RUM) (Grant et al., 2011). Differential expression was determined with EdgeR and values were normalized to counts per million. Gene

Ontology (GO) analysis of BMP target genes was performed using the PANTHER classification system for the enrichment analysis (http://pantherdb.org/) and Fisher's exact test and False Discovery Rate (FDR) <0.05 to determine terms that are statistically significant. (Ashburner et al., 2000; Mi et al., 2019).

Seurat Analysis of Single-cell RNA-sequencing Dataset

Previously published scRNA-sequencing from 6,100 individual cells dissociated from 75% epiboly embryos were used (Farrell et al., 2018). Any cell with less than 2,000 genes sequenced were excluded from analysis. Any gene sequenced in fewer than 3 cells were also excluded from analysis. Locations of the 47 landmark genes used are shown in Satija et al., 2015. Expression of target genes were mapped into bins using the Seurat package vesion 1.2 (Satija et al., 2015). Data were normalized in Seurat.

Statistical Analysis

Statistical tests were performed on GraphPad Prism software, and Student's t-tests (two groups) or analysis of variance (three groups) were performed. Error bars represent standard deviation. Figure legends indicate the number of n values for each analysis. Each experiment was performed at least two times.

CHAPTER 4: Conclusions and Future Directions

4.1 Summary of findings

The fundamental developmental biology question of how morphogen gradients impart positional information to pattern tissues has been understudied and is largely unknown. Although the role of BMP signaling in DV axial patterning is conserved from insects to mammals, it was not known how the gradient is interpreted during patterning. The mechanism of BMP gradient interpretation is especially interesting because it has been proposed to differ between biological contexts. This dissertation sought to address how the BMP signaling gradient is interpreted into positional information and multiple cell fates along the dorsal-ventral (DV) axis.

Chapter 1 discussed the intracellular regulation of BMP signaling and how the transcriptional effectors control gene expression. The chapter also explored the role of signaling concentration and duration in morphogen interpretation and potential mechanisms underlying different thresholds. In Chapter 2, I identified over 50 genes that are directly activated by BMP signaling to specify all ventral-lateral cell fates during embryogenesis. I determined that these target genes are expressed in at least three domains using Seurat analysis of single-cell RNA-sequencing data from mid-gastrula embryos. I distinguished between three models of BMP signal interpretation based on signal duration, signaling gradient slope, or signal activation thresholds. To distinguish between these models, I quantitatively measured the endogenous phospho-Smad5 (pSmad5) gradient and position of target gene expression within the embryo at a single-cell

resolution. I eliminated gradient slope or signal duration as mechanisms to activate spatially-distinct target gene expression. I determined that the gradient of BMP signaling is interpreted in a pSmad5 concentration-dependent manner to activate target genes underlying ventral-lateral cell fates. I found that cells respond to at least three distinct threshold levels of BMP signaling activity to activate and position target gene expression, regardless of signaling gradient shape, slope, or signal duration. Our work is the first to demonstrate that BMP signaling can activate gene expression in a concentration-dependent manner *in vivo*. Overall, this work has contributed to the understanding of how morphogens can impart positional information during tissue patterning.

4.2 Translating gene expression domains into cell fates

4.2.1 Identification of BMP target genes

We identified 57 genes directly upregulated and 15 genes directly downregulated by BMP signaling during DV patterning. While BMP signaling was previously thought to repress dorsal cell fates indirectly through expression of *vox*, *vent*, and *ved* (Imai et al., 2001; Shimizu et al., 2002), we have found that BMP signaling can directly repress the expression of the BMP antagonist *chordin,* as well as other neural ectodermal genes. A subset of the genes that are upregulated by BMP signaling have roles in ventral fate specification, such as *tp63* specifying the epidermis, *foxi1* specifying the preplacodal ectoderm, and *tfap2c* specifying the neural crest. Further investigations of the genetic networks downstream will determine how these transcription factors initiate the genetic

cascade that specify all of the ventral cell fates in the embryo. Nine of the 57 target genes directly regulate the BMP signaling pathway itself including both positive and negative regulators. BMP signaling activates the expression of extracellular inhibitors (*szl, bambia, tll1*), the *bmp4* ligand, I-Smads (*smad6a, smad6b, smad7*), and the R-Smads *smad9* during gastrulation. Positive and negative feedback of BMP signaling may be important for robustness during gradient formation and should be explored in future studies.

We found BMP signaling also directly regulates the components of other signaling pathways during DV patterning. While BMP signaling downregulates *ip6k2a*, an effector of the Hedgehog pathway (Sarmah and Wente, 2010), BMP signaling directly activates the canonical Wnt receptors *fzd4/5*, the Nodal signaling cofactor *foxh1*, and the Retinoic Acid binding protein *crabp2b*. As described in Chapter 1, Wnt, Nodal and RA signaling contribute to anterior-posterior axial patterning. Integration of these signaling pathways to pattern the two body axes has been shown to occur at the level of Smad phosphorylation and regulation, but our work suggests that additional signal integration may also occur through direct transcriptional feedback.

4.2.2 Refinement of expression domains

We have found that genes responding to the BMP signaling gradient are initially expressed in at least three overlapping domains across the DV axis. Analysis of additional target genes may uncover additional domains patterned by the BMP gradient. How precise is the BMP gradient to position these expression

boundaries in the embryo? Does variability in the level of BMP signaling activity correlate to variability in the position of gene expression boundaries? The variability in pSmad5 levels ranges from about 10% in the dorsal region to 24% in the ventral region (Zinski et al., 2017). The expression boundaries for the three target genes are located between 70º and 107º **(Figure 2.3K)**, and this is also the region that contains the lowest variability of pSmad5 levels **(Figure 4.1A-B)**. The current method of measuring pSmad5 levels and gene expression levels in separate embryos limits analysis to comparisons between average positions. Simultaneous measurements of single-molecule fluorescent *in situ* hybridization (smFISH) and pSmad5 immunostaining will be required to compare variability of pSmad5 levels to variability of target gene expression between individual cells. The use of intron-specific FISH probes will also enable measurements of nascent transcripts in response to the immediate readout of pSmad5 levels.

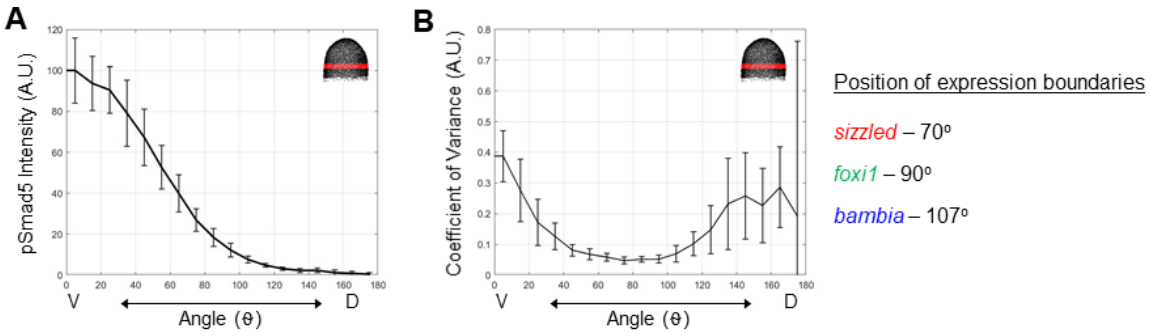

Figure 4.1 Variability of pSmad5 levels across the DV axis. (A) Average pSmad5 levels across the DV axis. Data presented in Figure 2.7. The intensity is averaged from a 40 µm band of cells around the DV axis at the location shown in red in the right corner embryo schematic of each panel. (B) The coefficient of variance of pSmad5 levels across the DV axis shown in (A).

The use of smFISH will enable quantitative measurements of target gene transcripts across the DV axis of the embryo. Recent work has demonstrated that the BMP signaling gradient in Drosophila produces a graded mRNA distribution of two target genes, *ush* and *hnt* (Hoppe et al., 2020). Interestingly, we also observe graded expression of three target genes across the DV axis **(Figure 2.6C-E)**, but expression levels would need to be validated using quantitative FISH. The graded mRNA distribution of *ush* and *hnt* in Drosophila was proposed to reflect differences in transcriptional burst kinetics that is regulated by the level of BMP signaling. Cells receiving high levels of BMP signaling have increased *ush* and *hnt* transcript levels and more active alleles than cells receiving low levels of BMP signaling. Whether the level of BMP signaling activity modulates the rate of promoter activation in zebrafish DV patterning will be an exciting area of future research.

The BMP gradient is highly dynamic from mid-blastula to mid-gastrula stages (Tucker et al., 2008; Zinski et al., 2017) **(Figure 4.2A)**. While the levels of pSmad5 increase 2-fold in the ventral region of the embryo, the pSmad5 levels in the lateral region remain stable (Zinski et al., 2017). The shape of the gradient is also rapidly changing during gastrulation. A shallow gradient becomes increasingly steep and the gradient slope is highest in the lateral region of the embryo **(Figure 2.7G-I)**. Steepening of the slope over time may allow for the formation of sharper gene expression boundaries. The expression domains are also dynamic from mid-blastula to mid-gastrula stages **(Figure 4.2B-C)**. The

expression of *sizzled* and *foxi1* is not observed until 6.3 hpf. The expression domains of both *sizzled* and *foxi1* expand along the DV axis during gastrulation. Interestingly, expression of *foxi1* was not detected by FISH at 5.7 hpf even though cells have reached pSmad5 levels above the predicted threshold level **(Figure 4.2C)**. While *foxi1* expression levels need to be validated by qPCR, it is possible the embryo may not be competent to express *foxi1* at 5.7 hpf, even in response to sufficiently high levels of pSmad5. Competency to BMP signaling will be addressed later in the chapter.

The initial readout of the BMP gradient results in the formation of broad overlapping domains of target genes. The refinement of these domains into discrete domains of gene expression requires downstream genetic regulatory networks and interaction with other signaling pathways. The most dramatic refinement of an expression domain patterned initially by BMP signaling specifies the preplacodal ectoderm, which contributes to the formation of sensory organs. Progenitors of the preplacodal ectoderm are initially broadly specified by BMP signaling across the DV axis. We have found that markers for preplacodal ectoderm respond to intermediate (*foxi1*) and low (*tfap2c*) levels of pSmad5. By the end of gastrulation, the preplacodal ectoderm progenitors are restricted to a narrow band around the anterior neural plate (Kwon et al., 2010). BMP signaling is not required for specification of preplacodal ectoderm after early-gastrula stages and is no longer required to maintain the expression of *foxi1* and *tfap2c.* FGF signaling is then required for refinement and specification of preplacodal

tissues. How other domains become resolved and differentiate into cell fates is not known for many ventral tissues, but our identification of the initial readout of the BMP gradient may inform the identity of the upstream master-regulators that control cell fate specification.

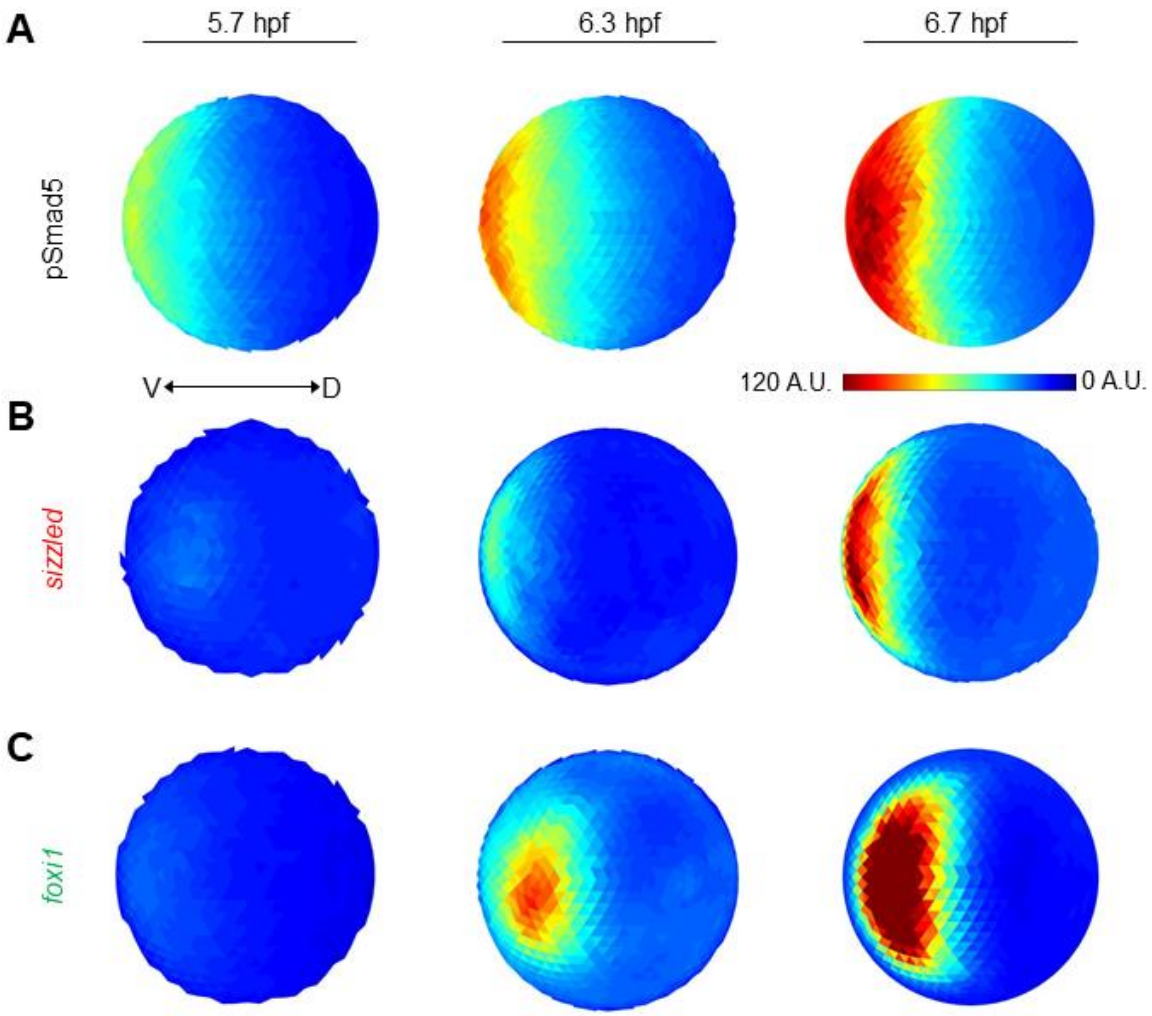

Figure 4.2 Dynamic pSmad5 levels and target gene expression during gastrulation. (A) Animal view, dorsal to right of mean pSmad5 intensities in wild-type embryos at 5.7 hpf (n=5), 6.3 hpf (n=5), and 6.7 hpf (n=5). (B-C) Animal views of average fluorescent *in situ* hybridization signal in wild-type embryos at early-gastrula 5.7 hpf, 6.3 hpf, and 6.7 hpf of *sizzled* (E) (n=5,5,5) and *foxi1* (F) (n=8,8,8). A.U. is arbitrary units.

4.3 Generation of different thresholds

4.3.1 Differences in pSmad5 binding site affinity

We have identified three target genes that are activated by distinct concentration-thresholds of pSmad5. The essential question remains how these genes are regulated by different levels of signaling activity. Differences in binding site affinity is classically thought to be the mechanism of concentration-dependent responsiveness. Identification of pSmad5 binding sites at the regulatory region of target genes will allow the comparison of the binding site affinity between genes activated by different pSmad5 threshold levels. The pSmad5 binding sites can be identified by chromatin immunoprecipitation (ChIP)-seq, but antibody availability and heterogeneity within the embryo make the experiment challenging. The small size of the SBE makes it difficult to predict Smad binding sites by searching for enrichment of the consensus sequence within regulatory regions. However, differences in Smad5 binding site affinity have been identified in response to BMP signaling in human endothelial cells (Morikawa et al., 2011). The sequences GGCGCC, GGAGCC, and GCCG were all found to be enriched in Smad1/5 binding regions by ChIP-seq, and Smad1/5 was shown to have a lower affinity for the GGAGCC sequence. Once the binding sites of pSmad5 have been identified, the sequences could be cloned into a reporter construct to determine whether differences in the pSmad5 binding site is sufficient to drive expression within the endogenous expression domain.

4.3.2 Smad5 cofactors during DV patterning

To increase affinity and selectivity for DNA, Smad transcription factors bind to other DNA-binding cofactors. It is not known which cofactors are required for targeting pSmad5 to DNA during DV patterning in the zebrafish, and very few cofactors have been identified for Smad1/5/9 in general. One likely candidate cofactor is the zebrafish Oct4 homolog, Pou5f3. Maternal-zygotic (MZ) Pou5f3 mutants are dorsalized and lack *tp63* expression, a known BMP target gene we also found by RNA-seq (Belting et al., 2011). It is not known if the expression of other BMP target genes is reduced in the MZ-*pou5f3* mutant embryos. The interaction between Smad5 and Pou5f3 needs to be validated in zebrafish. It will be interesting to determine if there is a common set of cofactors for all BMP target genes, or if there are differences in cofactors associated with genes activated by different threshold levels of signaling.

Differences in cofactor association have been shown to target Smads to different transcriptional targets and may underlie differences in concentration-thresholds. The transcription factors Zelda and Zen were found to bind the regulatory regions of BMP target genes in Drosophila (Deignan et al., 2016). The expression domain of the low threshold target gene *ush* was reduced in *zen* mutants, while the expression of the high threshold target gene *hnt* was lost. This suggests that Zen increases responsiveness to BMP signaling. Zelda was found to be required for positioning the expression boundary of another high threshold target *Race*. Mutations in the Zelda binding site of the *Race* enhancer reduced

the expression of *Race*, while additional Zelda binding sites broadened the expression domain in the embryo. Zen and Zelda may act as cofactors for pMad to increase the expression domains of *ush* and *hnt*. Association with cofactors may increase pSmad5 affinity for DNA for a subset of target genes and allow genes to respond to lower levels of signal. It will be exciting to explore whether cofactor association with pSmad5 mediates BMP gradient interpretation in DV axial patterning.

4.3.3 Differences in pSmad5 threshold across the AV axis

Simultaneous patterning of the DV and AV axis in the zebrafish requires the integration of multiple signaling pathways. Just as varying the level of BMP signaling specifies more ventral cell fates, gradients of FGF and Nodal signaling specify more posterior fates. Ultimately, cell fate specification depends on cells responding to multiple signaling inputs. We have observed that cells respond to BMP signaling differently depending on their location across the AV axis for a subset of target gene expression. By comparing the level of pSmad5 and the level of gene expression at different positions of the embryo, we see that cells uniformly express *sizzled* in response to BMP signaling across the AV axis **(Figure 4.3A)**. However, the expression of *foxi1* is restricted to the animal pole of the embryo **(Figure 4.3B)**. FGF and Nodal signaling emanating from the margin restrict expression of *foxi1,* as well as other ventral ectodermal genes. When FGF signaling is inhibited, *foxi1* expression is expanded all the way to the margin of the embryo (Hans et al., 2007). Interestingly, we have found that cells at the

margin are more responsive to express *bambia* than cells at the animal pole **(Figure 4.3C)**. This suggests that cells at the margin have a lower threshold for *bambia* expression then those at the animal pole. It is possible that integration between FGF and Nodal signaling or repression in the animal pole modulates BMP responsiveness and the pSmad5 threshold for a subset of target genes.

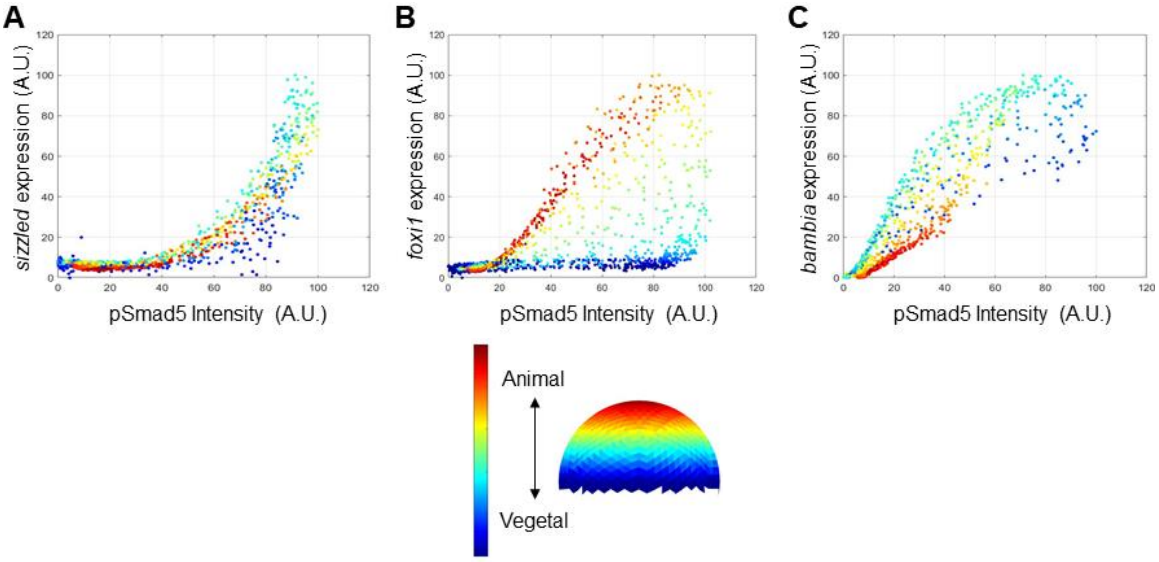

Figure 4.3 Response to BMP signaling across the animal-vegetal axis. (A-C) Average pSmad5 level and fluorescent *in situ* hybridization intensity for *sizzled* (A), *foxi1* (B), and *bambia* (C) in individual positions of the embryo. The color of the marker indicates the location along the AV axis.

4.4 Competency of BMP signaling during patterning

Previous work from our lab has identified the temporal window when the DV axis is patterned in the zebrafish embryo (Tucker et al., 2008). Inhibiting BMP signaling after 8 hpf has no effect on DV patterning and the embryos develop normally. This suggests that cells become refractory to reductions in BMP signaling after mid-gastrula stages. However, there is recent evidence that cells in the animal pole remain responsive to BMP signaling even after the temporal window of endogenous patterning has passed. MZ mutants for Bmp1a, a

metalloprotease that inactivates Chordin, display severely reduced pSmad5 levels at early gastrula stages but still develop into wild-type adults (Tuazon et al., 2020). By mid-gastrula stages, high pSmad5 levels in ventral regions are restored and the gradient partially recovers in MZ-*bmp1a* mutant embryo. To test if cells remain responsive to BMP signaling at mid-gastrula stages to express ventral anterior markers, we injected BMP2/7 protein into the intercellular space of mid-gastrula *bmp7* mutant embryos **(Figure 4.4A)**. Embryos were fixed 1.5 hours post injection and for FISH for *foxi1* expression, a preplacodal ectoderm marker. We surprisingly saw the induction of *foxi1* expression after initiating BMP signaling at timepoints later than when ventral-anterior domains were thought to be specified **(Figure 4.4B)**. This raises questions on the plasticity of the embryo during DV patterning and how responsiveness to BMP signaling is maintained.

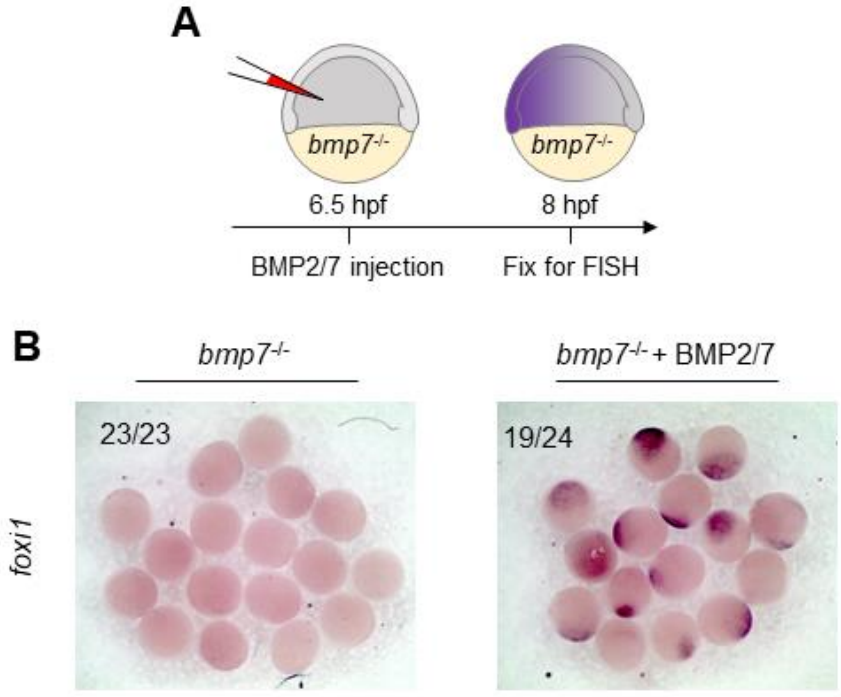

Figure 4.4 Mid-gastrula embryos remain competent to BMP signaling. (A) Experimental schematic of a *bmp7* mutant embryo injected with 10 pg BMP2/7

protein that is fixed 1.5 post-injection for FISH. (B) FISH for *foxi1* in *bmp7* mutants uninjected or injected with 10 pg BMP2/7 protein.

4.5 Concluding Remarks

Overall, this work provides a better understanding of how the gradient of BMP signaling positions gene expression during dorsal-ventral axial patterning in the zebrafish embryo. Gradients of BMP signaling pattern many tissues during development, and this work will further the understanding of how BMP signaling gradients are translated into multiple cell fates. Additionally, BMP signaling is associated with many congenital and adult diseases, including cancers, pulmonary hypertension, and osteoporosis, and BMP signaling has exciting roles in medical applications and tissue engineering. Uncovering the mechanism of how BMP regulates gene expression has broad implications to our understanding of both development and disease.

BIBLIOGRAPHY

Affolter, M., and Basler, K. (2007). The Decapentaplegic morphogen gradient: from pattern formation to growth regulation. Nature reviews Genetics *8*, 663-674.

Akizu, N., Estarás, C., Guerrero, L., Martí, E., and Martínez-Balbás, M.A. (2010). H3K27me3 regulates BMP activity in developing spinal cord. Development (Cambridge, England) *137*, 2915-2925.

Alarcón, C., Zaromytidou, A.I., Xi, Q., Gao, S., Yu, J., Fujisawa, S., Barlas, A., Miller, A.N., Manova-Todorova, K., Macias, M.J.*, et al.* (2009). Nuclear CDKs drive Smad transcriptional activation and turnover in BMP and TGF-beta pathways. Cell *139*, 757-769.

Andrews, M.G., Del Castillo, L.M., Ochoa-Bolton, E., Yamauchi, K., Smogorzewski, J., and Butler, S.J. (2017). BMPs direct sensory interneuron identity in the developing spinal cord using signal-specific not morphogenic activities. eLife *6*.

Aragón, E., Goerner, N., Zaromytidou, A.I., Xi, Q., Escobedo, A., Massagué, J., and Macias, M.J. (2011). A Smad action turnover switch operated by WW domain readers of a phosphoserine code. Genes & development *25*, 1275-1288.

Armes, N.A., and Smith, J.C. (1997). The ALK-2 and ALK-4 activin receptors transduce distinct mesoderm-inducing signals during early Xenopus development but do not co-operate to establish thresholds. Development (Cambridge, England) *124*, 3797-3804.

Arora, K., Dai, H., Kazuko, S.G., Jamal, J., O'Connor, M.B., Letsou, A., and Warrior, R. (1995). The Drosophila schnurri gene acts in the Dpp/TGF beta signaling pathway and encodes a transcription factor homologous to the human MBP family. Cell *81*, 781-790.

Ashburner, M., Ball, C.A., Blake, J.A., Botstein, D., Butler, H., Cherry, J.M., Davis, A.P., Dolinski, K., Dwight, S.S., Eppig, J.T.*, et al.* (2000). Gene ontology: tool for the unification of biology. The Gene Ontology Consortium. Nature genetics *25*, 25-29.

Ashe, H.L., and Briscoe, J. (2006). The interpretation of morphogen gradients. Development (Cambridge, England) *133*, 385-394.

Ashe, H.L., Mannervik, M., and Levine, M. (2000). Dpp signaling thresholds in the dorsal ectoderm of the Drosophila embryo. Development (Cambridge, England) *127*, 3305-3312.

Aubin, J., Davy, A., and Soriano, P. (2004). In vivo convergence of BMP and MAPK signaling pathways: impact of differential Smad1 phosphorylation on development and homeostasis. Genes & development *18*, 1482-1494.

BabuRajendran, N., Palasingam, P., Narasimhan, K., Sun, W., Prabhakar, S., Jauch, R., and Kolatkar, P.R. (2010). Structure of Smad1 MH1/DNA complex reveals distinctive rearrangements of BMP and TGF-beta effectors. Nucleic acids research *38*, 3477-3488.

Balaskas, N., Ribeiro, A., Panovska, J., Dessaud, E., Sasai, N., Page, K.M., Briscoe, J., and Ribes, V. (2012). Gene regulatory logic for reading the Sonic Hedgehog signaling gradient in the vertebrate neural tube. Cell *148*, 273-284.

Beddington, R.S., and Robertson, E.J. (1999). Axis development and early asymmetry in mammals. Cell *96*, 195-209.

Belting, H.G., Wendik, B., Lunde, K., Leichsenring, M., Mössner, R., Driever, W., and Onichtchouk, D. (2011). Pou5f1 contributes to dorsoventral patterning by positive regulation of vox and modulation of fgf8a expression. Developmental biology *356*, 323-336.

Ben-Haim, N., Lu, C., Guzman-Ayala, M., Pescatore, L., Mesnard, D., Bischofberger, M., Naef, F., Robertson, E.J., and Constam, D.B. (2006). The nodal precursor acting via activin receptors induces mesoderm by maintaining a source of its convertases and BMP4. Developmental cell *11*, 313-323.

Bhat, N., Kwon, H.J., and Riley, B.B. (2013). A gene network that coordinates preplacodal competence and neural crest specification in zebrafish. Developmental biology *373*, 107-117.

Bier, E., and De Robertis, E.M. (2015). EMBRYO DEVELOPMENT. BMP gradients: A paradigm for morphogen-mediated developmental patterning. Science (New York, NY) *348*, aaa5838.

Blanco Calvo, M., Bolós Fernández, V., Medina Villaamil, V., Aparicio Gallego, G., Díaz Prado, S., and Grande Pulido, E. (2009). Biology of BMP signalling and cancer. Clinical & translational oncology : official publication of the Federation of Spanish Oncology Societies and of the National Cancer Institute of Mexico *11*, 126-137.

Blitz, I.L., and Cho, K.W. (2009). Finding partners: how BMPs select their targets. Developmental dynamics : an official publication of the American Association of Anatomists *238*, 1321-1331.

Briscoe, J., and Small, S. (2015). Morphogen rules: design principles of gradient-mediated embryo patterning. Development (Cambridge, England) *142*, 3996-4009.

Brugger, S.M., Merrill, A.E., Torres-Vazquez, J., Wu, N., Ting, M.C., Cho, J.Y., Dobias, S.L., Yi, S.E., Lyons, K., Bell, J.R.*, et al.* (2004). A phylogenetically conserved cis-regulatory module in the Msx2 promoter is sufficient for BMP-dependent transcription in murine and Drosophila embryos. Development (Cambridge, England) *131*, 5153-5165.

Cechmanek, P.B., and McFarlane, S. (2017). Retinal pigment epithelium expansion around the neural retina occurs in two separate phases with distinct mechanisms. Developmental dynamics : an official publication of the American Association of Anatomists *246*, 598-609.

Ceinos, R.M., Torres-Nuñez, E., Chamorro, R., Novoa, B., Figueras, A., Ruane, N.M., and Rotllant, J. (2013). Critical role of the matricellular protein SPARC in mediating erythroid progenitor cell development in zebrafish. Cells, tissues, organs *197*, 196-208.

Chacko, B.M., Qin, B.Y., Tiwari, A., Shi, G., Lam, S., Hayward, L.J., De Caestecker, M., and Lin, K. (2004). Structural basis of heteromeric smad protein assembly in TGF-beta signaling. Molecular cell *15*, 813-823.

Chai, N., Li, W.X., Wang, J., Wang, Z.X., Yang, S.M., and Wu, J.W. (2015). Structural basis for the Smad5 MH1 domain to recognize different DNA sequences. Nucleic acids research *43*, 9051-9064.

Chaikuad, A., and Bullock, A.N. (2016). Structural Basis of Intracellular TGF-β Signaling: Receptors and Smads. Cold Spring Harbor perspectives in biology *8*.

Chen, H.B., Shen, J., Ip, Y.T., and Xu, L. (2006). Identification of phosphatases for Smad in the BMP/DPP pathway. Genes & development *20*, 648-653.

Chen, X., Rubock, M.J., and Whitman, M. (1996). A transcriptional partner for MAD proteins in TGF-beta signalling. Nature *383*, 691-696.

Collery, R.F., and Link, B.A. (2011). Dynamic smad-mediated BMP signaling revealed through transgenic zebrafish. Developmental dynamics : an official publication of the American Association of Anatomists *240*, 712-722.

Dahle, Ø., Kumar, A., and Kuehn, M.R. (2010). Nodal signaling recruits the histone demethylase Jmjd3 to counteract polycomb-mediated repression at target genes. Science signaling *3*, ra48.

Dal-Pra, S., Fürthauer, M., Van-Celst, J., Thisse, B., and Thisse, C. (2006). Noggin1 and Follistatin-like2 function redundantly to Chordin to antagonize BMP activity. Developmental biology *298*, 514-526.

De Robertis, E.M., and Kuroda, H. (2004). Dorsal-ventral patterning and neural induction in Xenopus embryos. Annual review of cell and developmental biology *20*, 285-308.

Deignan, L., Pinheiro, M.T., Sutcliffe, C., Saunders, A., Wilcockson, S.G., Zeef, L.A., Donaldson, I.J., and Ashe, H.L. (2016). Regulation of the BMP Signaling-Responsive Transcriptional Network in the Drosophila Embryo. PLoS genetics *12*, e1006164.

Dennler, S., Itoh, S., Vivien, D., ten Dijke, P., Huet, S., and Gauthier, J.M. (1998). Direct binding of Smad3 and Smad4 to critical TGF beta-inducible elements in the promoter of human plasminogen activator inhibitor-type 1 gene. The EMBO journal *17*, 3091-3100.

Dessaud, E., Ribes, V., Balaskas, N., Yang, L.L., Pierani, A., Kicheva, A., Novitch, B.G., Briscoe, J., and Sasai, N. (2010). Dynamic assignment and maintenance of positional identity in the ventral neural tube by the morphogen sonic hedgehog. PLoS biology *8*, e1000382.

Dessaud, E., Yang, L.L., Hill, K., Cox, B., Ulloa, F., Ribeiro, A., Mynett, A., Novitch, B.G., and Briscoe, J. (2007). Interpretation of the sonic hedgehog morphogen gradient by a temporal adaptation mechanism. Nature *450*, 717-720.

Dick, A., Hild, M., Bauer, H., Imai, Y., Maifeld, H., Schier, A.F., Talbot, W.S., Bouwmeester, T., and Hammerschmidt, M. (2000). Essential role of Bmp7 (snailhouse) and its prodomain in dorsoventral patterning of the zebrafish embryo. Development (Cambridge, England) *127*, 343-354.

Dorey, K., and Amaya, E. (2010). FGF signalling: diverse roles during early vertebrate embryogenesis. Development (Cambridge, England) *137*, 3731-3742.

Dubrulle, J., Jordan, B.M., Akhmetova, L., Farrell, J.A., Kim, S.H., Solnica-Krezel, L., and Schier, A.F. (2015). Response to Nodal morphogen gradient is determined by the kinetics of target gene induction. eLife *4*.

Dunipace, L., Ozdemir, A., and Stathopoulos, A. (2011). Complex interactions between cis-regulatory modules in native conformation are critical for Drosophila snail expression. Development (Cambridge, England) *138*, 4075-4084.

Dutko, J.A., and Mullins, M.C. (2011). SnapShot: BMP signaling in development. Cell *145*, 636, 636.e631-632.

Duval, N., Vaslin, C., Barata, T.C., Frarma, Y., Contremoulins, V., Baudin, X., Nedelec, S., and Ribes, V.C. (2019). BMP4 patterns Smad activity and generates stereotyped cell fate organization in spinal organoids. Development (Cambridge, England) *146*.

Dyson, S., and Gurdon, J.B. (1998). The interpretation of position in a morphogen gradient as revealed by occupancy of activin receptors. Cell *93*, 557-568.

Economou, A.D., and Hill, C.S. (2020). Temporal dynamics in the formation and interpretation of Nodal and BMP morphogen gradients. Current topics in developmental biology *137*, 363-389.

Farrell, J.A., Wang, Y., Riesenfeld, S.J., Shekhar, K., Regev, A., and Schier, A.F. (2018). Single-cell reconstruction of developmental trajectories during zebrafish embryogenesis. Science (New York, NY) *360*.

Feng, X.H., Zhang, Y., Wu, R.Y., and Derynck, R. (1998). The tumor suppressor Smad4/DPC4 and transcriptional adaptor CBP/p300 are coactivators for smad3 in TGF-beta-induced transcriptional activation. Genes & development *12*, 2153-2163.

Fuentealba, L.C., Eivers, E., Ikeda, A., Hurtado, C., Kuroda, H., Pera, E.M., and De Robertis, E.M. (2007). Integrating patterning signals: Wnt/GSK3 regulates the duration of the BMP/Smad1 signal. Cell *131*, 980-993.

Fürthauer, M., Thisse, B., and Thisse, C. (1999). Three different noggin genes antagonize the activity of bone morphogenetic proteins in the zebrafish embryo. Developmental biology *214*, 181-196.

Goudevenou, K., Martin, P., Yeh, Y.J., Jones, P., and Sablitzky, F. (2011). Def6 is required for convergent extension movements during zebrafish gastrulation downstream of Wnt5b signaling. PloS one *6*, e26548.

Graff, J.M., Thies, R.S., Song, J.J., Celeste, A.J., and Melton, D.A. (1994). Studies with a Xenopus BMP receptor suggest that ventral mesoderm-inducing signals override dorsal signals in vivo. Cell *79*, 169-179.

Grant, G.R., Farkas, M.H., Pizarro, A.D., Lahens, N.F., Schug, J., Brunk, B.P., Stoeckert, C.J., Hogenesch, J.B., and Pierce, E.A. (2011). Comparative analysis of RNA-Seq alignment algorithms and the RNA-Seq unified mapper (RUM). Bioinformatics (Oxford, England) *27*, 2518-2528.

Green, J.B., New, H.V., and Smith, J.C. (1992). Responses of embryonic Xenopus cells to activin and FGF are separated by multiple dose thresholds and correspond to distinct axes of the mesoderm. Cell *71*, 731-739.

Green, J.B., and Smith, J.C. (1990). Graded changes in dose of a Xenopus activin A homologue elicit stepwise transitions in embryonic cell fate. Nature *347*, 391-394.

Gurdon, J.B., Mitchell, A., and Mahony, D. (1995). Direct and continuous assessment by cells of their position in a morphogen gradient. Nature *376*, 520-521.

Hannon, C.E., Blythe, S.A., and Wieschaus, E.F. (2017). Concentration dependent chromatin states induced by the bicoid morphogen gradient. eLife *6*.

Hans, S., Christison, J., Liu, D., and Westerfield, M. (2007). Fgf-dependent otic induction requires competence provided by Foxi1 and Dlx3b. BMC developmental biology *7*, 5.

Harfe, B.D., Scherz, P.J., Nissim, S., Tian, H., McMahon, A.P., and Tabin, C.J. (2004). Evidence for an expansion-based temporal Shh gradient in specifying vertebrate digit identities. Cell *118*, 517-528.

Hashiguchi, M., and Mullins, M.C. (2013). Anteroposterior and dorsoventral patterning are coordinated by an identical patterning clock. Development (Cambridge, England) *140*, 1970-1980.

Heemskerk, I., Burt, K., Miller, M., Chhabra, S., Guerra, M.C., Liu, L., and Warmflash, A. (2019). Rapid changes in morphogen concentration control self-organized patterning in human embryonic stem cells. eLife *8*.

Hikasa, H., and Sokol, S.Y. (2013). Wnt signaling in vertebrate axis specification. Cold Spring Harbor perspectives in biology *5*, a007955.

Hild, M., Dick, A., Rauch, G.J., Meier, A., Bouwmeester, T., Haffter, P., and Hammerschmidt, M. (1999). The smad5 mutation somitabun blocks Bmp2b signaling during early dorsoventral patterning of the zebrafish embryo. Development (Cambridge, England) *126*, 2149-2159.

Hill, C.S. (2016). Transcriptional Control by the SMADs. Cold Spring Harbor perspectives in biology *8*.

Hoppe, C., Bowles, J.R., Minchington, T.G., Sutcliffe, C., Upadhyai, P., Rattray, M., and Ashe, H.L. (2020). Modulation of the Promoter Activation Rate Dictates the Transcriptional Response to Graded BMP Signaling Levels in the Drosophila Embryo. Developmental cell *54*, 727-741.e727.

Huang, A., Amourda, C., Zhang, S., Tolwinski, N.S., and Saunders, T.E. (2017). Decoding temporal interpretation of the morphogen Bicoid in the early Drosophila embryo. eLife *6*.

Imai, Y., Gates, M.A., Melby, A.E., Kimelman, D., Schier, A.F., and Talbot, W.S. (2001). The homeobox genes vox and vent are redundant repressors of dorsal fates in zebrafish. Development (Cambridge, England) *128*, 2407-2420.

Ishida, W., Hamamoto, T., Kusanagi, K., Yagi, K., Kawabata, M., Takehara, K., Sampath, T.K., Kato, M., and Miyazono, K. (2000). Smad6 is a Smad1/5-induced smad inhibitor. Characterization of bone morphogenetic protein-responsive element in the mouse Smad6 promoter. The Journal of biological chemistry *275*, 6075-6079.

Joly, J.S., Joly, C., Schulte-Merker, S., Boulekbache, H., and Condamine, H. (1993). The ventral and posterior expression of the zebrafish homeobox gene eve1 is perturbed in dorsalized and mutant embryos. Development (Cambridge, England) *119*, 1261-1275.

Kang, J.S., Alliston, T., Delston, R., and Derynck, R. (2005). Repression of Runx2 function by TGF-beta through recruitment of class II histone deacetylases by Smad3. The EMBO journal *24*, 2543-2555.

Karaulanov, E., Knöchel, W., and Niehrs, C. (2004). Transcriptional regulation of BMP4 synexpression in transgenic Xenopus. The EMBO journal *23*, 844-856.

Kim, J., Johnson, K., Chen, H.J., Carroll, S., and Laughon, A. (1997). Drosophila Mad binds to DNA and directly mediates activation of vestigial by Decapentaplegic. Nature *388*, 304-308.

Knockaert, M., Sapkota, G., Alarcón, C., Massagué, J., and Brivanlou, A.H. (2006). Unique players in the BMP pathway: small C-terminal domain phosphatases dephosphorylate Smad1 to attenuate BMP signaling. Proceedings of the National Academy of Sciences of the United States of America *103*, 11940-11945.

Kramer, C., Mayr, T., Nowak, M., Schumacher, J., Runke, G., Bauer, H., Wagner, D.S., Schmid, B., Imai, Y., Talbot, W.S.*, et al.* (2002). Maternally supplied Smad5 is required for ventral specification in zebrafish embryos prior to zygotic Bmp signaling. Developmental biology *250*, 263-279.

Kretzschmar, M., Doody, J., and Massagué, J. (1997). Opposing BMP and EGF signalling pathways converge on the TGF-beta family mediator Smad1. Nature *389*, 618-622.

Kudoh, T., Concha, M.L., Houart, C., Dawid, I.B., and Wilson, S.W. (2004). Combinatorial Fgf and Bmp signalling patterns the gastrula ectoderm into prospective neural and epidermal domains. Development (Cambridge, England) *131*, 3581-3592.

Kunwar, P.S., Zimmerman, S., Bennett, J.T., Chen, Y., Whitman, M., and Schier, A.F. (2003). Mixer/Bon and FoxH1/Sur have overlapping and divergent roles in Nodal signaling and mesendoderm induction. Development (Cambridge, England) *130*, 5589-5599.

Kwon, H.J., Bhat, N., Sweet, E.M., Cornell, R.A., and Riley, B.B. (2010). Identification of early requirements for preplacodal ectoderm and sensory organ development. PLoS genetics *6*, e1001133.

Lane, K.B., Machado, R.D., Pauciulo, M.W., Thomson, J.R., Phillips, J.A., 3rd, Loyd, J.E., Nichols, W.C., and Trembath, R.C. (2000). Heterozygous germline mutations in BMPR2, encoding a TGF-beta receptor, cause familial primary pulmonary hypertension. Nature genetics *26*, 81-84.

Langdon, Y.G., and Mullins, M.C. (2011). Maternal and zygotic control of zebrafish dorsoventral axial patterning. Annual review of genetics *45*, 357-377.

Lee, M.T., Bonneau, A.R., Takacs, C.M., Bazzini, A.A., DiVito, K.R., Fleming, E.S., and Giraldez, A.J. (2013). Nanog, Pou5f1 and SoxB1 activate zygotic gene expression during the maternal-to-zygotic transition. Nature *503*, 360-364.

Lee, S.H., So, J.H., Kim, H.T., Choi, J.H., Lee, M.S., Choi, S.Y., Kim, C.H., and Kim, M.J. (2014). Angiopoietin-like 3 regulates hepatocyte proliferation and lipid metabolism in zebrafish. Biochemical and biophysical research communications *446*, 1237-1242.

Lin, X., Duan, X., Liang, Y.Y., Su, Y., Wrighton, K.H., Long, J., Hu, M., Davis, C.M., Wang, J., Brunicardi, F.C.*, et al.* (2006). PPM1A functions as a Smad phosphatase to terminate TGFbeta signaling. Cell *125*, 915-928.

Little, S.C., and Mullins, M.C. (2009). Bone morphogenetic protein heterodimers assemble heteromeric type I receptor complexes to pattern the dorsoventral axis. Nature cell biology *11*, 637-643.

Liu, Z., Lin, X., Cai, Z., Zhang, Z., Han, C., Jia, S., Meng, A., and Wang, Q. (2011). Global identification of SMAD2 target genes reveals a role for multiple co-regulatory factors in zebrafish early gastrulas. The Journal of biological chemistry *286*, 28520-28532.

Löhr, U., Chung, H.R., Beller, M., and Jäckle, H. (2009). Antagonistic action of Bicoid and the repressor Capicua determines the spatial limits of Drosophila head gene expression domains. Proceedings of the National Academy of Sciences of the United States of America *106*, 21695-21700.

Lyons, P.J., Ma, L.H., Baker, R., and Fricker, L.D. (2010). Carboxypeptidase A6 in zebrafish development and implications for VIth cranial nerve pathfinding. PloS one *5*, e12967.

Marigo, V., and Tabin, C.J. (1996). Regulation of patched by sonic hedgehog in the developing neural tube. Proceedings of the National Academy of Sciences of the United States of America *93*, 9346-9351.

Massagué, J. (2012). TGFβ signalling in context. Nature reviews Molecular cell biology *13*, 616-630.

Massague, J., Seoane, J., and Wotton, D. (2005). Smad transcription factors. Genes & development *19*, 2783-2810.

Mi, H., Muruganujan, A., Ebert, D., Huang, X., and Thomas, P.D. (2019). PANTHER version 14: more genomes, a new PANTHER GO-slim and improvements in enrichment analysis tools. Nucleic acids research *47*, D419-d426.

Mills, A.A., Zheng, B., Wang, X.J., Vogel, H., Roop, D.R., and Bradley, A. (1999). p63 is a p53 homologue required for limb and epidermal morphogenesis. Nature *398*, 708-713.

Miyazawa, K., and Miyazono, K. (2017). Regulation of TGF-β Family Signaling by Inhibitory Smads. Cold Spring Harbor perspectives in biology *9*.

Miyazawa, K., Shinozaki, M., Hara, T., Furuya, T., and Miyazono, K. (2002). Two major Smad pathways in TGF-beta superfamily signalling. Genes to cells : devoted to molecular & cellular mechanisms *7*, 1191-1204.

Morgani, S.M., Metzger, J.J., Nichols, J., Siggia, E.D., and Hadjantonakis, A.K. (2018). Micropattern differentiation of mouse pluripotent stem cells recapitulates embryo regionalized cell fate patterning. eLife *7*.

Morikawa, M., Koinuma, D., Tsutsumi, S., Vasilaki, E., Kanki, Y., Heldin, C.H., Aburatani, H., and Miyazono, K. (2011). ChIP-seq reveals cell type-specific binding patterns of BMP-specific Smads and a novel binding motif. Nucleic acids research *39*, 8712-8727.

Mullen, A.C., Orlando, D.A., Newman, J.J., Lovén, J., Kumar, R.M., Bilodeau, S., Reddy, J., Guenther, M.G., DeKoter, R.P., and Young, R.A. (2011). Master transcription factors determine cell-type-specific responses to TGF-β signaling. Cell *147*, 565-576.

Mullins, M.C., Hammerschmidt, M., Kane, D.A., Odenthal, J., Brand, M., van Eeden, F.J., Furutani-Seiki, M., Granato, M., Haffter, P., Heisenberg, C.P.*, et al.* (1996). Genes establishing dorsoventral pattern formation in the zebrafish embryo: the ventral specifying genes. Development (Cambridge, England) *123*, 81-93.

Muraoka, O., Shimizu, T., Yabe, T., Nojima, H., Bae, Y.K., Hashimoto, H., and Hibi, M. (2006). Sizzled controls dorso-ventral polarity by repressing cleavage of the Chordin protein. Nature cell biology *8*, 329-338.

Neave, B., Holder, N., and Patient, R. (1997). A graded response to BMP-4 spatially coordinates patterning of the mesoderm and ectoderm in the zebrafish. Mechanisms of development *62*, 183-195.

Nguyen, V.H., Schmid, B., Trout, J., Connors, S.A., Ekker, M., and Mullins, M.C. (1998). Ventral and lateral regions of the zebrafish gastrula, including the neural crest progenitors, are established by a bmp2b/swirl pathway of genes. Developmental biology *199*, 93-110.

Nguyen, V.H., Trout, J., Connors, S.A., Andermann, P., Weinberg, E., and Mullins, M.C. (2000). Dorsal and intermediate neuronal cell types of the spinal cord are established by a BMP signaling pathway. Development (Cambridge, England) *127*, 1209-1220.

Nordin, K., and LaBonne, C. (2014). Sox5 Is a DNA-binding cofactor for BMP R-Smads that directs target specificity during patterning of the early ectoderm. Developmental cell *31*, 374-382.

Ochoa-Espinosa, A., Yu, D., Tsirigos, A., Struffi, P., and Small, S. (2009). Anterior-posterior positional information in the absence of a strong Bicoid gradient. Proceedings of the National Academy of Sciences of the United States of America *106*, 3823-3828.

Ochoa-Espinosa, A., Yucel, G., Kaplan, L., Pare, A., Pura, N., Oberstein, A., Papatsenko, D., and Small, S. (2005). The role of binding site cluster strength in Bicoid-dependent patterning in Drosophila. Proceedings of the National Academy of Sciences of the United States of America *102*, 4960-4965.

Ogryzko, V.V., Schiltz, R.L., Russanova, V., Howard, B.H., and Nakatani, Y. (1996). The transcriptional coactivators p300 and CBP are histone acetyltransferases. Cell *87*, 953-959.

Pera, E.M., Ikeda, A., Eivers, E., and De Robertis, E.M. (2003). Integration of IGF, FGF, and anti-BMP signals via Smad1 phosphorylation in neural induction. Genes & development *17*, 3023-3028.

Piccolo, S., Sasai, Y., Lu, B., and De Robertis, E.M. (1996). Dorsoventral patterning in Xenopus: inhibition of ventral signals by direct binding of chordin to BMP-4. Cell *86*, 589-598.

Podos, S.D., Hanson, K.K., Wang, Y.C., and Ferguson, E.L. (2001). The DSmurf ubiquitin-protein ligase restricts BMP signaling spatially and temporally during Drosophila embryogenesis. Developmental cell *1*, 567-578.

Pomreinke, A.P., Soh, G.H., Rogers, K.W., Bergmann, J.K., Blassle, A.J., and Muller, P. (2017). Dynamics of BMP signaling and distribution during zebrafish dorsal-ventral patterning. eLife *6*.

Pouponnot, C., Jayaraman, L., and Massagué, J. (1998). Physical and functional interaction of SMADs and p300/CBP. The Journal of biological chemistry *273*, 22865-22868.

Pyati, U.J., Webb, A.E., and Kimelman, D. (2005). Transgenic zebrafish reveal stage-specific roles for Bmp signaling in ventral and posterior mesoderm development. Development (Cambridge, England) *132*, 2333-2343.

Pyrowolakis, G., Hartmann, B., Müller, B., Basler, K., and Affolter, M. (2004). A simple molecular complex mediates widespread BMP-induced repression during Drosophila development. Developmental cell *7*, 229-240.

Qin, B.Y., Chacko, B.M., Lam, S.S., de Caestecker, M.P., Correia, J.J., and Lin, K. (2001). Structural basis of Smad1 activation by receptor kinase phosphorylation. Molecular cell *8*, 1303-1312.

Ramel, M.C., and Hill, C.S. (2013). The ventral to dorsal BMP activity gradient in the early zebrafish embryo is determined by graded expression of BMP ligands. Developmental biology *378*, 170-182.

Reeves, G.T., and Stathopoulos, A. (2009). Graded dorsal and differential gene regulation in the Drosophila embryo. Cold Spring Harbor perspectives in biology *1*, a000836.

Restrepo, S., Zartman, J.J., and Basler, K. (2014). Coordination of patterning and growth by the morphogen DPP. Current biology : CB *24*, R245-255.

Reversade, B., and De Robertis, E.M. (2005). Regulation of ADMP and BMP2/4/7 at opposite embryonic poles generates a self-regulating morphogenetic field. Cell *123*, 1147-1160.

Ribes, V., Balaskas, N., Sasai, N., Cruz, C., Dessaud, E., Cayuso, J., Tozer, S., Yang, L.L., Novitch, B., Marti, E.*, et al.* (2010). Distinct Sonic Hedgehog signaling dynamics specify floor plate and ventral neuronal progenitors in the vertebrate neural tube. Genes & development *24*, 1186-1200.

Rinner, O., Makhankov, Y.V., Biehlmaier, O., and Neuhauss, S.C. (2005). Knockdown of cone-specific kinase GRK7 in larval zebrafish leads to impaired cone response recovery and delayed dark adaptation. Neuron *47*, 231-242.

Rogers, K.W., and Schier, A.F. (2011). Morphogen gradients: from generation to interpretation. Annual review of cell and developmental biology *27*, 377-407.

Rogulja, D., and Irvine, K.D. (2005). Regulation of cell proliferation by a morphogen gradient. Cell *123*, 449-461.

Rogulja, D., Rauskolb, C., and Irvine, K.D. (2008). Morphogen control of wing growth through the Fat signaling pathway. Developmental cell *15*, 309-321.

Ross, S., Cheung, E., Petrakis, T.G., Howell, M., Kraus, W.L., and Hill, C.S. (2006). Smads orchestrate specific histone modifications and chromatin remodeling to activate transcription. The EMBO journal *25*, 4490-4502.

Sagerström, C.G., Gammill, L.S., Veale, R., and Sive, H. (2005). Specification of the enveloping layer and lack of autoneuralization in zebrafish embryonic explants. Developmental dynamics : an official publication of the American Association of Anatomists *232*, 85-97.

Sagner, A., and Briscoe, J. (2017). Morphogen interpretation: concentration, time, competence, and signaling dynamics. Wiley interdisciplinary reviews Developmental biology *6*.

Santos-Pereira, J.M., Gallardo-Fuentes, L., Neto, A., Acemel, R.D., and Tena, J.J. (2019). Pioneer and repressive functions of p63 during zebrafish embryonic ectoderm specification. Nature communications *10*, 3049.

Santos, D., Luzio, A., and Coimbra, A.M. (2017). Zebrafish sex differentiation and gonad development: A review on the impact of environmental factors. Aquat Toxicol *191*, 141-163.

Sapkota, G., Alarcón, C., Spagnoli, F.M., Brivanlou, A.H., and Massagué, J. (2007). Balancing BMP signaling through integrated inputs into the Smad1 linker. Molecular cell *25*, 441-454.

Sarmah, B., and Wente, S.R. (2010). Inositol hexakisphosphate kinase-2 acts as an effector of the vertebrate Hedgehog pathway. Proceedings of the National Academy of Sciences of the United States of America *107*, 19921-19926.

Satija, R., Farrell, J.A., Gennert, D., Schier, A.F., and Regev, A. (2015). Spatial reconstruction of single-cell gene expression data. Nature biotechnology *33*, 495-502.

Schier, A.F., and Talbot, W.S. (2005). Molecular genetics of axis formation in zebrafish. Annual review of genetics *39*, 561-613.

Schmid, B., Furthauer, M., Connors, S.A., Trout, J., Thisse, B., Thisse, C., and Mullins, M.C. (2000). Equivalent genetic roles for bmp7/snailhouse and bmp2b/swirl in dorsoventral pattern formation. Development (Cambridge, England) *127*, 957-967.

Schmierer, B., and Hill, C.S. (2007). TGFbeta-SMAD signal transduction: molecular specificity and functional flexibility. Nature reviews Molecular cell biology *8*, 970-982.

Schulte-Merker, S., Lee, K.J., McMahon, A.P., and Hammerschmidt, M. (1997). The zebrafish organizer requires chordino. Nature *387*, 862-863.

Schumacher, J.A., Hashiguchi, M., Nguyen, V.H., and Mullins, M.C. (2011). An intermediate level of BMP signaling directly specifies cranial neural crest progenitor cells in zebrafish. PloS one *6*, e27403.

Shi, Y., and Massagué, J. (2003). Mechanisms of TGF-beta signaling from cell membrane to the nucleus. Cell *113*, 685-700.

Shi, Y., Wang, Y.F., Jayaraman, L., Yang, H., Massague, J., and Pavletich, N.P. (1998a). Crystal structure of a Smad MH1 domain bound to DNA: insights on DNA binding in TGF-beta signaling. Cell *94*, 585-594.

Shi, Y., Wang, Y.F., Jayaraman, L., Yang, H., Massagué, J., and Pavletich, N.P. (1998b). Crystal structure of a Smad MH1 domain bound to DNA: insights on DNA binding in TGF-beta signaling. Cell *94*, 585-594.

Shimizu, T., Yamanaka, Y., Nojima, H., Yabe, T., Hibi, M., and Hirano, T. (2002). A novel repressor-type homeobox gene, ved, is involved in dharma/bozozok-mediated dorsal organizer formation in zebrafish. Mechanisms of development *118*, 125-138.

Shore, E.M., Xu, M., Feldman, G.J., Fenstermacher, D.A., Cho, T.J., Choi, I.H., Connor, J.M., Delai, P., Glaser, D.L., LeMerrer, M.*, et al.* (2006). A recurrent mutation in the BMP type I receptor ACVR1 causes inherited and sporadic fibrodysplasia ossificans progressiva. Nature genetics *38*, 525-527.

Sirotkin, H.I., Gates, M.A., Kelly, P.D., Schier, A.F., and Talbot, W.S. (2000). Fast1 is required for the development of dorsal axial structures in zebrafish. Current biology : CB *10*, 1051-1054.

Sjödal, M., Edlund, T., and Gunhaga, L. (2007). Time of exposure to BMP signals plays a key role in the specification of the olfactory and lens placodes ex vivo. Developmental cell *13*, 141-149.

Slagle, C.E., Aoki, T., and Burdine, R.D. (2011). Nodal-dependent mesendoderm specification requires the combinatorial activities of FoxH1 and Eomesodermin. PLoS genetics *7*, e1002072.

Smith, S.M., and Maughan, P.J. (2015). SNP genotyping using KASPar assays. Methods Mol Biol *1245*, 243-256.

Stachel, S.E., Grunwald, D.J., and Myers, P.Z. (1993). Lithium perturbation and goosecoid expression identify a dorsal specification pathway in the pregastrula zebrafish. Development (Cambridge, England) *117*, 1261-1274.

Stern, C.D., Charité, J., Deschamps, J., Duboule, D., Durston, A.J., Kmita, M., Nicolas, J.F., Palmeirim, I., Smith, J.C., and Wolpert, L. (2006). Head-tail patterning of the vertebrate embryo: one, two or many unresolved problems? The International journal of developmental biology *50*, 3-15.

Stevens, M.L., Chaturvedi, P., Rankin, S.A., Macdonald, M., Jagannathan, S., Yukawa, M., Barski, A., and Zorn, A.M. (2017). Genomic integration of Wnt/β-catenin and BMP/Smad1 signaling coordinates foregut and hindgut transcriptional programs. Development (Cambridge, England) *144*, 1283-1295.

Stickney, H.L., Imai, Y., Draper, B., Moens, C., and Talbot, W.S. (2007). Zebrafish bmp4 functions during late gastrulation to specify ventroposterior cell fates. Developmental biology *310*, 71-84.

Tozer, S., Le Dreau, G., Marti, E., and Briscoe, J. (2013). Temporal control of BMP signalling determines neuronal subtype identity in the dorsal neural tube. Development (Cambridge, England) *140*, 1467-1474.

Tribulo, C., Aybar, M.J., Nguyen, V.H., Mullins, M.C., and Mayor, R. (2003). Regulation of Msx genes by a Bmp gradient is essential for neural crest specification. Development (Cambridge, England) *130*, 6441-6452.

Troilo, H., Zuk, A.V., Tunnicliffe, R.B., Wohl, A.P., Berry, R., Collins, R.F., Jowitt, T.A., Sengle, G., and Baldock, C. (2014). Nanoscale structure of the BMP antagonist chordin supports cooperative BMP binding. Proceedings of the National Academy of Sciences of the United States of America *111*, 13063-13068.

Tuazon, F.B., and Mullins, M.C. (2015). Temporally coordinated signals progressively pattern the anteroposterior and dorsoventral body axes. Seminars in cell & developmental biology *42*, 118-133.

Tuazon, F.B., Wang, X., Andrade, J.L., Umulis, D., and Mullins, M.C. (2020). Proteolytic Restriction of Chordin Range Underlies BMP Gradient Formation. Cell reports *32*, 108039.

Tucker, J.A., Mintzer, K.A., and Mullins, M.C. (2008). The BMP signaling gradient patterns dorsoventral tissues in a temporally progressive manner along the anteroposterior axis. Developmental cell *14*, 108-119.

Vastenhouw, N.L., Zhang, Y., Woods, I.G., Imam, F., Regev, A., Liu, X.S., Rinn, J., and Schier, A.F. (2010). Chromatin signature of embryonic pluripotency is established during genome activation. Nature *464*, 922-926.

Vincent, T., Neve, E.P., Johnson, J.R., Kukalev, A., Rojo, F., Albanell, J., Pietras, K., Virtanen, I., Philipson, L., Leopold, P.L.*, et al.* (2009). A SNAIL1-SMAD3/4 transcriptional repressor complex promotes TGF-beta mediated epithelial-mesenchymal transition. Nature cell biology *11*, 943-950.

Wagner, D.S., and Mullins, M.C. (2002). Modulation of BMP activity in dorsal-ventral pattern formation by the chordin and ogon antagonists. Developmental biology *245*, 109-123.

Warmflash, A., Sorre, B., Etoc, F., Siggia, E.D., and Brivanlou, A.H. (2014). A method to recapitulate early embryonic spatial patterning in human embryonic stem cells. Nature methods *11*, 847-854.

Wartlick, O., Mumcu, P., Kicheva, A., Bittig, T., Seum, C., Julicher, F., and Gonzalez-Gaitan, M. (2011). Dynamics of Dpp signaling and proliferation control. Science (New York, NY) *331*, 1154-1159.

Watanabe, M., Fung, E.S., Chan, F.B., Wong, J.S., Coutts, M., and Monuki, E.S. (2016). BMP4 acts as a dorsal telencephalic morphogen in a mouse embryonic stem cell culture system. Biology open *5*, 1834-1843.

Webb, K.J., Coolen, M., Gloeckner, C.J., Stigloher, C., Bahn, B., Topp, S., Ueffing, M., and Bally-Cuif, L. (2011). The Enhancer of split transcription factor Her8a is a novel dimerisation partner for Her3 that controls anterior hindbrain neurogenesis in zebrafish. BMC developmental biology *11*, 27.

Wei, C.Y., Wang, H.P., Zhu, Z.Y., and Sun, Y.H. (2014). Transcriptional factors smad1 and smad9 act redundantly to mediate zebrafish ventral specification downstream of smad5. The Journal of biological chemistry *289*, 6604-6618.

Wharton, S.J., Basu, S.P., and Ashe, H.L. (2004). Smad affinity can direct distinct readouts of the embryonic extracellular Dpp gradient in Drosophila. Current biology : CB *14*, 1550-1558.

Wilson, P.A., Lagna, G., Suzuki, A., and Hemmati-Brivanlou, A. (1997). Concentration-dependent patterning of the Xenopus ectoderm by BMP4 and its signal transducer Smad1. Development (Cambridge, England) *124*, 3177-3184.

Wolpert, L. (1969). Positional information and the spatial pattern of cellular differentiation. Journal of theoretical biology *25*, 1-47.

Wong, C., Rougier-Chapman, E.M., Frederick, J.P., Datto, M.B., Liberati, N.T., Li, J.M., and Wang, X.F. (1999). Smad3-Smad4 and AP-1 complexes synergize in transcriptional activation of the c-Jun promoter by transforming growth factor beta. Molecular and cellular biology *19*, 1821-1830.

Wotton, D., Lo, R.S., Lee, S., and Massagué, J. (1999). A Smad transcriptional corepressor. Cell *97*, 29-39.

Wu, X.B., Li, Y., Schneider, A., Yu, W., Rajendren, G., Iqbal, J., Yamamoto, M., Alam, M., Brunet, L.J., Blair, H.C.*, et al.* (2003). Impaired osteoblastic differentiation, reduced bone formation, and severe osteoporosis in noggin-overexpressing mice. The Journal of clinical investigation *112*, 924-934.

Yamakawa, N., Vanbeselaere, J., Chang, L.Y., Yu, S.Y., Ducrocq, L., Harduin-Lepers, A., Kurata, J., Aoki-Kinoshita, K.F., Sato, C., Khoo, K.H.*, et al.* (2018). Systems glycomics of adult zebrafish identifies organ-specific sialylation and glycosylation patterns. Nature communications *9*, 4647.

Yamashita, M., Ying, S.X., Zhang, G.M., Li, C., Cheng, S.Y., Deng, C.X., and Zhang, Y.E. (2005). Ubiquitin ligase Smurf1 controls osteoblast activity and bone homeostasis by targeting MEKK2 for degradation. Cell *121*, 101-113.

Yao, L.C., Blitz, I.L., Peiffer, D.A., Phin, S., Wang, Y., Ogata, S., Cho, K.W., Arora, K., and Warrior, R. (2006). Schnurri transcription factors from Drosophila and vertebrates can mediate Bmp signaling through a phylogenetically conserved mechanism. Development (Cambridge, England) *133*, 4025-4034.

Zagorski, M., Tabata, Y., Brandenberg, N., Lutolf, M.P., Tkacik, G., Bollenbach, T., Briscoe, J., and Kicheva, A. (2017). Decoding of position in the developing neural tube from antiparallel morphogen gradients. Science (New York, NY) *356*, 1379-1383.

Zawel, L., Dai, J.L., Buckhaults, P., Zhou, S., Kinzler, K.W., Vogelstein, B., and Kern, S.E. (1998). Human Smad3 and Smad4 are sequence-specific transcription activators. Molecular cell *1*, 611-617.

Zhang, Y., Chang, C., Gehling, D.J., Hemmati-Brivanlou, A., and Derynck, R. (2001). Regulation of Smad degradation and activity by Smurf2, an E3 ubiquitin ligase. Proceedings of the National Academy of Sciences of the United States of America *98*, 974-979.

Zhu, H., Kavsak, P., Abdollah, S., Wrana, J.L., and Thomsen, G.H. (1999). A SMAD ubiquitin ligase targets the BMP pathway and affects embryonic pattern formation. Nature *400*, 687-693.

Zinski, J., Bu, Y., Wang, X., Dou, W., Umulis, D., and Mullins, M.C. (2017). Systems biology derived source-sink mechanism of BMP gradient formation. eLife *6*.

Zinski, J., Tajer, B., and Mullins, M.C. (2018). TGF-beta Family Signaling in Early Vertebrate Development. Cold Spring Harbor perspectives in biology *10*.

Zinski, J., Tuazon, F., Huang, Y., Mullins, M., and Umulis, D. (2019). Imaging and Quantification of P-Smad1/5 in Zebrafish Blastula and Gastrula Embryos. Methods in molecular biology (Clifton, NJ) *1891*, 135-154.